Master's Thesis
MSc Biomedical Engineering
August 2024

Proactive Radiation Protection

Utilizing 3D Camera for Real-Time Feedback, Minimizing the Scatter Radiation Exposure for Medical Staff.

P.S. (Pepijn) van Ardenne

TU Delft
Delft University of Technology
Reinier de Graaf

Proactive Radiation Protection

Utilizing 3D Camera for Real-Time Feedback, Minimizing the Scatter Radiation Exposure for Medical Staff.

P.S. (Pepijn) van Ardenne
13 Augustus 2024

Thesis in partial fulfilment of the requirements for the joint degree of Master of Science in Technical Medicine – Imaging & Intervention
Delft University

Master's Thesis Project (TM30005 – 35 ECTS)
Faculty of Mechanical Engineering, Biomechanical Engineering, TU Delft
Reinier de Graaf Gasthuis
October 2022 - August 2024

Supervisors
Prof. Dr. J.J. (John) van den Dobbelsteen, TU Delft (Technical Supervisor)
T.S. (Teddy) Vijfvinkel, MD, TU Delft and Reinier de Graaf Gasthuis (Daily Supervisor)
E. (Emanuele) Frassini, TU Delft (Supervisor)

Thesis committee members
Prof. Dr. J.J. (John) van den Dobbelsteen, TU Delft (Chair and Technical Supervisor)
Prof. Dr. M. (Maarten) van der Elst, Reinier de Graaf Gasthuis (Medical Supervisor)
Prof. Dr. B.H.W. (Benno) Hendriks, TU Delft and Philips (Independent committee member)

TU Delft
Delft University of Technology

Reinier de Graaf

Preface and Acknowledgements

With this master's thesis, my three years studying at the Technical University of Delft comes to an end. I gained valuable knowledge about the field and personal growth. I explored additional learning opportunities beyond the standard curriculum outside my studies. Such as working as a Project Engineer for a contracting agency, where I was employed at various companies like TATA Steel, Windunie, and BBIO. Here I worked four days a week and was involved in task for the various companies as a maintenance consultant, primarily focusing on mechanical and energy projects.

When searching for a graduation project, I wanted to work on developing a product that could bridge the gap between technical and medical worlds. When I was last minute informed that my internship at Phillips was canceled due to budget cuts, this project caught my interest through the orientation videos. After an exploratory conversation with John, my interest grew further, and I chose this graduation program.

I would like to express my gratitude to John van Dobbelsteen for the guidance, feedback, and critical opinion, which kept me motivated and enthusiastic on the project. Additionally, I thank Teddy Vijfvinkel for the daily support and his friendly help with the implementation of this project. Also, I appreciate the help of Emmanuele Frassini for his help with finding a solution for the program errors I encountered. In line with this I appreciate the help of Rick Butler with his council for the technical aspects for the implementation of the Camera. Lastly, I want to thank Maarten van der Elst and Benno Hendriks for their feedback during the meetings with the research team.

Pepijn van Ardenne
Amsterdam, August 2024

Summary

Introduction – Procedures related to cardiac catheterization are increasing, resulting in increased radiation exposure for medical staff and the associated health risks. To limit the amount of radiation exposure measures are used. In many cases those measures are not properly used due to the lack of awareness from the medical staff. The primary goal of this research is to integrate a radiation model with a tool, the Azure Kinect, to locate the medical staff and calculate the radiation exposure. The secondary goal is to track the lead shield resulting in the possibility to adjust to the optimal position for the staff while executing the surgery. This study may contribute to real-time dosimetry, the optimal position of both the medical staff and the lead shield, better awareness of radiation exposure, and generally a minimization of the exposure of the medical staff during procedures in the cath lab.

Method – The Azure Kinect DK is used to track the position of the medical staff and, with help of the Aruco markers the lead shield. By using an existing radiation model, the exposure of radiation can be calculated. Firstly, the accuracy of the tracking was ensured. Subsequently, the Azure Kinect's ability was tested to capture difficult situations. Then, the applicability of the radiation model to the Azure Kinect measurements was tested. Finally, the ability to visualize changes and demonstrate their effect on radiation exposure was examined.

Results – The inaccuracy was higher than the Azure Kinect developers reported due to non-optimal conditions; the accuracy deviation had an absolute value of 6,25%. It was found that the deviation of the coordinates between the different measurement points are moderate, with a few outliers and the y-coordinates decreasing deviation as the cardiologist moves farther away from the phantom. By combining medical staff tracking software with the radiation model, radiation exposure can be calculated. The results show that the software detected a decrease in radiation exposure as the distance towards the source increased and the lead shield is placed closer to the cardiologist.

Discussion and Conclusion – This research aims to improve the awareness of radiation exposure in real-time during a procedure. This software represents a significant improvement over the equipment currently used, such as the Phillips Dose Aware badges and the Dosimetry badges.

Despite the error sensitivity of the Azure Kinect, the combination of the device and software can measure the radiation exposure of the medical staff in simulated procedural scenarios in the cath lab. However, there are some limitations resulting in not yet being applicable during a procedure.

Future research directions should enhance the system to increase the applicability during procedures. Optimization can be achieved by positioning of the Azure Kinect to reduce the change of possible occlusion during a procedure and tracking of the lead shield with the help of AI object detection.

By accomplishing these objectives, the gap can be narrowed between the use of this software in a test environment and its application during a procedure. Ultimately, this will lead to an increased awareness of unnecessary radiation exposure among medical staff during procedures.

1.0. Introduction

The cath lab (catheterization laboratory) is utilized for the procedures and diagnosis related to the blood vessels and heart. The number of procedures is increasing due to the rise in lifestyle-related conditions and ageing. A vast majority of these procedures in the cath lab use radiation for diagnostic imaging procedures. When the X-ray interacts with the patient or another material, the primary radiation beam is scattered into the surroundings [1]. The scatter radiation can reach the medical staff performing the procedure, resulting in health risks such as cancer, tissue damage, cataracts, and genetic effects [2]. These risks are for both the medical staff and the patient. However, the medical staff is exposed to a significantly higher number of procedures, thus resulting in an increased chance of health risks, which should require the use of protection for scatter radiation. Because the medical staff lacks awareness of the radiation protection parameters, they do not use all the available protection measures or use them efficiently enough [3], resulting in higher exposure to radiation than necessary. This unnecessary exposure could be avoided by real-time dosimetry during the surgery [4]. Since quality assurance is a major theme in healthcare, the safety of the medical staff in the cath lab is an important subject. The question is whether it is possible to implement a simple system to provide real-time dosimetry.

1.1. Exposure of Radiation

The radiation beam scatters when it interacts with the patient, this can result in multiple downsides. In Figure 1, it is shown how scatter radiation reacts with the patient and affects the medical staff around the patient. In addition to changing the direction, scatter radiation results in degraded image quality and increased radiation exposure [2, 5]. The quality of the image decreases because scatter radiation results in background noise that will interfere with the original beam. The radiation beam can have multiple harmful health effects on humans, namely: stochastic and deterministic [6].

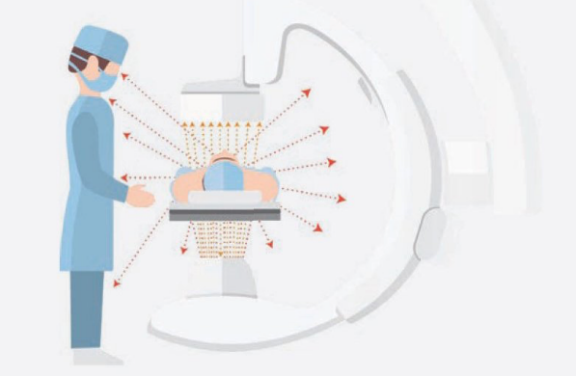

Figure 1: Shows how radiation from the C-arm behaves and interacts upon contacting the patient, where the radiation is reflected, resulting in what is known as scatter radiation, which affects the medical staff surrounding the surgeon's table [46].

The stochastic effects are associated with long-term and low-level exposure to radiation, resulting in an increased probability of health effects. These health effects follow a linear, no-threshold risk model, in which the risk of damage to the irradiated tissue increases with the amount of exposure [7]. Effects of the stochastic include cancers of the skin, thyroid, and gastrointestinal tract [8].

The deterministic effects are more associated with short-term and higher lever exposure to radiation, resulting in direct damage to the living cells. The severity of these effects is predictable with a dose-related increase and does not occur below a specific threshold [9]. Deterministic effects include cataracts, skin erythema and desquamation sterility [10].

Due to the serious medical concerns resulting from prolonged radiation exposure, there is a maximum allowed dose of radiation for the medical staff. The maximum dose limit for the staff is 20 mSv per year [11] and is measured with a personal radiation dosimeter during procedures. Table 1 shows the amount of radiation received on the extremities of the body of the medical staff. The dosimeters are put over the protection clothing of the medical staff and indicate the amount of radiation the staff receives. The results from Table 1 show that the highest radiation is received for the left hand. This can also be found in the number of stochastic health effects among cardiologists, working in the cath lab for a longer period, as a higher frequency of brain cancer is observed on the left side of the head [13].

Regarding the amount of radiation used during a procedure, there is a trade-off between the quality of the image and the safety of the medical staff [2]. Given that one concern outweighs the other, the medical staff operates according to the ALARA principle to keep the radiation exposure As Low as Reasonably Achievable. The amount of received radiation is influenced by the distance from the radiation source, exposure time, and the degree of shielding provided by radiation protection [14]. The received radiation by the physicians in Table 1 is remarkably high, taking into account it is just one procedure. Therefore, it is necessary to research real-time dosimetry, awareness, and radiation protection to limit the received radiation in the cath lab.

	Left wrist	Right wrist	Left finger	Right finger	Left leg	Right leg	Between the eyes	Left eye
	Physicians							
Average±SD	485±1158	108±232	324±718	88±213	124±363	103±313	64±232	37±120
Median	64	48	0	0	19	22	0	0
Range	[14–5239]	[16–1242]	[0–2877]	[0–814]	[10–1959]	[4–1691]	[0–1129]	[0–557]
	Nurses							
Average±SD	26±12	26±6	4±8	2±5	15±2	18±4	4±8	1±3
Median	25	24	0	0	15	18	0	0
Range	[13–41]	[19–32]	[0–15]	[0–9]	[14–17]	[15–22]	[0–16]	[0–5]

Table 1: An indication of the amount of dosimetry the Physician and nurse receive for their specific limbs per procedure measured for multiple operations, the dosage is in (µSv) [12].

1.2. Radiation Protection

Due to the severity of the health effects resulting from radiation, there is a significant emphasis on radiation protection. Safety can be classified into two categories: active protection and passive protection.

Active protection relates to measures regarding adjusting the behavior [15]. Measures for this have been mentioned above, such as creating awareness, ALARA, and dosimetry badges. Passive protection relates to physical measures and maintaining distance to reduce radiation exposure. Some of the passive protection that is used in the cath lab is shown in Figure 2. Protective measures the cardiologist wears during procedures are lead aprons, thyroid collar shields, lead glasses, absorbing surgical caps or headbands, and lead gloves. Wearable protective measures like lead aprons and thyroid collar shields are commonly worn during procedures [16]. However, protective measures like glasses, gloves, and absorbing headwear are used much less frequently during procedures for several reasons. What is concerning is that wearing lead glasses can reduce exposure to scattered radiation to the eyes by up to 85% [17]. Only 34.5% of the cardiologists use the lead glasses in the experiment. The lead gloves reduce up to 57% exposure to scatter radiation [18]. There are multiple reasons for not wearing radiation protective equipment, such as uncomfortable, limited freedom of movement, and insufficient awareness of the dangers [19]. Thereafter, lead flaps are hanging from the surgeon's table and a movable lead shield between the medical staff and the radiation source to prevent exposure to radiation for the medical staff.

The lead shield is an important protection measure since it reduces radiation up to 93.5% [20]. However, the extent to which the shield reduces the radiation exposure greatly depends on

how the shield is used, since the positioning of the shield impacts the reduction. To use the shield correctly, some steps must be followed. Firstly, the shield must be precisely positioned perpendicular to the line from the scatter radiation source to the medical staff [20]. Secondly, the shield should be placed as close as possible to the medical staff [20]. Unfortunately, the shield is not always in this optimal position during procedures, possibly due to a lack of awareness of the danger of radiation, restricting the movements of the medical staff, and not realizing it is not in the optimal position [19]. A system providing real-time feedback on the optimal position of the lead shield would reduce the amount of radiation exposure, thereby making a positive contribution to preventing health risks for medical staff in the cath lab.

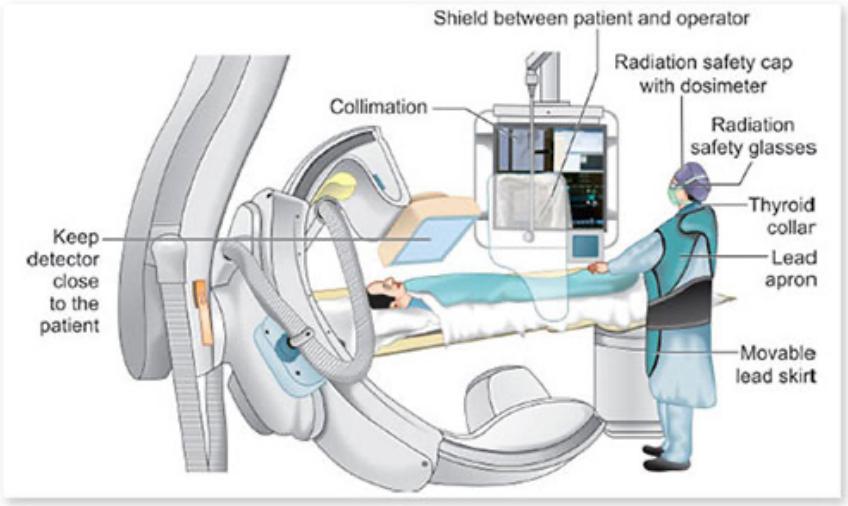

Figure 2: provides a schematic example of the setup in a catheterization laboratory and some of the passive radiation safety equipment used during procedures.

1.3. Video-based tracking

Video recording in healthcare can be useful and is used for multiple different purposes. One of these purposes is tracking the movements of the bodies of the medical staff, which serves multiple applications: detecting phases during surgery, analyzing the workflow, evaluating the procedure, and education in healthcare [21]. In addition, utilizing body tracking through a camera can assist in creating awareness and determining the optimal position for medical staff to minimize exposure to scatter radiation. The software can warn the medical staff when they are unnecessarily exposed to radiation so that they can adjust their position. The recording must be in 3D, since the cath lab needs to be mapped in three axes [22].

There are multiple methods to create a 3D image, such as multiple cameras, multiple lenses and InfraRed depth cameras. By using multiple cameras, 2D images from various angles are combined to generate a 3D representation of the room. However, the use of 2D images from multiple cameras to create a 3D representation comes with various disadvantages. Such as a representation that captures the depth with less accuracy [23, 24, 26]; the need for calibrating multiple cameras can lead to more errors and is more time-consuming [22, 23]; many more frames, leading to a need for higher computational power [23]. Another method to create a 3-dimensional representation is with the help of two lenses of a camera integrated into a single device, which then generates the 3D image. This does mitigate the issue of the high computational power requirement to some extent. Moreover, the 3D representation from a depth camera such as an InfraRed camera is more accurate [22]. Infrared cameras generate 3D images by emitting infrared light, measuring the time it takes for light to travel to objects and back, and converting this depth information into a 3D scene [24]. To reduce possible errors that may occur with the recording of an InfraRed depth camera a color camera can be used alongside [30]. The color (RGB) camera generates a 2D colored image by capturing light in red, green, and blue wavelengths [25]. The image captured by this hybrid setup provides an accurate 3D representation of the environment, keeps the computational power

requirement limited, and can be easily put in operation. In this study, the Azure Kinect DK is used because it combines RGB and InfraRed Incameras, has low-cost, and can be easily used to develop software for tasks such as tracking. The accuracy of the camera system is affected by factors in the cath lab such as occlusion [27] and lighting [28]. In addition, the accuracy of tracking the bodies is also influenced by specific body parts; the lower extremities [23], and the outer parts of the extremities [22] show lower accuracy. However, by combining the InfraRed and RGB cameras the medical staff's position can in real-time be accurately located in the cath lab. To be able to make a statement about the received radiation of the medical staff, the lead shield should be traced as well. Since the lead shield is transparent it is difficult to be traced by video recording. By placing an Aruco marker on the lead shield it can be accurately traced by the Azure Kinect. Since the orientation of the Aruco markers relative to the camera can be determined, and the accuracy of tracking is higher than without a marker [42].

1.4. Goals and Objectives

The primary goal of this study is to integrate a radiation model with the 3D positioning of the cardiologist to accurately determine their exposure to scatter radiation in the cath lab. This will be achieved by using a 3-dimensional camera to record the cath lab and track the position of the medical staff. The radiation model will then calculate the radiation exposure based on the staff's specific location and the amount of radiation used during a procedure. This approach is the first step in providing real-time feedback to the staff regarding their radiation exposure, potentially adjusting their behavior [4] to enhance safety protocols in daily practice. With the help of this model, the implementation of the 3D camera will be explored to accurately determine the radiation exposure of the staff in a cath lab. Several sub-objectives will be investigated:

- Operating conditions of the Azure Kinect DK.
- Applicability in the cath Lab.

The secondary goal of this study is tracking the lead shield with the help of the Aruco markers with the 3D camera for the position. This results in adjusting the shield to the optimal position for a reduction in radiation. Since the amount of scatter radiation exposure is influenced by both the distance between the lead shield and the staff and the perpendicular position of the shield in line with the scatter radiation source to the staff [20]. This study aims to determine the feasibility of locating the medical staff and the lead shield, and calculate their exposure to radiation, to raise awareness and adjust the behavior to reduce health risks.

Addressing these goals and objectives may lead to real-time dosimetry, the optimal position of both the medical staff and the lead shield, better awareness of radiation exposure, and generally a minimization of the exposure of the radiation during procedures.

2.0. Method

This study follows a systematic methodology to implement a 3-dimensional camera for the tracking of the body of the cardiologist and the lead shield for radiation safety in the catheterization laboratory. The camera records the cath Lab and tracks the cardiologist, and by applying an existing radiation model [29], the dosimetry for the cardiologist can be calculated for the different coordinates with and without the lead shield. In this study, the radiation model [29] using fluoroscopic mode with the C-arm not angled was employed, the other models can be applied as well. Three different measurements are being considered: assessing the equipment's limitations, applying the radiation exposure model, and visualizing changes in radiation exposure.

2.1. Azure Kinect DK

For the tracking of the bodies of the medical staff to ascertain their specific location in the cath lab, there is a need to virtually represent the room in three axes (x-, y-, z-axis). In order to create this representation, the recordings of the environment of the medical staff should be as well in 3D. Thereby, the recordings in this study were performed by the Azure Kinect DK, shown in Figure 3.

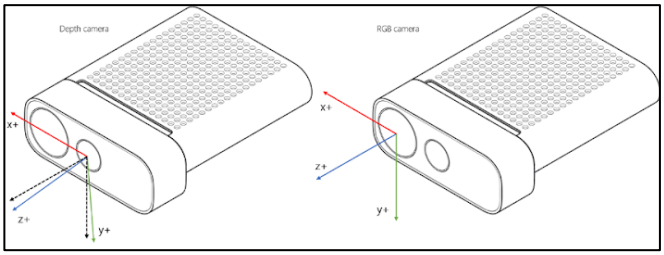

Figure 3: A schematic overview of the Azure Kinect DK and the two cameras it includes [34]. The Kinect on the left shows the depth camera and the direction of the three different axis and the small adjustment the camera has for the Z- and Y-Axes. The Kinect on the right shows the direction of the axes, this is used as the origin of the Azure Kinect in this research.

The Azure Kinect DK is a developer's kit from Microsoft that comes with a variety of software kits, settings, and multiple sensors. An example of a software kit from Microsoft is body tracking. There is a wide range of different settings and sensors, that can be adjusted or be turned off. Taking into consideration there is a trade-off between increasing the accuracy, by adjusting the settings, and the required computational capacity [32]. Since a high computational capacity can possibly lead to problems in the processing of the data in real-time, the objective is to keep the computational capacity as low as reasonably possible without reducing the accuracy of the data.

During the measurements, the depth camera and the color camera are the only sensors that are turned on. The microphone and Inertia Measurement Units (IMUs) have no added value in creating a representation of the cath lab in this experiment. To keep the amount of data limited during the measurement, the microphone and IMUs are therefore turned off.

There are 5 different settings for the depth camera. Some of the different settings are abbreviated with the Narrow Field of View (NFOV) and others with a Wide Field of View (WFOV). In addition, a setting refers to the possibility of combining multiple small pixels into a megapixel, which is called (un)binned. The last setting is the passive IR setting which does not emit light but only absorbs the light of the surroundings to calculate the distance. The average distance from the (scatter)radiation source (using the chest of the patient as the reference point shown in figure 4) to the medical staff was measured for the clinician at 103 cm and the assistant at 158 cm [33]. Since the camera cannot be positioned directly on the radiation source, a margin should be accounted for the space between the source and the camera. This ensures that the camera can be placed at an appropriate distance from the radiation source without obstructing the work of the medical staff. The camera must measure not only the distance of the medical staff but also a greater distance and a wide field of interest, as the entire surgeon's table needs to be captured in the captured image. Therefore, the optimal setting for the depth camera should be around 2.5 meters with a wider field of interest. This is the reason the WFOV unbinned

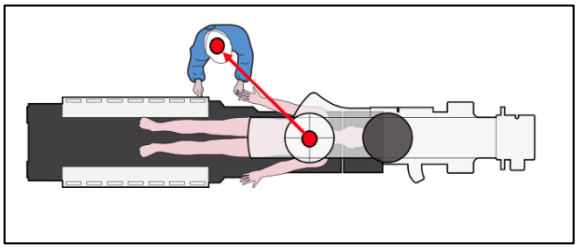

Figure 4: Shows a schematic top view of the cardiologist at the surgeon's table with the C-arm position above the patient. The distance between the cardiologist and the C-arm is marked red, as this needs to be measured with the Azure Kinect to calculate the amount of scattered radiation the cardiologist receives.

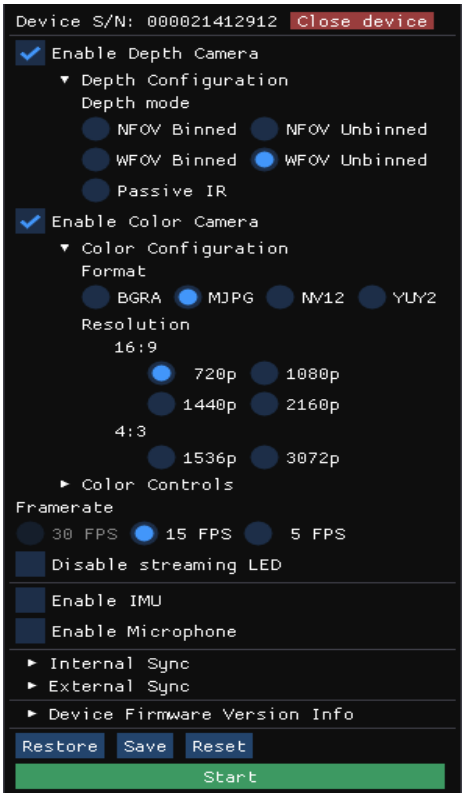

Figure 5: Shows preview of the selected settings of the Azure Kinect during the measurement in viewer mode. When a recording needs to be made, these are the settings that can be chosen, but they must be configured via the cmd window [31].

setting is chosen for the measurements, that will record in a round view. A downside is the increased computational capacity for the higher resolution due to the unbinned setting. However, this does result in a potentially lower error sensitivity [26] in the tracking of the cardiologist and the lead shield.

The settings of the color camera can be adjusted to change the color configuration format and the resolution. The depth camera is the primary source for mapping the environment while the color camera is used as a referential image in the measurement. Therefore, it is not necessary to use a high resolution for the color camera. Since the computational capacity should be as low as reasonably possible a lower resolution is preferred. Therefore, a resolution of 720p has been chosen and the only compatible color configuration format with this resolution is MJPG.

The framerate is set to a value of 15 FPS, to keep the capacity reasonably low and the images relatively smooth, since the measurements are recordings of a cardiologist who makes movements, and they are not high-speed movements. The setting for disabling streaming LED should not be used, to assure accurate depth measurement. The used settings are shown in figure 5 in the Azure Kinect viewer mode.

An important aspect of the Azure Kinect for usage in the cath lab is the accuracy of the device. With the settings configured, according to the developers the following can be said about the camera [31]; the reach of the camera sensor is optimized between 0,25-2,88 meter. However, the device can measure distances outside of this reach. The device has a random error of std. dev. ≤ 17 mm and a typical systematic error of < 11 mm + 0,1%. During a recording, a radiation intensity of 2,2 µW/cm²/nm is used for the InfraRed light. The developers included a disclaimer that the aforementioned errors apply to ideal conditions, while not taking in account the measurements being disturbed by reflection. The recordings of the Azure Kinect can be influenced by factors in the cath lab, such as: bright light, darkness, and reflection [45]. Therefore, the accuracy in the cath lab might differ from the accuracy mentioned by the developers of the Azure Kinect.

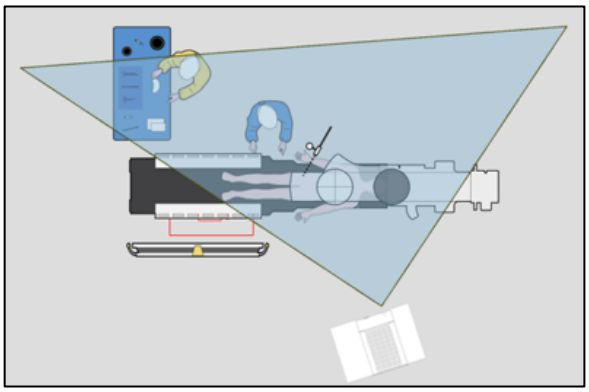

Figure 6: Shows a schematic overview from the top view of the positioning of the Azure Kinect that the camera will have during a procedure in the catheterization laboratory with the cardiologist and assistant present. Additionally, the field of view of the camera is sketched. The figure also shows the lead shield positioned between the cardiologist and the patient. Additionally, the monitor is positioned next to the Azure Kinect and the surgeon's stable.

2.2. Measurement set-up

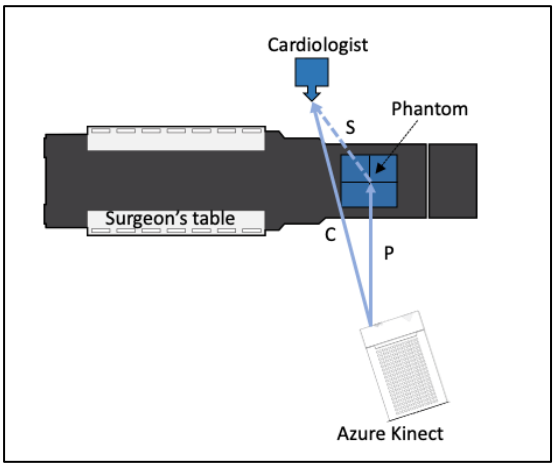

Figure 7: Shows a schematic overview of the of catheterization laboratory and the position of the Azure Kinect. Through a vector sketch, this figure shows how the vector from the phantom is calculated to the cardiologist to calculate the scatter radiation (S.). The Azure measures the vector to the cardiologist (C.) through the measurements and the vector to the Phantom (P.) through the calibration.

The measurements were conducted in the cath lab in the Reinier de Graaf Gasthuis, simulating certain situations for the cardiologist. In the room, there are some small some changes. The Kinect is positioned on a table opposite to the surgeon's table from the cardiologist, with a line on the floor and the wall serving as reference points for the table and the Azure Kinect's position (Appendix B, figure 22). The Azure Kinect DK is elevated above the tabletop, so that the LED light on the Kinect does not blind his own view. Additionally, a laptop is placed on the table to control the Azure Kinect. The table and the Azure Kinect are positioned at an angle to the surgeon's table, ensuring that the entire surgeon's table is visible during the recordings and that the monitor does not occlude the view. This set-up is shown in figure 6. The angle the Azure Kinect makes with the surgeon's table is crucial because it is needed to calculate the transformation of the coordinate system for the radiation model [29]. This angle is measured relative to the surgeon's table, with the Azure Kinect aligned parallel to the edge of its table and the surgeon's table positioned parallel to the edge of the phantom. The angle of the table relative to the surgeon's table can be considered equal to the angle of the Azure Kinect to the phantom. Additionally, the lead shield is covered with five 5x5 Aruco markers, each measuring 20 to 30 cm in size. Thirty centimeters from the left edge of the surgeon's table, a piece of tape is placed on the floor to mark the cardiologist's position. Measured from the middle of the surgeon's table, this distance is 60 centimeters. During the measurements the phantom is removed, and the c-arm is retracted, to reduce the possibility of occlusion. However, the location where the phantom should be, with the edges and center are marked with tape, to serve as a reference point to determine the positions of the lead shield or cardiologist.

To verify the software of the Azure Kinect, a simple calibration measurement to validate the accuracy of the measurement needs to be done of the distance to the cardiologist, center of the phantom, and the distance and orientation to the lead shield. The measurements from the Azure Kinect are validated by measuring tape.

The Azure Kinect measures the distance of the cardiologist relative to the Kinect itself, while the radiation model [29] uses the center of the phantom as the origin of the coordinate system. Since the camera measures distances in three axes, it can be considered as a vector. To recalculate the distances to the cardiologist in three axes from the Azure Kinect to the center of the phantom, a vector can be used as translation. This vector is the distance to the center of the phantom and is visible in figure 7. Since this distance is constant, the distance to the radiation source can be calculated for each measurement by the cardiologist when the coordinates of the center of the phantom are known. To determine the correct coordinates of the phantom using the Azure Kinect, an Aruco marker is placed at the exact location of the center point of the phantom, which is then measured by the Azure Kinect. These values will be applied to the coordinate system of the cardiologist and lead shield that will be incorporated into a radiation model.

The first measurement that were executed for this research are static and tests the limitations of the Azure Kinect and the body tracking software in difficult situations, since occlusion [27] often leads to inaccurate measurements during video recording. During this measurement, a short recording is made of the cardiologist standing behind the surgeon's table in an anatomical posture in three different positions: rotated 0 degrees compared to the camera, rotated 45 degrees, and rotated 90 degrees. During the various positions of the cardiologist, the lead screen is also placed in three different positions: is located next to the cardiologist in the Kinect image, partially obstructing the view of the cardiologist, and completely obstructing the view of the cardiologist. The purpose of this measurement is to cross-check whether the correct distance of the cardiologist can be detected when they are standing behind the lead shield and whether the cardiologist can be correctly detected at all in difficult situations to avoid any invalid outcome.

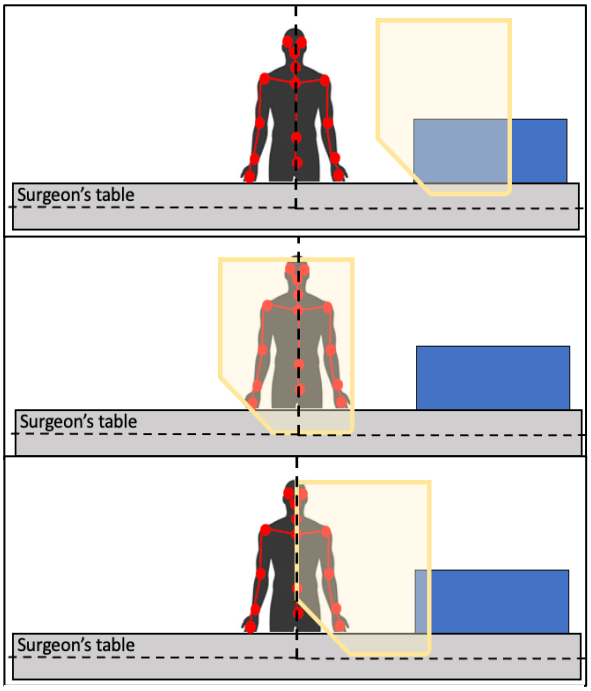

Figure 8: Shows a schematic overview of the positioning of the lead shield relative to the cardiologist in the first measurement, the cardiologist is only positioned in his anatomically position. Firstly, the lead shield is not obstructing the view of the camera on the cardiologist. Secondly, the lead shield is completely obstructing the view on the cardiologist. Finally, the lead shield is partially obstructing the view on the cardiologist.

The second measurement executed for this research is dynamic and tests the applicability of the radiation exposure model. The positioning of the cardiologist and the lead shield will therefore correspond to the positions investigated in the study of Deudekom [29]. During the measurement, the applicability of the model and the Kinect is tested, as well as whether the accuracy is high enough to make a validf statement about radiation exposure. The position of the cardiologist at the edge of the surgeon's table with a distances of 100, 130 160 cm to the center of the phantom. During each measurement, the cardiologist assumes one of these positions, while the lead shield is placed in three different positions. Additionally, for each position, the cardiologist adopts three different postures. The model indicated reduced exposure when the lead shield was positioned perpendicular to the surgeon's table, 20 cm closer to the cardiologist instead of 5 cm away from the left upper corner of the phantom. The positioning is replicated, and at position 1, the lead shield will be at 51.06 cm, and position 2 will be 36.06 cm from the center of the phantom. The third placement of the lead shield is on the edge of the surgeon's table at the level of the phantom's center. The three different placements of the lead shield each represent a method of placement: position one is a correctly

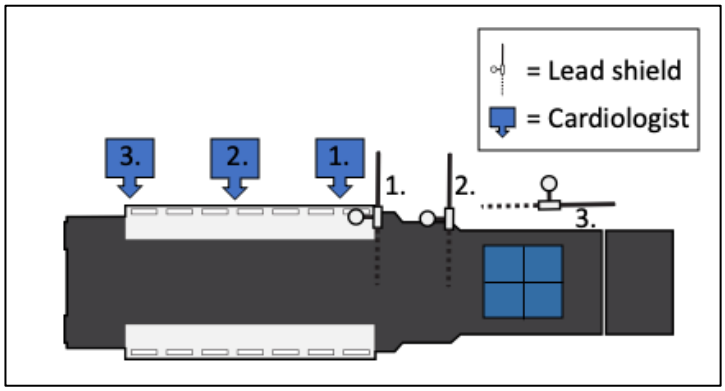

Figure 9: A schematic overview of the positioning of the cardiologist and lead shield during the second measurement. The cardiologist is positioned in a line to increase the distance towards the radiation source. The lead shield is positioned in three different positions; 1 correctly positioned close to the cardiologist, 2 correctly positioned but further away from the cardiologist, and 3 incorrectly

positioned shield close to the cardiologist, position two is a correctly positioned shield close to the radiation source, and position three represents an incorrectly positioned shield. During the measurements, the cardiologist assumes three different postures for each position of the lead shield; an anatomical perpendicular to the table, rotated 45 degrees, and perpendicular to the table with extended arms. The different postures allow for an assessment of estimating adjustments in body tracking while mimicking possible movements in the cath lab. The purpose of this measurement is to check whether this dynamical situation can lead to the same result as the radiation model [29] and if it is possible to estimate the exposure to radiation.

The third measurement that is researched involves visualization and tests the degree of adaptability of the collaboration between the Azure Kinect and the radiation exposure model. During these measurements, situations are simulated when radiation exposure will increase or decrease. This verifies whether the software can detect adjustments and can be easily visualized, enabling the cardiologist to be informed about radiation exposure through a simple feedback system. In these measurements, two different situations are simulated. Situation 1 changes the distance of the cardiologist relative to the radiation source, and the second situation involves placing the lead shield between the cardiologist and the radiation source while adjusting the distance relative to the cardiologist. The first situation is shown in Figure 10 adjusting the distance between the radiation source and the cardiologist by placing the cardiologist between four different points. The first point is at the foot end of the surgeon's table, the second and third points are aligned with the first position one meter and two meters to the right, and the last position is aligned with the second position 50 cm further back compared to the surgeon's table. By assuming these positions, the cardiologist has determined various distances from the radiation source, namely: 210.5, 126.5, 88.6, and 167.5 centimeters. During the first part of the measurement the cardiologist moves from position 1 to position 2, then to position 3, back to 2, and finally to position 4. In the second part of the measurement of the first situation, the cardiologist starts close to the radiation source starting at position 3, moving to position 2, then to position 1, back to position 2 and finally to position 4.

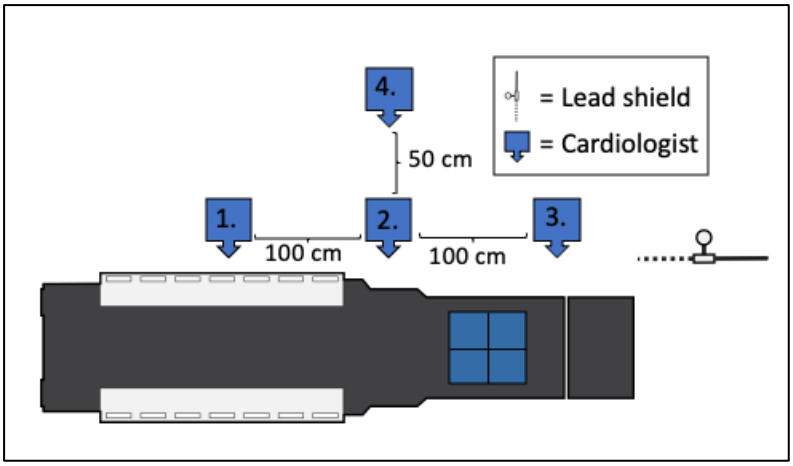

Figure 10: A schematic overview of the positions of the cardiologist for the first part of the third measurement. The distances for the four different positions are shown and the lead shield is positioned outside the

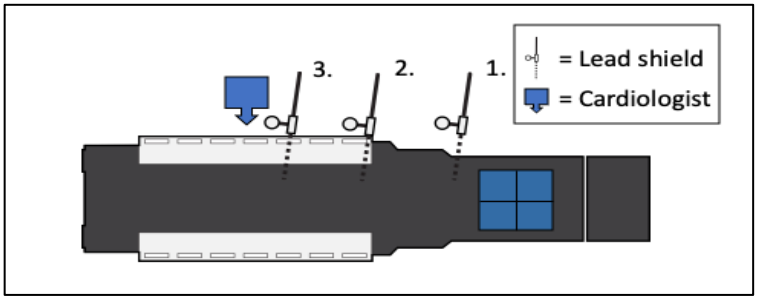

Figure 11: A schematic overview of the positions of the lead shield for the second part of the third measurement. The cardiologist is positioned left of the third position of the lead shield.

In the second measurement, akin to the first, the lead shield's distance towards the phantom is altered, shown in Figure 11. The positions are between the scattered radiation source and the cardiologist. The cardiologist is standing at the same position as position 1 in the initial situation of this measurement. The lead screen has been placed in three different positions, where the

connection of the C-arm to the ceiling had three different references points, where 1 is closest to the radiation source and 3 is closest to the cardiologist. In the initial measurement of this situation, the lead shield is positioned at position 1 and then moves closer to the cardiologist. In the second measurement, the reverse occurs, with the shield starting at position 3, close to the cardiologist and then moving closer to the scatter radiation source. The purpose of this measurement is to test whether the combination of software would still work in a dynamic situation and whether the movement of the cardiologist and lead shield would cause problems in tracking.

2.3. Modelling

Python and Visual Studio were used to create the software for the tracking of the cardiologist and the lead shield and Python was used for processing the data. Github [34] was used to implement specific functions or examples in the program. The important parts of the programming process are discussed. The program has been divided into certain parts to facilitate future enhancement of the python script. The parts can be replaced or improved without affecting the rest of the code.

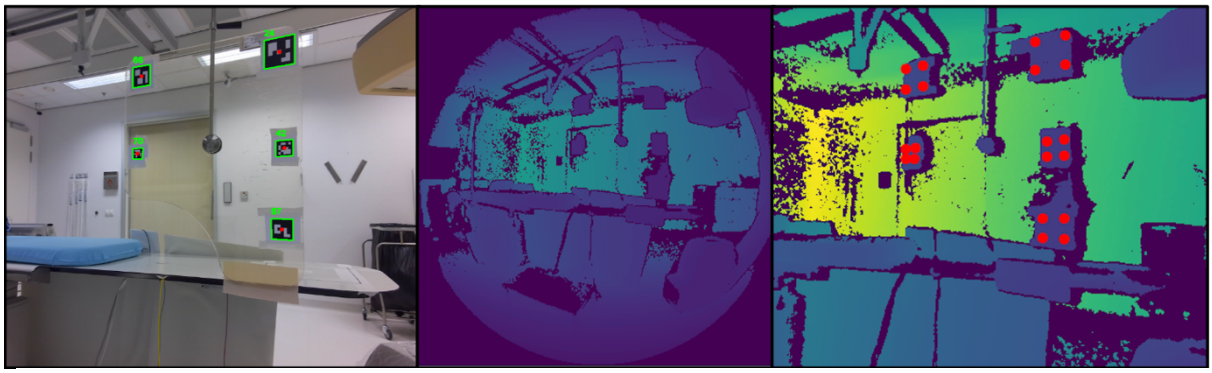

Figure 10: The different views of the calibration measurement of the lead shield. Left: shows the color image and the tracking of the Aruco marker. Middle: shows the round depth image, it has black edges because a lens is used that is convex. There is no tracking of the Aruco marker in this image. Right: shows the color image overlaid on the depth image, with the tracking of the corners of the Aruco marker. This allows obtaining the depth values from the depth image using the pixel coordinates of the color image.

For tracking the cardiologist, a combination of software was used which was provided by Microsoft for the Azure Kinect DK. This software is provided in the form of a header file and contains various functions to build an application that can track the limbs of a recorded person. These functions use an input and output queue during the tracking, allowing the Azure Kinect captures to be processed more efficiently through an asynchronous process. An advantage is that when assessing a frame for body tracking, it is not affected by the absence of a detected body in the previous frame, as each frame is evaluated independently. However, this method of assessing each frame independently requires a lot of computational capacity. The time for the input and output queuing is called the timeout value and differs per application. Since the computational capacity should be kept as low as reasonably possible, body parts are not traced during recording. Therefore, an offline_processing program is used to trace the body parts afterwards using the recording as input, this is a shared program on GitHub [34]. The software can also be modified to perform online processing during the recording itself. However, since this is a test phase, it is simpler to perform these adjustments offline to allow for further modifications and to verify the measurements. The output comprises a collection of body structures, a 3D body index map. The 3D body index map consists of the coordinates x-, y-, and z- coordinates for the depth image. The depth view is used to trace the body of the cardiologist. Since the depth view utilizes InfraRed radiation for measurement, it has the advantage that the cardiologist can be traced in a completely dark room. For example,

when the lights are dimmed during a procedure, the body tracking software will not have difficulties with tracing the cardiologist.

Aruco markers are a simple way to accurately track objects through video recording, as described in the literature review (Appendix A). This method is implemented with the help of the OpenCV toolkit, as Microsoft's toolkits do not directly support it for the Azure Kinect. OpenCV is a toolkit that provides various algorithms and tools for detecting and analyzing objects in images and videos [35]. With this toolkit, a custom algorithm can be created and trained to track the lead shield without Aruco markers. However, because it is extremely labor-intensive and is not directly related to the focus of this research, it falls outside the scope of this study. During the method, an offline method can be used to extract the coordinates of the Aruco markers from a recording. This reduces the computational capacity and allows optimizing the code more easily, as the recording can be replayed instead of being re-recorded. The tracking of the Aruco markers consists of two parts: obtaining information about which pixels the marker represents in the frame and determining the orientation of the markers.

The process of tracking the pixel values of the markers proceeds as follows: the recording of the color image is read frame by frame, and whenever the toolkit detects an Aruco marker, a green outline is drawn around it and the Aruco marker is named by a number, as shown in figure 12. The information from the numbered markers includes the pixel values of the frame's width and length, commonly referred to as pixels x and y of the color view, determined for each corner.

The orientation of the markers can be determined through a calculation using the intrinsic and extrinsic parameters of the Azure Kinect. The intrinsic parameters represent the value of certain settings in the camera, while the extrinsic parameters determine the camera's position in the 3D scene [36]. By doing a calibration measurement with a chessboard, these parameters are determined, from which the roll, pitch, and yaw values (rotation over the x-, y-, and z-axes) of the markers can be calculated per frame. The orientation of the axes is determined from the left upper corner of the Aruco marker, with the Z-axis extending straight out of the marker, the X-axis running to the right along the upper edge of the marker, and the Y-axis extending upwards along the left edge of the marker.

The output of these scripts includes, per frame the pixel values for the width and length of the color image for the corners of the Aruco marker, as well as the roll, pitch and yaw rotation. The Aruco markers are traced with the color view, which means that the software requires light for tracing and will have difficulties tracking in a dark operating room.

The output values from tracking the bodies and the Aruco markers do not contain the same information and do not provide details about the exact position in a 3D map. The Azure Kinect DK features its own toolkit, known as k4a.exe [37], designed for writing software and maximizing the camera's capabilities. Since the software needs to be written in Python to align with the radiation model [29], a wrapper named pyk4a must be utilized [38].

The output from tracking the Aruco markers lacks the depth value, which is necessary for converting the coordinates in a 3D map. Coupling

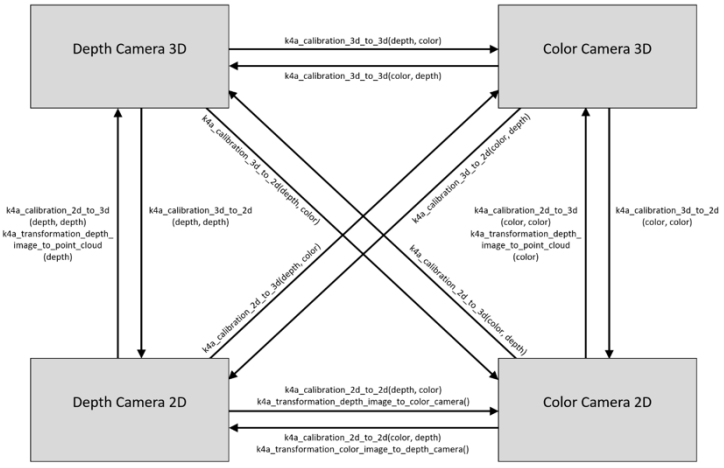

Figure 11: Shows an indication on the different images the Azure Kinect uses [31]. Which function of the K4A should be used to transform the coordinates of an images to coordinates of a different image. Since it is necessary to use coordinates in the same image for having a clear representation of the environment.

the acquired x- and y-pixel coordinates from the color image with the depth image was not possible due to the difference in resolution. To solve this problem, the color image was overlaid onto the depth image. This allowed the depth values to be obtained using the x- and y-pixel coordinates of the corners of the Aruco markers in the color image, as shown in Figure 12.

The 3D depth and 2D color values are available for the cardiologist and the Aruco markers. Figure 13 shows the different functions of the pyk4a toolkit, where the coordinates can be converted into the 2D or 3D pixels of the color and depth image. By converting to 3D coordinates, it is possible to represent both the cardiologist and the Aruco marker in the same 3D map. The 3D coordinates are calculated for the depth view in millimeters with the Azure Kinect as the origin of the coordinate system.

The radiation model [29] uses two different coordinate systems with two different origins. The three axes are oriented in the same direction. The first origin is located in the center of the phantom. This position has been precisely mapped using a calibration measurement of the position of the center of the phantom and the angle of the Azure Kinect DK with the surgeon's table. The second origin is established near the left foot end of the surgeon's table at ground level. The exact coordinates of this point are relative to the first origin in the radiation model. Once the first origin is determined, this point can be calculated.

The coordinates of the cardiologist and the lead shield must first be converted from the Azure Kinect coordinate system to the first coordinate system of the radiation model. Through the calibration measurements, the coordinates and orientation of the center of the phantom are known. By applying a translation and rotation vector [39], shown in equation 1, the origin and axes direction of the Azure Kinect coordinate system are adjusted to match those of the first coordinate system in the radiation model. Since the axes directions of the second origin are the same as those of the first origin in the radiation model, only a translation vector is needed to convert the coordinate system. When the coordinates have been converted to the coordinate system of the second origin, the radiation exposure can be calculated manually. The coordinates in centimeters are looked up manually in the radiation model [29] that maps the amount of radiation exposure in mSv. The second origin of the coordinate system is used to calculate the radiation exposure, and the first origin is used to display the measured coordinates since this has a simple reference point, the center of the phantom.

A drawback is that the radiation model only calculates the radiation up to a limited distance

$$\begin{bmatrix} X' \\ Y' \\ Z' \\ 1 \end{bmatrix} = \begin{bmatrix} 1 & 0 & 0 & Tx \\ 0 & 1 & 0 & Ty \\ 0 & 0 & 1 & Tz \\ 0 & 0 & 0 & 1 \end{bmatrix} + \begin{bmatrix} X \\ Y \\ Z \\ 1 \end{bmatrix}$$

$$R_x(\theta) = \begin{bmatrix} 1 & 0 & 0 \\ 0 & cos(\theta) & -sin(\theta) \\ 0 & sin(\theta) & cos(\theta) \end{bmatrix}$$

$$R_y(\theta) = \begin{bmatrix} cos(\theta) & 0 & sin(\theta) \\ 0 & 1 & 0 \\ -sin(\theta) & 0 & cos(\theta) \end{bmatrix}$$

$$R_z(\theta) = \begin{bmatrix} cos(\theta) & 0 & sin(\theta) \\ 0 & 1 & 0 \\ -sin(\theta) & 0 & cos(\theta) \end{bmatrix}$$

Equation 1: Left the translation vector. The translation (Tx, Ty, and Tz) values are added to the old coordinates for the x-, y-, and z-axis to calculate the new coordinates (X', Y', Z'). Right the rotation vector, which then need to be multiplied by the old coordinates. The rotation matrices (Rx, Ry, and Rz) are calculated by the cosines and sines of the angels [39].

from the center of the phantom. Since measurements beyond this limit distances were measured during this study, The following assumption was made. When the distances of points outside and inside the model range are known, the radiation at the point within the model can be calculated using the model. Suppose there are no objects between these two points. In that case, the assumption is made that the radiation at the point outside the model can be calculated using the inverse square law [40]. This is shown in equation 2, based on the distances from the two different

points to the radiation source and the amount of radiation remaining at the position within the model.

$$\frac{I1}{I2} \propto \left(\frac{d2}{d1}\right)^2$$

Equation 2: Shows the inverse square law. The intention of the first point divided by the second is proportional to the square of the second's distance divided by the first's distance. It shows that if the distance from the source doubles, the intensity becomes four times smaller [40].

Another assumption is that the limbs of the cardiologist, where the radiation is measured, are considered as discrete points within the radiation model. The amount of radiation at a measured point will therefore not be influenced by objects that have not been accounted for in the radiation model. This differs in two different reasons from the reality. First, the dosimetry will be lower than measured for certain body parts when the entire body of the cardiologist is positioned between the radiation source and this body part [41]. Second, the calculated dosimetry does not take any reduction in radiation in account due any possible reduction in radiation due to the use of protective clothing [7].

3.0. Results

During the measurements 15 recordings were made, which caused for 52 measuring points. It was not possible to successfully trace the body in three situations, resulting in a total of 49 measurements. These measurements are displayed in a table 3 till 10 in Appendix C. For these measurements the center of the radiation source is considered the origin of the coordinate system; where the x-axis is parallel to the edges of the surgeon's table with positive values extending towards the head end, the y-axis has positive values extending perpendicularly towards the surgeon's table where the cardiologist stands, and the z-axis has positive values extending towards the ceiling.

3.1. Coordinates Acquisition

The calibration measurements that were performed beforehand to determine the position of the camera relative to the cath Lab and to validate the accuracy of the software are shown in table 2. The measurements of the orientation of the Aruco markers were not included in the results, despite the software being effective.

Measurement points	Validation Measurement	Azure Kinect Measurement	Percentage Deviation
Left Shoulder	236,8	252,6	6,25 %
Right Shoulder	249,2	262,4	5,03 %
Left Wrist	230,6	238,2	3,19 %
Right Wrist	246,0	248,3	-0,93 %
Nose	226,4	240,5	-6,23 %
Lead Shield	100,5	102,5	1,95 %
Center Phantom	123,0	117,8	4,41 %

Table 2: This table shows the distance of the measurement with the Azure Kinect, the validation measurement measured with measuring tape, and the deviation in percentage for certain body parts, lead shield, and the center of the phantom. The distance is measured from the Azure Kinect in centimeters.

To better understand the coordinates in Appendix C's tables, the coordinates are shown in the Figure 26 till 30 in Appendix D for the second measurement and the first part of the third

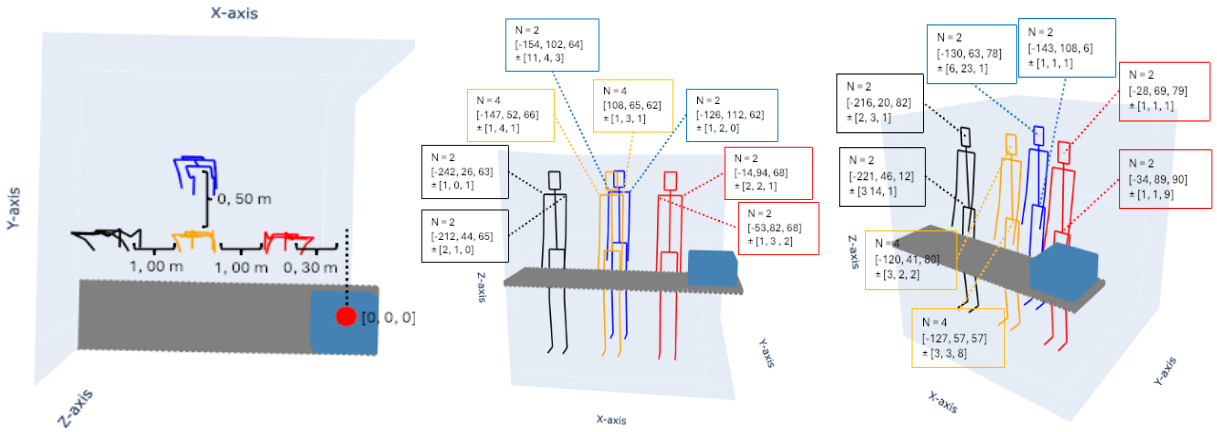

Figure 14: Shows the positions of the cardiologist in part 1 of the measurement 3, the cardiologist takes on an anatomical posture perpendicular to the surgeon's table. A: Gives the distances between the different positions of the cardiologist and the center of the phantom in meters, marked with tape prior to the measurements. B: Gives the coordinates of the different positions of the cardiologist in centimeters for the left and the right shoulder and the deviations between the multiple measurements, the center of the phantom is the origin of the coordinate system. C: The same figure as B, but with the nose and the middle of the pelvis as body parts.

measurement that has been executed. One of these visualizations of the third measurement is shown in figure 14. The deviations of the coordinates between the different measurement points are moderate, with a few outliers: the right shoulder in blue, the nose in blue and the pelvis in black. The second measurement has only a few outliers, namely 5. However, the coordinates do not entirely correspond with the expected values based on the reference points visible in figure 14A. Since the Y-coordinates for red, yellow, and black cardiologist differ from each other, even though these values should be nearly identical. These differences are smaller for the second measurement, with the observation that the y-coordinates decrease as the cardiologist moves farther away from the phantom

3.2. Static Measurement

During the first measurement, the software was tested to determine if difficult positions of the cardiologist and the lead shield could be accurately measured. Table 3 of appendix C shows the values of this measurement. In Appendix E the different situations are shown in the figures. Figure 15 displays the difference in distance between the lead shield and the cardiologist. This shows that the cardiologist can be traced even when the lead shield is in front of them. However, for measurement 5, 6, and 8 the software did not provide a value for the cardiologist's position. Measurement 5 and 6 is the cardiologist partly behind the lead shield, and measurement 8 is the cardiologist completely behind the lead shield. These measurements demonstrate that the software has difficulties with tracing the cardiologist when they are positioned at an angle relative to the camera and when there is an object in front of them. The color view and depth view of the Azure Kinect for measurement 5 is shown in Figure 16. This shows that the images are not affected by the reflections of the lead shield.

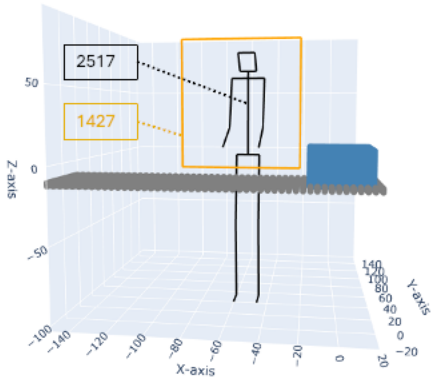

Figure 15: Shows an illustration of the measurements of the Azure Kinect, when the cardiologist is positioned behind the lead shield. The distance is in millimeters and measured from the Azure Kinect.

3.3. Dynamic Measurement

The second measurement is shown in tables 4, 5, and 6 of Appendix C. To gain a better understanding of these results the data is illustrated in Appendix F. These figures compare different situations, where according to the radiation model [29], the amount of radiation received by the cardiologist decreases when the distance from the source increases or when the lead shield is placed closer to the cardiologist. The effect of adjusting the distance of the cardiologist towards the radiation source is shown in Figure 17. This demonstrates that the radiation exposure indeed decreases as the distance increases. In Figure 18 the different positions of the lead screen are demonstrated. This shows that radiation exposure decreases when a lead shield is used. To provide

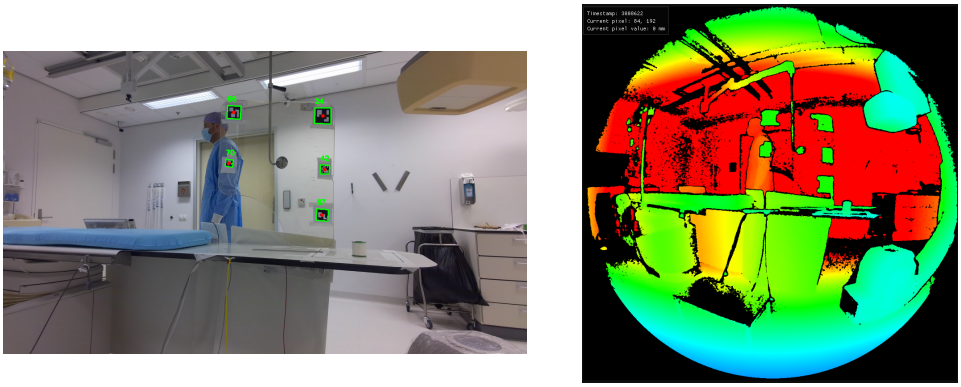

Figure 16: Shows the different views of the Azure Kinect for measurement 5. A: Shows the RGB view of the Azure Kinect with the tracking of the Aruco markers. B: Shows the depth image of the Azure Kinect.

an indication of this effect table 4 in Appendix B shows an overview. For the positions of the cardiologist closest to the phantom (100 cm), the lead shield's impact on radiation exposure to the nose is as following: compared to a situation without a lead shield, a lead shield at 36 cm from the phantom results in a 62,7% reduction in radiation exposure and at 51 cm results in a 96,4% reduction in radiation exposure. However, this decrease in value was not visible for all body parts.

Body Parts	Different Position's Cardiologist:		
	100 cm	130 cm	160 cm
	Radiation levels [mSv]		
L Wrist	2,7006	1,8759	0,9122
L Elbow	2,0373	1,9481	1,0351
L Shoulder	1,1978	1,1600	0,9949
Nose	1,0393	0,9977	0,7879
Pelvis	0,8350	0,9250	0,7739
R Shoulder	1,1013	0,8015	0,5995
R Elbow	1,4181	0,8674	0,5568
R Wrist	1,1285	0,9505	0,7432

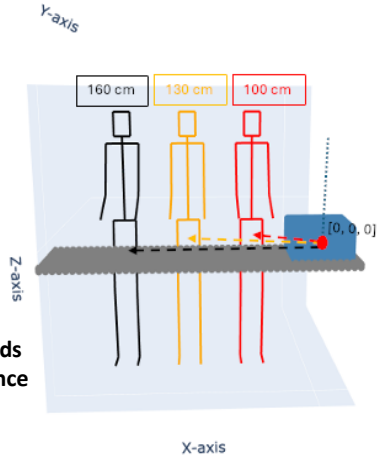

Figure 17 & Table 3: Shows the difference in radiation exposure for the cardiologists with various distances. The cardiologist has a posture with his hands raised. The amount of radiation is given in mSv in the provided table. The distance of the cardiologist is 100, 130, and 160 cm.

Body Parts	Different position's Lead Shield:		
	-	36 cm	51 cm
	Radiation levels [mSv]		
L Wrist	1,3571	0,1327	0,5170
L Elbow	1,2345	0,9724	0,6719
L Shoulder	1,0835	0,6654	0,6719
Nose	1,0148	0,6598	0,1983
Pelvis	0,9338	0,8671	0,2360
R Shoulder	0,7707	0,7713	0,4277
R Elbow	0,8457	0,8806	0,7726
R Wrist	0,8587	0,9033	0,8875

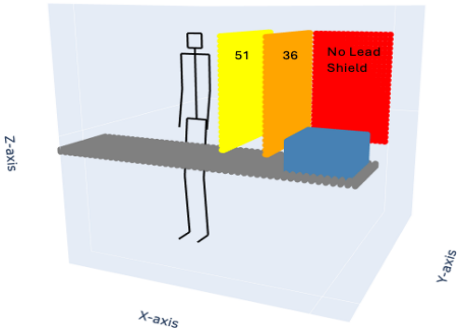

Figure 18 & Table 4: Shows the difference in radiation exposure with different positions of the lead shield. The cardiologist is positioned 130 cm away from the radiation source with an anatomical posture. the amount of radiation is given in mSv in the provided table. The lead shield is placed at 36 and 51 cm away from the center of the phantom and not positioned between the phantom and cardiologist.

3.4. Visualization Measurement

The results of the third measurement that has been executed are shown in the tables 7 till 10 in Appendix C. These graphs are illustrated for a better understanding of the two measurements of part 1 (table 7 and 8) are illustrated in Appendix G, and the two measurement of part 2 (table 9 and 10) are illustrated in Appendix H. The first measurement of part one is shown in figure 19. The position of the cardiologist closest to the radiation source is omitted since the radiation model did not provide logical values. This position is shown in figure 20 in the depth and color view from the Azure Kinect. The depth view demonstrates that the cardiologist is positioned to the right of the radiation source. Because the radiation model [29] does not deliver accurate data points for this position, the position is omitted. The measurements show that the Azure Kinect can distinguish positions and illustrate that a greater distance reduces the radiation exposure. The measurements of part two is shown in Appendix H. Since the radiation model [29] has a limited selection of lead shield positions, only two positions can be used. Therefore, the model was only used for the first two positions of the first measurement of part two and the last two positions of the second measurement of part two to determine the radiation exposure with the lead shield positioned at a distance of 36 and 51 cm from the radiation source. Therefore, the last measurement of the first set and the first measurement of the second set do not have calculated radiation exposure. The difference between the two-measurement is that in the first measurement the lead shield is positioned parallel to the surgeon's table resulting in a completely visible Aruco marker. In the second measurement the lead shield is positioned under an angle, so that the Aruco marker is not completely visible. In both measurements the location of the lead shield can be measured relative to the phantom and the cardiologist in order to make a statement about the radiation exposure. In figure 21, the second part of the measurement is shown with the lead shield positioned in the two closest positions to the phantom. The coordinates in the middle of the lead shield are derived from the measured coordinates of the Aruco markers and the distance of them towards the center point. The coordinates of the Aruco markers on the lead shield may deviate from the expected value in some cases. Especially the Y-coordinates deviate from the expected values, but X- and Z-coordinates to a lesser extent. The software makes errors in tracing the coordinates when the Aruco marker is positioned under an

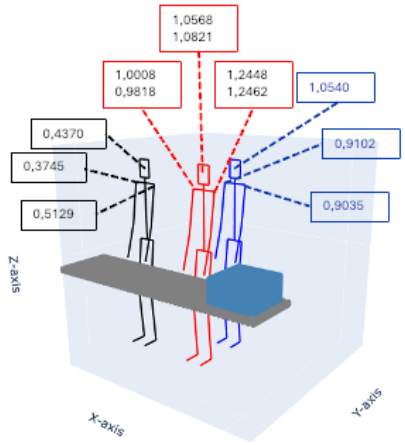

Figure 19: Shows the received radiation for position 1, 2, and 4 for both parts of the first measurement. The radiation exposure is visible for the nose, left shoulder, and right shoulder in mSv.

angle, and with marker 66 and 70 when the lead shield is positioned further away from the phantom. Due to the positioning of the Azure Kinect, these markers are also under an angle during the first part of the measurement when the lead shield is positioned farther from the phantom.

Figure 10: Shows the color and depth view of the Azure Kinect of the cardiologist standing at the position closest to the phantom of measurement 1 of part 1 of the visualization measurement. The views show that the position of the cardiologist is not left of the radiation

During the visualization measurements, the software had no difficulty tracking the cardiologist frame by frame. In addition, the software could also trace the Aruco markers frame by frame virtually without any flaws. However, during the tracking of the Aruco markers, there were instances where not all markers could be recognized. This could occur, when the Aruco markers moved in the view of the recording causing a blurry image, this could result in a missed tracked frame. Since the Azure Kinect records at a frame rate 15 frames per second, there were enough frames per second where the markers were successfully traced. Due to the length of the recordings for the measurements, the body tracking software encountered issues with saving the data, as the matrix storing the coordinates was large. This problem was solved by dividing the recordings into shorter segments, which ensures that the matrices of data are shorter and easier to store.

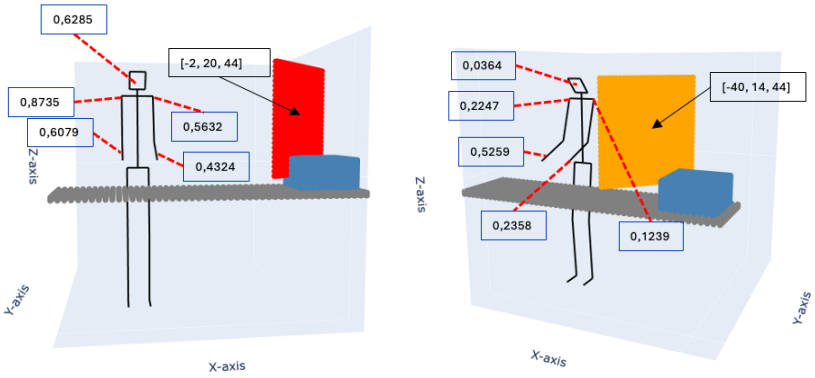

Figure 21: Shows the difference in distances of the middle of the lead shield in centimeters for [x, y, z] axes in centimeters and the radiation exposure in mSv. A: The lead shield positioned at 2 centimeters from the phantom. B: The lead shield positioned at 40 centimeters from the phantom.

4.0. Discussion

Radiation safety in the catheterization Laboratory is of great importance as it has a significant impact on the health of the medical staff. This research aims to improve the awareness of radiation exposure in real-time during a procedure, thereby reducing the amount of radiations exposure of the medical staff in their daily routine. Since the medical staff often do not realize that their positioning and the placement of themselves or the lead shield are not optimal, it can result in higher radiation exposure [19]. A method is developed to track the location of the medical staff and the lead shield in the cath lab and apply these locations to a radiation model to make a statement about the radiation exposure for the specific location. The locations are measured with the help of the 3D camera the Azure Kinect DK and the radiation exposure statement is made with a radiation model [29].

4.1. 3-Dimensional tracking

The developers of the Azure Kinect DK stated that a certain accuracy, and the standard & random error margin provided by the recordings are done in the ideal conditions [35]. However, the measurements of this study were not conducted under these ideal conditions of the Azure Kinect. Besides the standard procedure where we eventually want to use the software is far from this ideal condition. As the calibration measurements showed, the accuracy deviation fluctuated between 0 and 6.25% in absolute terms from the validation measurements taken with a measuring tape. The fact that this deviation is higher than the developers claim could be due to non-ideal conditions, or small movements of the medical staff, interference with the InfraRed signal, and inherent measurement inaccuracies. Hence, the highest deviations derive from for the body parts of the medical staff. The fluctuation in accuracy deviation could potentially lead to a misinterpretation assuming the cardiologist is behind the lead shield, when in reality this is not the case.

During the measurements, the following findings were observed regarding the tracking of coordinates: diverging coordinates for the y-axis, deviations in the coordinates, and challenges in tracking during difficult situations.

In the second and third measurements the coordinates for the y-axis do not remain constant, even though they should. As the distance between the cardiologist and the phantom increases, the value for the y-coordinates decreases. This is a result of the incorrect calculation of the value used for the rotation of the coordinate system, where the zero point is located at the center of the phantom. This can be caused by incorrectly measuring the angle of the Azure Kinect's table relative to the surgeon's table. A slight change in the position of the Azure Kinect's table during the measurements causes the angle to change, or a systematic underestimation leading to an invalid outcome.

During the measurement of the coordinates, there is a small difference in coordinates when the cardiologist stands in the same position. Since the position where the cardiologist should stand is marked with tape on the ground, the upper body can make small movements, causing the coordinates to slightly vary.

The tracking of the body of the cardiologist is reasonable durable in difficult situations. Measurement one showed that the software can correctly track the cardiologist without being affected by reflection of the lead shield. Besides, the software can track the medical staff in surgical clothing. Since the lead shield and clothing's are not occluding the measurement of the cardiologist, it results in a more applicable software during procedures. However, the software has difficulty with tracing when the cardiologist or Aruco marker are positioned under an angle in the direction to the Azure Kinect. These two are tracked by two different methods, so the difficulty with tracing is not related. The difficulty of tracking the cardiologist under an angle, shown in measurement one, will not be an issue during a standard procedure since the cardiologist is facing most of the time toward de surgeon's table. Meanwhile, tracking the markers under an angle, shown in the second part of measurement two, could indeed lead to problems if executed as just described this way during a procedure. This will be addressed in the limitations of this study. Additionally, the depth values for the Aruco markers sometimes do not have a value interpreting the color pixels in the depth image, read as 'No depth value'. This occurs because a black pixel is found at the exact location, which may be due to issues with reflecting or capturing the InfraRed radiation of the depth image, such as being too far away, lack of reflection, or moving too quickly for the frame rate.

The recordings of the Azure Kinect can be influenced by factors in the cath lab such as: bright light, darkness, and reflection [45]. These factors result in recordings not meeting the ideal conditions of the Azure Kinect. Some studies that used a similar device in a surgeon's room indicated that the measurements were quite accurate, within a margin of error of up to 5 cm [43; 44]. This is lower than the error margin in the calibration measurements of this study. The higher error margin in this study can be caused by small movements of the medical staff resulting in a difference between the measurement and validation's measurement, or a closer positioning of the camera in the other

studies resulting in a lower error due the smaller proportions.

During the calibration measurements the Azure Kinect recorded over an extended period, fluctuations in the measured distances were observed, which should have been reasonably constant across different frames. These variations had an absolute value of 40 millimeters. These fluctuations in distance measurements result in inaccuracies when calculating the coordinates along the three axes. These differences in the measured distances are caused by interference with the InfraRed signal.

The measurements from the Azure Kinect will contain, beside these fluctuations, other inaccuracies. The deviation in accuracy might be relatively lower than what the calibration measurements showed, as those measurements included small movements and measurement errors that normally would not occur. Nevertheless, the error sensitivity of the Azure Kinect is relatively low for determining the position of medical staff. At a distance of 2.5 meters from the Azure Kinect, the deviation of accuracy, including maximum inaccuracy and fluctuation, would be 15 to 20 centimeters. This is comparable to the span from tip of the little finger to the thumb of an adult male, which is relatively small. Besides, this software is designed to increase awareness of radiation exposure at specific positions of the cardiologist and the lead shield. The cardiologist always can visually verify if his complete body is actually behind the lead shield. A statement can be made that the tracking of the position of the medical staff and the lead shield is accurate in order to calculate the radiation exposure.

4.2. Measuring the scatter radiation

By applying the measured coordinates of the cardiologist's body parts in a radiation model [29], it was possible to make a statement about the radiation exposure. The dynamical and visualization measurements revealed the following aspects about radiation exposure. First, the level of radiation exposure decreases as the distance from the cardiologist to the radiation source increases. Second, the lead shield reduces radiation exposure, and when it is closer to the cardiologist, it results in a greater reduction in radiation exposure. From the literature study, it can be confirmed that the distance of the cardiologist to the scatter radiation source [12] and the distance of the lead shield to the cardiologist [20] influence the radiation exposure of the cardiologist. From measurement two, it emerged that for certain coordinates, the attenuation percentage for the lead shield at positions 51 cm and for 36 cm was almost the same as the attenuation percentages by the radiation model [29], comparable to the situation where no lead shield was used. The reason that the percentage is not exactly the same is because different coordinates for the cardiologist were used. However, it is not evident for all body parts that the distance of the lead shield relative to the cardiologist affects the amount of radiation exposure. This could be explained by the fact that certain body parts are not completely behind the lead shield. Furthermore, it can also be seen in the radiation model [29] that the scattered radiation is present at the edge behind the lead shield. Resulting in some body parts that have a higher radiation exposure than expected.

A statement can be made that the software can measure the scatter radiation in the cath lab. However, the software is not yet applicable in a procedure to measure the actual exposure to radiation due to certain limitations and assumptions being made. A good consideration to keep in mind is that a first version of the model was used in this study, and improvements are needed to apply the software during a procedure to measure the radiation exposure for the medical staff.

4.3. Progress & Perspective

The cath lab is a complex environment, and for successful operating the Azure Kinect, certain conditions need to be established to be applicable in the cath lab. The Azure Kinect must be usable during procedures and not be adversely affected by darkness, bright lights, occlusion, or reflections

[45]. Additionally, it must be capable of creating a 3D representation, utilize limited computational capacity while maintaining adequate accuracy, easy to use, low in cost, and requires specialized software development.

During procedures the Azure Kinect might be affected by several factors [45]. Firstly, during surgery the lights are dimmed, resulting in a significantly darker cath lab environment. Since, the Azure Kinect is tracking the medical staff with the depth view using InfraRed light, this will not result in complications. Conversely, the Aruco markers are traced using the color view, which could potentially lead to issues. Secondly, bright light is used to illuminate the incision site for improved vision for the cardiologist. This might affect the reflection of the InfraRed radiation from the Azure Kinect for distance calculation [27]. During this experiment it did not interfere with the InfraRed radiation of the depth view. Thirdly, occlusion during an actual procedure might lead to potential errors [28]. In this study no occlusion occurred during the measurements, partly because these measurements were framed for a specific situation in the cath lab. When a procedure takes place in a general operating room, there is a significantly higher risk of occlusion. This is due to the presence of more medical staff, additional equipment, the C-arm in an extracted position, and a patient laying on the table. A simple solution for this problem is repositioning the Azure Kinect or the usage of a second Azure Kinect, positioned under a different angle to add another view to record the situation. The developers of Microsoft offer a comprehensive suite of software that enables the creation of 3D representations through the collaboration of multiple Azure Kinects DK. Lastly, reflection in the cath lab might interfere with the InfraRed of the depth view [45]. However, this did not affect the measurements of this study. All the possible objects that can reflect InfraRed were present during the measurement, like medical instruments, surface of the lead shield, and components of the C-arm.

During this study, the settings for the Azure Kinect were chosen based on the compromise between limited computational capacity and maintaining sufficient accuracy. Such as choosing a fps of 15 for the recording which was sufficient to get smooth images. The software had difficulty with tracing the cardiologist in recordings longer than 80 seconds during the measurements. The problem was that the matrix containing the data of all coordinates for all body parts became too large for the environment used during the writing of the code. The solution was to split these recordings in two parts. However, the solution could be simple when switching to online processing of the body tracking. Since not all data needs to be stored but the exposure to radiation can be calculated directly. This results in significantly less data that needs to be stored. The outcome will be a good compromise with a low computational capacity but sufficient accuracy for the tracking.

This software is a significant improvement over the previously used equipment for detecting radiation exposure, such as the dose aware badges from Phillips and the dosimetry badges. These devices are limited in the extent to which they can deliver information, provide unusable information if not use correctly, contain limited information, and naturally also exhibit fluctuations in accuracy. These limitations would occur much less frequently when using this software. The fluctuation in the accuracy is higher than expected compared to the deviation in accuracy observed in other research and what the Microsoft developers claimed. Despite these fluctuations being relatively small and will not result in any issues with tracking medical staff, it is essential to put this into perspective.

Ultimately, this software is being developed into a product to measure real-time exposure to scatter radiation for medical staff during a procedure and provide feedback to the medical staff. Although this product is primarily intended to raise awareness of unnecessary radiation exposure, it is necessary to account for the error sensitivity of the Azure Kinect. Otherwise, medical staff might receive incorrect feedback indicating they are improperly positioned while they are actually not. If this occurs repeatedly, it could lead to issues in the credibility of the use of this software during procedures. A potential solution for these errors in feedback could be a filter that accounts for the error sensitivity when alerting the medical staff. For example, a filter of 15 to 20 centimeters could

be used as a margin to warn the medical staff, indicating whether their position within this margin is correctly covered by the lead shield or not. Using the fluctuation in accuracy as a margin for the filter may be excessive, as the over- or underestimation of the positions is most likely to be smaller.

The Azure Kinect is able to recreate a 3D representation of the cath lab and would also be able to represent a generic surgery room. Additionally, the recording could be represented in 3D frame by frame because the software had barely any difficulty with tracking. The software of the body tracking had no issues during the measurements in this study in tracking the cardiologist frame by frame. Meanwhile, during some frames the software for tracking the Aruco markers was not able to find the marker due to movement. This will not result in an issue since the lead shield is measured exclusively in a stationary situation.

4.4. Applicability in a Procedure

The Azure Kinect DK is low cost and easy to use device to increase the awareness of medical staff about their radiation exposure in operating rooms in general. Since software can be easily designed within the device, it can prevent problems that may occur during the recording. For actual implementation, the software must directly track the bodies of the medical staff and calculate their radiation exposure, which is possible with the online method. Since this study is a trial, it was decided to do this offline. It is possible to directly calculate the radiation exposure of the medical staff and provide it in a form of feedback.

Eventually, the software will be used to provide real-time feedback to medical staff during procedures to adjust their position from the lead shield to prevent and educate the medical staff in unnecessary radiation exposure. However, there is still a significant step to be taken from these trial measurements to actual measurements during a procedure. During an actual procedure significantly, more occlusions can occur due to the presence of additional objects, increased medical staff, the patient and covered equipment. This could result in issues with the Azure Kinect's view of the cardiologist and lead shield. Therefore, the optimal positioning of the Azure Kinect must be considered. Since there is a lot of staff, the Azure Kinect might be knocked of the table, and a patient lying on the surgeon's table could block the camera's view. During a procedure, the cardiologist must always have a clear view on the monitor, which means that the monitor is always oriented towards the cardiologist. Therefore, it is easier to mount the Azure Kinect to the top edge of the monitor so it cannot be knocked over and can provide an unobstructed view on the cardiologist and the rest of the medical staff. However, a challenge arises from the camera's movement, caused by the movement of the monitor. This complicates the orientation of both the lead shield and the cardiologist relative to the scattered radiation source. If there is a fixed point in the operating room that the Azure Kinect can track, using for example an Aruco marker, the distance and orientation of the camera to that point can be calculated. Once the constant and relative distances in the three axes from this point to the scattered radiation source are known, it becomes possible to calculate the distance from the Azure Kinect to the scattered radiation at any time, regardless of the movement of the monitor. A second Azure Kinect can always be added in another corner pointing at the same direction reducing the change of occlusion, tracking the movement of the Azure Kinect added to the monitor, and adding a validation measurement.

Additionally, consideration must be given to the method of delivering real-time feedback for adjusting the cardiologist's behavior. Thus, presenting the feedback on the lead shield is considered the preferred option [29]. One potential solution could be the traffic light system that illuminates the entire lead shield, where red indicates a misplaced shield, orange signifies correctly positioned but too far from the medical staff, and green denotes correctly positioned at the appropriate distance. Using this system, the medical staff can be easily alerted without disrupting the procedure when they

need to adjust the position of the lead shield, either because they are not protected at all or because there is room for improvement.

4.5. Limitations of the Model

The model that is used in this study had several limitations and required some assumptions, which will cause trouble in the application during a procedure.

Firstly, the radiation model [29] that is used is limited. Since the radiation mode has only a select number of positions for the lead shield and a limited range of position for the cardiologist. However, the model is based on the findings that the distance from the scatter radiation source to the surgeon is 103 cm and the assistant at 158 cm [33]. Despite, some measurements were outside the range of the model. The limited position for the cardiologist is resolved by assuming that when there is no object that can influence the scatter radiation, this results in the radiation exposure outside the range of the model can be calculated with the inverse square law. Another assumption that has been made is that the body parts are considered discrete points and the exposure to radiation is not influenced by the other body parts or protective clothing.

Secondly, the model consists of actual measurements of scattered radiation. Between those data points the amount of radiation is calculated with a quadratic decay. The model is dependent on those data points where the scattered radiation is measured; the model has limited measuring points, especially on the surgeon's table itself and at the level of the phantom and on the right side of it. An example of this is the radiation values for the body parts during part 1 of the visualization measurements for the position closest to the phantom. This value was therefore lower than the value measured for the position further to the left, which would not be logical. Also, during the dynamical measurements, it occasionally occurred that the radiation exposure for body parts was lower when the position was closer to the scatter radiation source. This is because the position, where a lower value is calculated but a higher value would be expected, falls between two measuring point and is calculated by a quadratic decay. At the same time the higher value is close to a measuring point. This occurs because the values between two measuring points drop as they are calculated by the decay between those two points and the measuring points result to be higher than expected. This can result in a lower value than expected. However, the deviation of the values in question are so low that it would have little to no effect on the outcome.

4.6. Limitations of the Measurements

During the measurements some limitations emerged, resulting in possible errors that occur when measuring the coordinates of the Aruco markers. The software is programmed to use the coordinates of the left upper corner of the marker to calculate the distance to the marker. Since the Azure Kinect is positioned under an angle with the lead shield, there is a possibility the distance is overestimated because the tracer is placed further to the left. This problem could arise in reading the depth in the depth view. Firstly, the colour view, in which the markers are tracked, is overlaid on the depth view to calculate the distance. Since the resolution of the colour view is higher, the pixels of the different views will not correlate on a one-to-one basis. Secondly, the lens of the depth view is round, resulting in a relatively more distorted view when the traced object is placed further to the edges of the view. This resulting in a higher possibility of an error in estimating the distance of the depth view with the pixels of the colour view. Due to the positioning of the camera, the tracking of the top left corner, and the issues present in the depth view, the coordinates for the Aruco marker can read an incorrect depth value, which results in incorrect coordinates when transformed to a new coordinate system. In Figure 12, the upper left corners of markers 66 and 70 are in the combined view on the edge of the Aruco markers and can easily overestimated. In the second part of the

visualization measurements especially for Aruco marker 66 and 70 these errors arise. The error was mainly in the y-coordinates, as these were primarily calculated from the depth values. In addition, when the lead shield is positioned under an angle there is more often an overestimation. A possible solution could be to choose a different corner or to calculate the center of the Aruco marker and use that as the 2D pixel coordinate when converting to the depth view. During procedures the lead shield will be covered by a sleeve, resulting in an obstructed view of the Aruco markers. This will cause issues in tracking the lead shield, since the software will not be able to track the Aruco markers.

4.7. Future Research

Future research directions should prioritize to overcome the current study limitations and improve the assumptions, with the goal of enhancing the system to increase the applicability in real-time feedback system during procedures. The radiation model is limited and needs to be optimized, by adding additional measuring points in the entire surgery room, especially on the surgeon's table and right of the phantom. Also, the model should be able to calculate radiation exposure for the lead shield in virtually all possible positions. The decision here should be made to have the model calculate the influence of the lead shield on the environment of the surgeon's room, rather than conducting measurements with a lead shield and only applying these positions in the model. Subsequently, the body parts should not be considered as a discrete point. Since the radiation exposure for the body parts are influenced by protective clothing and other body parts in front of the scatter radiation source. This Results in an estimation of the radiation exposure and not the actual exposure.

In addition, it would be beneficial to resolve the issues of the increased change of occlusion during a procedure. For instance, to place the Azure Kinect on the top edge of the monitor in order to reduce the amount of possible occlusion and prevent unwanted movements of the camera. This method is in need of a constant fixation point to calibrate the distance of the Azure Kinect towards the scatter radiation source. An option that aligns with this approach is the use of a second Azure Kinect that has a different view angle on the medical staff and surgeon's table. This Provides an increased solution for possible occlusion that may occur during a procedure, validating the position of the first camera, and reducing the possible inaccuracies or non-detections.

Another aspect that needs further examination is the tracking of the lead shield. Since a cover is used over the lead shield during surgery, visibility on the Aruco markers is limited. Therefore, it is important to be able to apply AI object detection software to the lead shield to facilitate the tracking during a procedure.

5.0. Conclusion

Radiation exposure can lead to significant health risks for the medical staff during procedures where radiation is used. In this study the Azure Kinect DK is used to track the coordinates of the medical staff during a test environment. By combining an already existing radiation model, the amount of radiation exposure can be calculated. This enables to measure the received exposure of scatter radiation for the medical staff based on a simple recording of the operation room. By creating awareness of the unnecessary radiation exposure, the behavior of the medical staff can be adjusted to reduce radiation exposure. This system can measure changes of exposure through positions of the medical staff or the lead shield and provide feedback on how the changes in movement affect exposure to scatter radiation.

Critical areas for future research include reducing the step between the test environment and the actual usage during a procedure. For instance, by improving the model to enable its application across a wider range of situations. Moreover, reducing possible occlusion with strategic

placement of the Azure Kinect or adding a second Azure Kinect. Lastly, the usage AI object detection needs to be further investigated since the Aruco marker will not be completely visible due to a cover during the procedure.

Although this is a preliminary step towards proactive radiation proception, by realization these objectives, it becomes feasible to integrate a real-time feedback system into the operating room using the Azure Kinect DK, alerting medical staff to adjust their behavior to minimize radiation exposure during procedures.

References

[1.] Partridge J. (2005) Radiation in the cardiac catheter laboratory. Heart. ;91(12):1615-20. doi: 10.1136/hrt.2005.061150. Erratum in: Heart. 2009 Apr;95(7):594. PMID: 16287755; PMCID: PMC1769234.

[2.] de Ceuninck M., Muyldermans P., van de Walle S., Bergez B., Haspeslagh R., Stammen F., Dujardin K. (2019) A quality project for radiation reduction in the cath lab. Acta Cardiol. (1):38-44. doi: 10.1080/00015385.2018.1439705. Epub 2018 Feb 19. PMID: 29457955.

[3.] Jafri, M. A., Farrukh, S., Zafar, R., & Ilyas, N. (2022). A survey on radiation protection awareness at various hospitals in Karachi, Pakistan. Heliyon, 8(11), e11236. https://doi.org/10.1016/j.heliyon.2022.e11236

[4.] Murat, D., Wilken-Tergau, C., Gottwald, U., Nemitz, O., Uher, T., & Schulz, E. (2021). Effects of Real-Time Dosimetry on staff radiation exposure in the cardiac Catheterization Laboratory. Journal of Invasive Cardiology, 33(5). https://europepmc.org/article/MED/33833127

[5.] Wu, G., Mainprize, J. G., Boone, J. M., & Yaffe, M. J. (2009). Evaluation of scatter effects on image quality for breast tomosynthesis. Medical Physics, 36(10), 4425–4432. https://doi.org/10.1118/1.3215926

[6.] Biso, S., & Vidovich, M. I. (2020). Radiation protection in the cardiac Catheterization Laboratory. Journal of Thoracic Disease, 12(4), 1648–1655. https://doi.org/10.21037/jtd.2019.12.86

[7.] Gutiérrez-Barrios, A., Cañadas, D., Noval-Morillas, I., Gheorghe, L., Zayas-Rueda, R., & Calle-Pérez, G. (2022). Radiation protection for the interventional cardiologist: Practical approach and Innovations. World Journal of Cardiology, 14(1), 1–12. https://doi.org/10.4330/wjc.v14.i1.1

[8.] Smilowitz NR, Balter S, Weisz G. Occupational hazards of interventional cardiology. Cardiovasc Revasc Med 2013;14:223-8.

[9.] Buys, D., & Brown, S. (2021). Radiation exposure protection: Small things matter. Cardiovascular journal of South Africa : official journal for Southern Africa Cardiac Society [and] South African Society of Cardiac Practitioners, 32(5), 5–6. https://doi.org/10.5830/cvja-2021-052

[10.] Karatasakis A, Danek BA, Brilakis E. Radiation Protection. 2018:199-216.3

[11.] Radiation protection of medical staff in orthopaedic surgery. (z.d.). IAEA. https://www.iaea.org/resources/rpop/health-professionals/other-specialities-and-imaging-modalities/orthopedic-surgery/staff

[12.] Efstathopoulos, E., Pantos, I., Andreou, M., Gkatzis, A., Carinou, E., Koukorava, C., Kelekis, N., & Brountzos, E. (2011). Occupational radiation doses to the extremities and the eyes in interventional radiology and cardiology procedures. British Journal of Radiology, 84(997), 70–77. https://doi.org/10.1259/bjr/83222759

[13.] Roguin, A., Goldstein, J., Bar, O., & Goldstein, J. A. (2013). Brain and neck tumors among physicians performing interventional procedures. American Journal of Cardiology, 111(9), 1368–1372. https://doi.org/10.1016/j.amjcard.2012.12.060

[14.] Faroux, L., Blanpain, T., Nazeyrollas, P., Tassan-Mangina, S., Heroguelle, V., Tourneux, C., Baudin, F., & Metz, D. (2018). Reduction in exposure of interventional cardiologists to ionising radiation over a 10-year period. International Journal of Cardiology, 259, 57–59. https://doi.org/10.1016/j.ijcard.2018.02.026

[15.] De Brún, A., Alcaraz-Mor, R., Bourrelly, M., Dalivoust, G., Gazazian, G., Boufercha, R., Lehucher-Michel, M., & Sari-Minodier, I. (2018). Radiation protection for surgeons and anesthetists: Practices and knowledge before and after training. Journal of Radiological Protection, 38(1), 175–188. https://doi.org/10.1088/1361-6498/aa9dbd

[16.] Boice, J. D., Dauer, L. T., Kase, K. R., Mettler, F. A., & Vetter, R. J. (2020). Evolution of radiation protection for medical workers. British Journal of Radiology, 93(1112), 20200282. https://doi.org/10.1259/bjr.20200282

[17.] Behr-Meenen, C., Von Boetticher, H., Kersten, J. F., & Nienhaus, A. (2021). Radiation protection in Interventional Radiology/Cardiology—Is State-of-the-Art equipment used? International Journal of Environmental Research and Public Health, 18(24), 13131. https://doi.org/10.3390/ijerph182413131

[18.] Kamusella, P., Scheer, F., Lüdtke, C. W., Wiggermann, P., Wissgott, C., & Andresen, R. (2017). Interventional angiography: radiation protection for the examiner by using lead-free gloves. Journal of Clinical and Diagnostic Research. https://doi.org/10.7860/jcdr/2017/25226.10305

[19.] Sommer, P., Sciacca, V., Anselmino, M., Tilz, R. R., Bourier, F., Lehrmann, H., & Bulava, A. (2023). Practical guidance to reduce radiation exposure in electrophysiology applying ultra low-dose protocols: A European Heart Rhythm Association Review. Europace, 25(7). https://doi.org/10.1093/europace/euad191

[20.] Jia, Q., Chen, Z., Jiang, X., Zhao, Z., Huang, M., Li, J., Zhuang, J., Liu, X., Hu, T., & Liang, W. (2017). Operator radiation and the Efficacy of Ceiling-Suspended lead

screen shielding during coronary angiography: An Anthropomorphic phantom Study using Real-Time Dosimeters. Scientific Reports, 7(1). https://doi.org/10.1038/srep42077

[21.] Baashar, Y., Alkawsi, G., Ahmad, W. N. W., Alomari, M. A., Alhussian, H., & Tiong, S. K. (2023). Towards Wearable Augmented Reality in Healthcare: A Comparative survey and analysis of Head-Mounted Displays. International Journal of Environmental Research and Public Health, 20(5), 3940. https://doi.org/10.3390/ijerph20053940

[22.] Belagiannis, V., Wang, X., Shitrit, H. B., Hashimoto, K., Stauder, R., Aoki, Y., Kranzfelder, M., Schneider, A., Fua, P., Ilic, S., Feussner, H., & Navab, N. (2016). Parsing human skeletons in an operating room. Journal of Machine Vision and Applications, 27(7), 1035–1046. https://doi.org/10.1007/s00138-016-0792-4

[23.] Beerend, G. A. (2022). 3D human pose estimation in multi-view operating room videos using differentiable camera projections. Computer Methods in Biomechanics and Biomedical Engineering: Imaging & Visualization, 11(4), 1197–1205. https://doi.org/10.1080/21681163.2022.2155580

[24.] Hansen, L., Siebert, M., Diesel, J., & Heinrich, M. P. (2019). Fusing information from multiple 2D depth cameras for 3D human pose estimation in the operating room. International Journal of Computer Assisted Radiology and Surgery, 14(11), 1871–1879. https://doi.org/10.1007/s11548-019-02044-7

[25.] Pan, F., Liu, J., Cen, Y., Chen, Y., Cai, R., Zhao, Z., Liao, W., & Wang, J. (2022). Accuracy of RGB-D camera-based and stereophotogrammetric facial scanners: A comparative study. Journal of Dentistry, 127, 104302. https://doi.org/10.1016/j.jdent.2022.104302

[26.] Kadkhodamohammadi, A., Gangi, A., De Mathelin, M., & Padoy, N. (2017). Articulated clinician detection using 3D pictorial structures on RGB-D data. Medical Image Analysis, 35, 215–224. https://doi.org/10.1016/j.media.2016.07.001

[27.] Rodrigues, V. F., Antunes, R. S., Seewald, L. A., Bazo, R., Reis, E. S. D., Santos, U. J. D., Da Rosa Righi, R., Da S, L. G., Da Costa, C. A., Bertollo, F. L., Maier, A., Eskofier, B. M., Horz, T., Pfister, M., & Fahrig, R. (2022). A multi-sensor architecture combining human pose estimation and real-time location systems for workflow monitoring on hybrid operating suites. Future Generation Computer Systems, 135, 283–298. https://doi.org/10.1016/j.future.2022.05.006

[28.] Strickland, M., Tremaine, J., Brigley, G., & Law, C. (2013). Using a depth-sensing infrared camera system to access and manipulate medical imaging from

within the sterile operating field. Canadian Journal of Surgery, 56(3), E1–E6. https://doi.org/10.1503/cjs.035311

[29.] Van Deudekom, T., Van den Dobbelsteen, J. J., vijfvinkel, T. S., & Hendriks, B. H. W. (2023, 25 mei). Reducing occupational radiation exposure in cardiac catheterisation laboratories: Dose rate predictions and feedback strategies. https://repository.tudelft.nl/islandora/object/uuid:f8ccae4b-17af-4f30-bf48-e26cb2d4f553.

[30.] Birkfellner, W., Watzinger, F., Wanschitz, F., Ewers, R., & Bergmann, H. (1998). Calibration of tracking systems in a surgical environment. IEEE Transactions on Medical Imaging, 17(5), 737–742. https://doi.org/10.1109/42.736028

[31.] Azure Kinect DK – AI-modellen ontwikkelen | Microsoft Azure. (z.d.). https://azure.microsoft.com/nl-nl/products/kinect-dk

[32.] Janisch, J., Mitoyen, C., Perinot, E., Spezie, G., Fusani, L., & Quigley, C. (2021). Video recording and analysis of avian movements and behavior: Insights from courtship case studies. Integrative and Comparative Biology, 61(4), 1378–1393. https://doi.org/10.1093/icb/icab095

[33.] T. Vijfvinkel, R. Butler, T. Ringers, J. Constandse, V. Verhoeven, B. Hendriks, J. v. d. Dobbelsteen and M. v. d. Elst, “Procedure-specific exposure to scattered radiation during cardiac catheterizations: The effects of distance, time and shielding.,” 2023.

[34.] microsoft. (z.d.). GitHub - microsoft/Azure-Kinect-Sensor-SDK: A cross-platform (Linux and Windows) user mode SDK to read data from your Azure Kinect device. GitHub. https://github.com/microsoft/Azure-Kinect-Sensor-SDK

[35.] OpenCV: Detection of ArUco Markers. (z.d.). https://docs.opencv.org/4.x/d5/dae/tutorial_aruco_detection.html

[36.] Guo, K., Ye, H., Gu, J., & Chen, H. (2021). A Novel Method for Intrinsic and Extrinsic Parameters Estimation by Solving Perspective-Three-Point Problem with Known Camera Position. Applied Sciences, 11(13), 6014. https://doi.org/10.3390/app11136014

[37.] microsoft. (z.d.-b). GitHub - microsoft/Azure-Kinect-Sensor-SDK: A cross platform (Linux and Windows) user mode SDK to read data from your Azure Kinect device. GitHub. https://github.com/microsoft/Azure-Kinect-Sensor-SDK

[38.] Etiennedub. (z.d.-a). GitHub - etiennedub/pyk4a: Python 3 wrapper for Azure-Kinect-Sensor-SDK. GitHub. https://github.com/etiennedub/pyk4a/tree/master

[39.] Wang, L., & Song, C. (2016). Geometry optimization made simple with translation and rotation coordinates. *Journal of Chemical Physics Online/□the □Journal of Chemical Physics/Journal of Chemical Physics*, *144*(21). https://doi.org/10.1063/1.4952956

[40.] Brownson, J. R. (2014). Laws of light. In *Elsevier eBooks* (pp. 41–66). https://doi.org/10.1016/b978-0-12-397021-3.00003-x

[41.] Martin, C. J. (2011). Personal dosimetry for interventional operators: when and how should monitoring be done? □*the □British Journal of Radiology/British Journal of Radiology*, *84*(1003), 639–648. https://doi.org/10.1259/bjr/24828606

[42.] Vörös, V., Page, A., Deprest, J., Kimpe, T., & Poorten, E. V. (2022). Motion and viewing analysis during minimally invasive surgery for autostereoscopic visualization. *International Journal of Computer Assisted Radiology and Surgery volume*, *18*, 527–535.

[43.] Stenmark, M., Omerbašić, E., Magnusson, M., Andersson, V., Abrahamsson, M., & Tran, P. (2022). Vision-Based Tracking of Surgical Motion During Live Open-Heart Surgery. □*The □Journal Of Surgical Research/Journal Of Surgical Research*, *271*, 106–116. https://doi.org/10.1016/j.jss.2021.10.025

[44.] Rodrigues, V. F., Antunes, R. S., Seewald, L. A., Bazo, R., Reis, E. S. D., Santos, U. J. D., Da R Righi, R., Da S, L. G., Da Costa, C. A., Bertollo, F. L., Maier, A., Eskofier, B., Horz, T., Pfister, M., & Fahrig, R. (2022). A multi-sensor architecture combining human pose estimation and real-time location systems for workflow monitoring on hybrid operating suites. *Future Generation Computer Systems*, *135*, 283–298. https://doi.org/10.1016/j.future.2022.05.006

[45.] Strickland, M., Tremaine, J., Brigley, G., & Law, C. (2013). Using a depth-sensing infrared camera system to access and manipulate medical imaging from

within the sterile operating field. *Canadian Journal Of Surgery*, *56*(3), E1–E6. https://doi.org/10.1503/cjs.035311

[46.] *Scatter radiation*. (n.d.). https://www.mml-medical.nl/en/blog/scatter-radiation/

Applications and Accuracy of Video-Based Body Tracking for Medical Staff in the Operating Room

P.S. (Pepijn) van Ardenne, 5656877, MSc student Biomedical Engineering

Delft University of Technology

16-11-2023

Abstract

Introduction: Video recording in healthcare can be used for various purposes like education, evaluation, and research. This review provides an overview of the application and the accuracy of body tracking for medical staff within the operating room using video recordings.

Method: Four systematic searches were conducted to collect relevant literature. The searches were performed in *Google Scholar*, *PubMed, Scopus,* and *Espacenet* databases. Data from thecf included articles were extracted to assess the measurement approach and compare the accuracy of video recordings across different methods.

Results: The included articles differed in the method for investigating body tracking. This showed that aspects of video recording or body tracking influenced the accuracy of the measurement. The aspects of video recording that influenced the accuracy are the usage of 2D images or 3D images, different cameras, and trackers. The aspects of body tracking that influenced the accuracy are differences in tracked body parts, constraints, and the amount of data.

Discussion: The accuracy was promising. However, it depends on the application if the body tracking is accurate or robust enough. There were still errors made during the tracking that can be reduced by adjusting certain aspects. The combination of the colour camera and InfraRed camera showed the highest applicability in the operation room. Future research can

be performed on the applications of body tracking to support medical staff in the surgery room.

Introduction

Healthcare is rapidly evolving, and one of the key areas is the usage of video recording. These healthcare recordings serve multiple valuable purposes, including education, evaluation, research, quality improvements, revalidation, and patient care [Prigoff et al., 2016; Quach et al., 2023]. However, there are opposing arguments for the usage of video recordings in healthcare, such as concerns related to privacy violations, distraction of the medical staff, and high equipment costs [Gordon et al., 2021]. Moreover, there are applications that can be implemented to reduce the effects of these opposing arguments. For instance, enhancing data security or editing the recordings can help protect the privacy of both the patient and medical staff [Quach, Vittetoe, and Langerman, 2023]. Enhanced data security can prevent data leakage and editing the faces of the patient and medical staff can make them unrecognizable in the recordings. In addition, as demonstrated by Levin et al. (2021), recording medical staff can lead to the so-called Hawthorne effect, resulting in improved work quality due to the presence of cameras. The Hawthorne effect refers to the fact that behaviour will be modified simply because it is observed. Finally, it is noteworthy that the use of low-cost cameras did not decrease the accuracy in comparison with more expensive cameras [Uslu et al., 2021]. Given the significant positive impact of video recording on healthcare and the criticism of the literature on the opposing arguments, it is sufficient to explore further research on this topic. Specifically for functions such as motion capturing and posture analysis, since these functions contribute to video recording.

Motion Capturing

Video recordings in healthcare have a wide range of applications. This study specifically targets the motion capturing of medical staff during surgical procedures. One valuable application of these capturings is tracking the body movements of the medical staff, which serves multiple purposes; detecting phases during surgery, analyzing the workflow, evaluating the procedure, and education in healthcare [Baashar et al., 2023]. There are multiple types of equipment available for capturing the movements of the medical staff during surgery. For example, HTC Vive [Niehorster, Li, and Lappe, 2017], Inertia Measurement Units (IMUs) [Ong et al., 2018], electromagnetic trackers [Datta et al., 2001], and radio-frequency identification tags [Kranzfelder et al., 2012], recurrent neural network-based systems [Moa et al., 2019], and video recordings Baashar et al., 2023]. Video recording is chosen over other methods because they have certain disadvantages, such as measuring only the wearer, restricting the movement of the wearer, and being error-prone in noisy and busy rooms. In addition, documenting visual information can serve various purposes during surgery, such as: tracking the movement of medical instruments, evaluating waste, and monitoring the progress of the procedure [Smith et al., 2014].

Due to the limitations of the other methods and the additional applications of video recording, this research focuses on visual information as a primary source of motion capturing, while other measuring equipment falls outside the scope of this research.

Analyze Posture

Movement and gait analysis are valuable tools in biomechanical research and have significant applications in healthcare. Posture analysis can aid in patient revalidation and monitoring fitness [Ong et al., 2018].

There are several methods for

tracking to analyze posture, with the use of IMUs and video recordings being the most common methods in the literature.

In the study of Jebeli et al. (2017) motion analysis of a simple walking pattern was compared with an expensive and comprehensive system of cameras and a cheap and basal camera system. This study evaluated that the accuracy of the two camera systems is the same in providing three-dimensional motion tracking. In the study of Ong et al.'s (2018) movement of the arm was measured with IMUs and compared with video recording. The results of the measurements were similar. While IMU measurements experience drift in the measurements [Ong et al., 2018]. The drift could be removed because the measurement involved cyclical movements, resulting in a reset of the occurred drift. However, clinical settings often involve non-cyclical movements, which may result in inaccurate measurements. The use of body sensors such as IMUs in clinical settings poses certain challenges. For example; the sterile packaging of sensors is necessary, attaching multiple sensors can be difficult, and sensors restrict the motion during use compromising the quality of performance. For these reasons, this research exclusively focuses on using video recordings to analyze the posture of medical staff.

Video Recording

Video recording can be used as a potential option for both motion capturing and analyzing the posture of medical staff in clinical settings. However, there are several challenges that may be encountered. Firstly, the precision of these measurements must be carefully evaluated to determine if body tracking can be applied in a clinical setting. In Jebelli et al.'s (2017) study, inaccuracies were already identified during a simple walking movement, and since body tracking in a clinical setting is considerably more complex, similar, or higher inaccuracies might arise. Secondly, positioning the video camera in clinical settings can cause certain challenges. The camera requires an unobstructed view of the operating room while not interfering with the work of the medical staff. Besides, the medical staff can obstruct the view of the camera among each other causing occlusion. Lastly, the camera should not compromise hygiene standards in the operating room. Thus, it is important to investigate the feasibility of body tracking using video recording in an operating room setting.

The objective of this review is to provide an overview of the accuracy of body tracking for medical staff within the operation room using video recordings. In addition, various approaches will be compared to assess their robustness and accuracy for potential utilization in a clinical setting. To assess factors influencing accuracy and whether the accuracy is sufficient for various applications. The required accuracy varies per specific application where body tracking is used. The need to be robust and accurate for a specific application is necessary to be used in the operating room. For example, it can be used for enhancing workflow planning or detecting radiation exposure. This has a significant advantage for the enhancement of healthcare.

Method

Search Strategy

A systematic search was conducted. This systematic literature search was performed using several databases: Google Scholar, PubMed, Scopus, and Epacenet. The aim was to

identify all clinical articles evaluating the body tracking of medical staff through video recordings. The search term consists of four parts. The first component ensured the focus on body tracking. The second component ensured that the information was obtained through video recording. The third component emphasized the recordings of medical staff, while the final component specified that the recordings occurred in the

operating room. The search term can be found in Appendix A. Several inclusion criteria were applied: (1) recording of solely the medical staff (2) recording around the surgeon's table (3) tracking the gaze or movement of the staff member, and (4) exclusion of articles involving image-guiding and computer vision. Articles were initially screened based on their titles and abstracts. Subsequently, full articles were reviewed, and those not meeting the inclusion criteria were excluded. Finally, the reference lists of the included articles were checked for any cited articles that met the inclusion criteria but were not initially found in the initial literature search.

Data extraction

Data was collected from the included articles regarding the recording approach and the accuracy. This information enabled the assessment of the quality of the measurement approach. Subsequently, results were combined, comparing the accuracy of the video recordings across various approaches.

Results

Eligible Studies

The selection process of the studies included in this review is shown in Appendix B. The search terms were applied in the databases on 10 October 2023. Following the search, 1329 of which 62 were duplicate articles. The 1267 potential records underwent screening based on titles and abstracts. Out of these, 1201 articles were excluded because the experiments did not meet the inclusion criteria. The remaining 66 articles underwent full screening of the text, and only 14 met the inclusion criteria. Additionally, a second search was conducted, resulting in the identification of four articles through the reference list that met the inclusion criteria but were initially missed in the initial search. In total, 18 articles were found using search terms from Appendix B.

Comparative Methods

Various methods were employed to track medical staff movements during surgery, resulting in a comparison of these approaches. The methods used in the included articles are described in Table 1. Accuracy margins of the measurement procedure are presented in terms of either accuracy or error percentage. A higher accuracy or lower error margin indicates how closely the 3D images represent the recorded environment, impacting the accuracy of medical staff body tracking. While the software responsible for calculations affects body tracking, its diversity in programming makes it challenging to compare, which is beyond the scope of this research. The primary analysis will focus on whether video recording accuracy is sufficient to make claims Belagiannis about medical staff locations.

Video Recording Possibilities

Various approaches to video recording were found in the literature. Multiple brands of video recording equipment were used to capture the 3D images of the operating room. The articles included in this review share one common feature: Providing 3D images of the filmed operating room. These 3D images were obtained through multiple manners, including the use of multiple cameras, InfraRed cameras, and cameras with multiple lenses. In some articles in this review, the accuracy of 3D images is compared with the 2D images [Kadkhodamhammadi et al., 2017; Beerends et al., 2022; Hansen et al., 2019; Belagiannis et al., 2016]. Although the accuracy of 3D was higher than 2D, both were considered high enough for measuring the workflow [Belagiannis et al., 2016; Aggarwal et al., 2007]. Because of the higher accuracy and the additional information, the 3D images are preferred over 2D images in representing the clinical

setting. Even though the calculation of the 3D images costs additional computational capacity [Belagiannis et al., 2016; Beerends et al., 2022].

The calculation of the 3D images is made differently per camera. The multiple cameras provide varying perspectives of 2D images, software combines these images into a 3D representation [Belagiannis et al., 2016]. Infrared cameras generate 3D images by emitting infrared light, measuring the time it takes for light to travel to objects and back, and converting this depth information into a 3D scene [Hansen et al., 2019]. Cameras with multiple lenses operate similarly to multiple-camera setups, with computational analysis of the 3D image occurring within the camera's software. The study of Beerends et al (2022) showed promising results for combining different camera systems that captured 3D and 2D images, such as InfraRed and colour cameras.

Besides the video recording, there were additional methods used in the measuring of the 3D position. For example, electromagnetic tracking, IMUs, and markers. Firstly, electromagnetic tracking was used in combination with video recording to deal with the possible occlusion in the recording [Birkfellner et al., 1998]. Which results in a higher accuracy of the body tracking in the video recording. Furthermore, IMUs were used as an addition to video recording. The IMUs are mostly used for parts of the research that have nothing to do with body tracking. For example, tracking the opening and closing of the door of the operation room [Azevedo-Coste et al., 2019; Birgand et al., 2019], to measure the contamination risk. This method had no impact on the accuracy of tracking the medical staff in the surgery room. Lastly, markers are used to identify particles that must be tracked by the video recorder. For example, paint patterns were applied to surgical tools to determine their orientation and precise location in a camera image, which also allowed for an indication of the surgeon's position [Stenmark et al., 2021]. Which results in the accuracy improved with the number of detected markers. Another example is where ArUco markers are placed on the hats of the medical staff and on the wall of the operation room to map the medical staff relative to the operation room [Vörös et al., 2023] resulting in additional accuracy for the tracking of the medical staff with video recording. These adjusted methods cause additional computational capacity for body tracking.

Usage of Body Tracking

Most of the articles used in this analysis demonstrated an accuracy high enough to perform the required task. However, the articles differ from each other that affect the accuracy, for example; the purpose of body tracking, measuring different body parts, susceptibility to occlusion, data augmentation, and adding constraints to the body the tracking.

Firstly, the difference in the investigated purpose is different. Body tracking is used for analyzing the workflow in the operation room or analyzing the movement of the surgeon. Using body tracking for the analysis of the workflow [Rodrigues et al., 2022] or movement jerks [Ganni et al., 2020] requires a lower accuracy in comparison with the analysis of the exact movement of the surgeon [Birkfellner et al., 1998; Kadkhodamhammadi et al., 2017].

Secondly, the body tracking includes different body parts in the articles, which influences the accuracy. For example, in the article of Beerends et al. (2022) accuracy was lower in the lower body limbs in comparison with the upper limb. Another example is that tracking accuracy was insufficient for measuring eye movements [Vörös et al., 2023; Stenmark et al., 2021], although it was sufficient for the accuracy required for body tracking in other articles [Rodrigues et al., 2022]. Thereafter, there is also tracking of solely the wrist [Mackenzie et al., 2021] or the medical instrument of the surgeon [Heilbrun et al., 2000], which influences the accuracy. Since the wrist and hand are difficult body parts to measure and have a higher detection error

or lower accuracy [Hansen et al., 2019; Kadkhodamhammadi et al., 2017]. The hips and elbows also have a higher detection error [Kadkhodamhammadi et al., 2017; Hansen et al., 2019]. Meanwhile, the head and the shoulder have a lower error in detection [Belagiannis et al., 2016].

Thirdly, the occurrence of occlusion reduces the accuracy [Rodrigues et al., 2022]. In the article of Hu et al. (2022) the amount of occlusion and misidentification of the medical staff was attempted to be reduced, through the usage of multi-camera multi-person tracking and re-identification during the tracking. However, the accuracy was higher than expected but is still affected by occlusion. Infrared cameras or cameras with multiple lenses are affected more by occlusion [Beerends et al., 2022; Hu et al., 2022].

The multiple-camera setups were found to be less affected by occlusion [Mateus et al., 2009; Belagiannis et al., 2016].

Fourthly, a higher amount of data increases the accuracy of the body tracking [Beerends et al., 2022]. Lastly, the accuracy can be influenced by adding constraints or using independent phase modelling in the body tracking software [Mateus et al., 2009]. Adding these adjustments to the software improves the accuracy of the tracking.

Title	Author (Year)	Video recording	Results
An Evaluation of the Feasibility, Validity, and Reliability of Laparoscopic Skills Assessment in the Operating Room	*Aggarwal et al. (2007)*	*Microsoft Webcam*	The objective of this study is to establish video-based motion tracking device of laparoscopic skill in the operating room. This study met the inclusion criteria to be included in the review. Each procedure was recorded with the ROVIMAS video-based motion tracking system to provide an objective measuring of the surgeons. The motion tracking and video-based assessment displayed interest reliability and validity of the device.
Tracking clinical staff behaviors in an operating room.	*Azevedo-Coste et al. (2019)*	*MOCAP & IMU*	In this study behavior in the operation room is investigated to reduce the contamination and infection risk. A setup combining a video camera and IMUs was used to continuously monitor staff movements and detect door opening and closing events. The IMUs are used to observe door movements and the video camera is used for detecting the movements of the medical staff. For the review only the measurement of the video camera matters and contributes to insight into the robustness of body tracking in the operation room. The quality of individual displacement was assessed, and the average percentage of underdetermined points for motion detection was 10.6% across all interventions.
3D human pose estimation in multi-view operating room videos using differentiable camera projections.	*Beerends et al. (2022)*	*RGB camera*	In this study using the Multi-View Operating Room (MVOR) dataset for pose estimation for 2D and 3D in an operating room. This study is included because it met the inclusion criteria and researching the difference between 2D and 3D gives new insights. The two different methods both have their advantages and disadvantages, clarity about the difference in accuracy can give a preference. The proposed method achieved an average MPJPE (Mean Per Joint Position Error) of 8.3 cm for 3D body joint locations, with varying scores for different body parts. For the 2D method, the precision decreased to an average MPJPE of 14.3 cm, particularly for the lower body and limbs. The study also evaluated the impact of data augmentations, showing improvements in results when more data is applied. Additionally, it found that using both colour and depth images together yielded the best results for pose estimation.
Parsing human skeletons in an operating room.	*Belagiannis et al. (2016)*	*Multiple GoPro's*	The study focuses on evaluating 2D and 3D human pose estimation in an operating room (OR) scenario. During the experiment 5 GoPro's are placed around the operating room each creating their own 2D human model of the medical staff. By combining the multiple images an 3D image of the pose of the staff can be created. This study met the inclusion criteria. The cameras placed around the room might give a solution to the occlusion that might occur, because the medical staff is recorded from every angle. The poses are measured with 9 parameters: 3 on each arm, head, chest, and hips. The 3D human pose estimation results showed that the head and torso were easily recognized, while the lower arms were more challenging. The 3D error results were around 10% lower than the 2D results (error total of 99.06 mm). Although, both were considered accurate enough for medical workflow analysis.
Motion-capture system to assess intraoperative staff movements and door openings: Impact	*Birgand et al. (2019)*	*VICON-Bonita*	This study observed and assessed the impact of the operating room (OR) staff movements and door openings on the infection risk. The measurements were executed with IMUs and eight infrared cameras (Vicon-Bonita). The IMUs were used for measuring the door opening and

on surrogates of the infectious risk in surgery.			the video camera was used to track the staff movements. The goal of this study is different, but the body-tracking part can contribute to this review. The study is not a typical body tracking investigation, but it shows that a camera system (consisting of 8 lenses) can follow the entire medical staff present at an orthopedic or cardiac surgery.
Calibration of Tracking Systems in a Surgical Environment.	*Birkfellner et al. (1998)*	Flashpoint 5000	In this research optical tracking was compared with electromagnetic tracking and combined for body tracking in surgery. The electromagnetic tracking would not be affected by an obstructed line-of-sight and should have a higher accuracy during the surgery. The registration of the electromagnetic and optical tracking was tested in different operation room environments, with varying positions and equipment. The full text of the research did not meet the inclusion criteria but the part of solely the optical tracking did meet the criteria. In this review the focus is on optical tracking. The optical tracking method had an accuracy deviation of 2.9 ± 1.4 mm. The average deviation between reading was approximately 2.9 ± 1.0 mm for solely electromagnetic tracking and 2.1 ± 0.8 mm for electromagnetic tracking corrected with the optical tracking method. The hybrid sensor setup resulting in the highest accuracy.
Validation of Motion Tracking Software for Evaluation of Surgical Performance in Laparoscopic Cholecystectomy	*Ganni et al (2020)*	*Not mentioned*	The aim of this study was identifying the best possible algorithm to benchmark different levels by motion tracking of the specific staff member. The identifying of the average movement and jerk index respectively resulted in identifying 23/24 performances. This study performs the body tracking measurement by measuring the jerk of the movement. This can lead to new insights as body tracking is often done through recognition. In Kinovea was a new algorithm tested for tracking system and scored using CAT-system. This system gives a score of the accuracy analyzed motion of the surgeon; the score was p = 0.01, R^2 = 0.844. The value of the motion tracking software provided an objective and accurate clinical evaluation on the performance.
Fusing information from multiple 2D depth cameras for 3D human pose estimation in the operating room.	*Hansen et al. (2019)*	*Multiple RGB-camera*	In the experiments a 2D-3D information fusion provided by multiple depth cameras to track the pose of the surgeons in the operating room. The first step, the 2D joints are predicted from a single depth image. Thereafter, the depth images of the multiple cameras are combined to predict the joints in a 3D image. This study met all the inclusion criteria for this review and gives insights for the accuracy. The Mean Per Joint Position (MPJP) error for the model was 8.0 cm, with a particular reduction in errors for challenging wrist joints, compared to 17.0 cm with only one view. When considering the number of cameras, the error decreased from 11.9 cm for one view to 7.1 cm for three views. The shoulders showed the lowest error in comparison with the wrist and hip.
Apparatus and method for photogrammetric surgical localization.	*Heilbrun et al. (2000)*	*Two cameras (Specific brands not mentioned)*	The article describes a state-of-the-art method for determining the position of a medical instrument relative to a medical workspace, often a patient's body region. This is achieved by capturing pairs of 2D images from different viewpoint using video cameras and after reconstruction a 3D image can be created. This allows for the tracking and guidance of medical instruments without the need for patient fixed device. This research did not specifically use body tracking, but instead used the tracking of the medical instruments. This could lead to new insight, as tracking bodies of multiple staff members can interfere with each other, which is not the case with tracking medical instruments. The accuracy of the device was tested and shows an accurate measurement within at least 2 mm (Video = 92.0 & -17.8).
Multi-Camera Multi-Person Tracking and Re-Identification in an Operating Room.	*Hu et al. (2022)*	*Inter-camera ReID*	The study uses multi-camera multi-person (MCMP) tracking and re-identification (ReID) to track the medical staff in the operation room. This study focuses on the staff in the operation room and tries to deal with identification and misidentification in a crowded room with obstacles. This research met all the inclusion criteria of this review and shed light on the fact that reducing occlusion is possible. The tracking is performed with a trajectory-based method, integrating tracking and ReID tasks. Firstly, the poses of the medical staff are detected by each camera frame by frame. Subsequently, the detected poses are exploited to track the trajectories of all members for each camera. Eventually, the different cameras are clustered to re-identify the medical staff in the room. This approach had a high accuracy (85,44 %) with the improved ReID accuracy due to temporal information utilization. However, the accuracy is influenced by the quality of detection, this is the reason the accuracy decreases in challenging scenarios such as occlusions.
Articulated clinician detection using 3D pictorial structures on RGB-D data.	*Kadkhodamhammadi et al. (2017)*	*Asus Xtion Pro Live* camera	In the experiment, pose estimation and clinician detection on a challenging RGB-D dataset recorded in a busy operating room during surgery. During the experiment the RGB-D camera created an 2D and 3D image and compared the tracking of solely the upper body. This study is included because the fourth inclusion criteria are met and the measuring of solely the upper body might result in higher accuracy and less computational time. The 3D model yielding the best performance,

			improving by approximately 11% over the baseline. The 3D (InfraRed) models consistently outperformed 2D (colour) ones, with an accuracy of 89.7 versus 77.3. For both methods, the head and shoulders had the highest accuracy of tracking in comparison with the elbow, wrist, and hips. The 3D model provided advantages in handling occlusions and improving detection accuracy, showcasing the value of 3D information in cluttered environments.
Enhanced training benefits of video recording surgery with automated hand motion analysis	*Mackenzie et al. (2021)*	*Nikon d600*	In this study the hand motion is analyzed by video recording during surgery for evaluation of the surgical performance. During the experiment solely the hands of the surgeons are measured with a camera and the camera is placed in the direction of the surgery table. The measures can be collected using consumer level cameras and analyzed automatically with free software. This study only tracked the hands of the medical staff instead of the whole body. The study is still included because the tracking of only the hands might lead to new insights. The video analysis results of body tracking were consistent and had a reduction in variability as part of increasing data.
Workflow monitoring based on 3D motion features.	*Mateus et al. (2009)*	*Multi-camera system (The specific cameras not mentioned)*	The goal of this study is the recognition of activity and interactions to monitor the workflow during surgery. The activities were recorded by a multi-camera system, resulting in a dataset of 22 videos with 3D reconstructions. This study does not have the primary goal of body tracking, but instead measuring the workflow with the help of body tracking. This may result in less importance to a higher accuracy. However, this study might still give insight for the robustness of the usage of body tracking with a video-camera. During the experiment three different variance of the hidden Markov models (HMM) were compared for analyzing the workflow by tracking the motion of the medical staff. Firstly, WHMM having temporal constraints on the workflow (accuracy online 89.2%). Secondly, MAP-HMM are all phases modeled independently by different HMMs trained on sub-windows of the data (accuracy online 70.5%). Lastly, CO-HMM this model uses sub-HMMs arranged in parallel and connected via sub-HMM background activities (accuracy online 78.2%). The error measures used included accuracy, recall, precision, and overall success. WHMM outperformed the other methods, with online results slightly worse than offline results. Anomalies were also identified in the detection process.
A multi-sensor architecture combining human pose estimation and real-time location systems for workflow monitoring on hybrid operating suites.	*Rodrigues et al. (2022)*	Kinect v2	During the experiment position and pose estimation data were combined to monitor the workflow of the medical staff in the hybrid operation room. The data was provided through the multi-camera human pose estimation methodology. The study was included because it had the exact criteria for this review. The noteworthy findings of this study are that the accuracy of the joints varied across body parts, with lower limbs having the lowest (1% to 20%) due to occlusions, and upper limbs having higher rates (12% to 57%). Eventually the accuracy of the used methodology (Human pose estimation) showed small joint detection errors (up to 5 cm) for all body parts. Overall, the system, had an accurate joint detection and efficient resource utilization, making it suitable for hybrid OR workflow monitoring.
Vision-Based Tracking of Surgical Motion During Live Open-Heart Surgery.	*Stenmark et al. (2021)*	Sony Handycam FDR-AX53	This research discusses the development and evaluation of a vision-based motion tracking system used in live open-hearth surgery. The motion tracking was provided by tracking dye attached on the surgical forceps. By tracking the path of the surgical forceps, the movement of the surgeon could be tracked. Surgeons subjectively reported a slight shift in balance and increased weight due to the die, but it did not affect their performance. This study deviates slightly from the standard criteria for this review, as the tracking is done using dye on the medical forceps. However, tracking the motion by following the paint on the surgical forceps, might result in additional accuracy in the body tracking. The detection reliability of the markers varied among surgeries, with an overall precision of 1.0 and recall of 0.81. The results showed, the motion tracking accuracy improved with the number of detected markers, and computational processing was performed in real time.
Using a depth-sensing infrared camera system to access and manipulate medical imaging from within the sterile operating field.	*Strickland et al. (2013)*	*Microsoft-kinect*	The article discusses the development and implementation of a touchless gesture-based system for intraoperative image navigation in surgical procedures. The system integrates an IR camera unit, image-processing unit, and feedback display onto a portable cart. Usability test showed that users quickly adapted to the gesture-based interface, finding it intuitive and easy to use. This study does not track the body with the camera, but solely track gestures. However, this might give insight on the advantages of using gesture tracking instead of the whole body. In a pilot study involving various surgical procedures, the system was used to access and manipulate imaging data, providing real-time guidance, and enhancing surgical precision. Challenges included potential interference from OR lighting. Overall, the system shows

			promise for improving intraoperative image navigation and in surgical settings.
Motion and viewing analysis during minimally invasive surgery for autostereoscopic visualization.	*Vörös et al. (2023)*	*Intel RealSense D415 depth camera*	In the study motion and viewing of the medical staff was tracked with depth cameras. The tracking with the camera was helped with ArUco markers that were placed on the caps of the clinicians and the wall of the operating room. The surgeons stood between 1200 to 2300 mm distance of the video camera. The looking of the surgeon remained mostly static during interventions, with only four repositioning recorded, all within 20 cm in all directions. This study meets the inclusion criteria and gives some insight if the accuracy is high enough to also track eye movement and the additional help of markers in body tracking. The motion tracking showed a standard deviation of 262 mm (x-axis), 157 mm (y-axis), and 297 mm (z-axis). Display rotations around the vertical y-axis exhibited variation.
Measuring teamwork for training in healthcare using eye tracking and pose estimation	*Weiss et al. (2023)*	*2 Logitech C270 webcams & 3 SMI ETG 2 wireless mobile eye tracking glasses*	This study is aimed to investigate the teamwork in simulated clinical situations. Behavior observation is executed by tracking the eye tracking by eye tracking glasses and pose estimation with two cameras. During the experiment the mobile eye tracking measuring where participants look, and multi-person pose estimation, measuring 3D human body and joint position. The measuring of the eye gaze does not contribute to this review. The pose estimation by video-camera does contribute to this review. The exact accuracy of the eye tracking and pose estimation is not mentioned, however the researchers spoke promisingly over the body tracking software named ROVIMAS. The rating scales were valid and demonstrated high interest reliabilities, highlighting the accuracy.

Table 1: This table represents the various studies included in the review. The table includes the title, author and type of camera used in the research. Additionally, there is a summary of the study and findings on accuracy, although not every study specifies exact accuracy.

Discussion

Tracking the movements of medical staff during surgery is a useful tool that can provide valuable information. However, there are some disadvantages mentioned to video recording such as privacy concerns, potential distraction, and high implementation costs [Gordon et al., 2021]. Nevertheless, there are counterarguments found in the literature, such as improved data security [Quach et al., 2023], the Hawthorne effect [Levin et al., 2021], and body tracking performances are not reduced in cost-effective cameras in comparison to elaborate and expensive camera systems [Uslu et al., 2021]. The tracking of the medical staff with optical information offers valuable insights. However, it is important to conduct research on the accuracy and aspects that influence the accuracy of localization of the medical staff. Then it is possible to make statements about the robustness and applicability of body tracking in the operating room. Without confirmation that the accuracy is sufficient, body tracking cannot be used as a tool for applications in the operating room.

Interpretation of the Results

The authors of the included articles found body tracking to be a promising tool. In the articles, the accuracy was considered high, and the standard error was considered low. In the article of Stenmark et al., (2021), the accuracy was considered on the low side to track the gaze of eyes during a procedure. However, the eyes are much smaller compared with the entire body, so when tracking the eyes there is a need for a much lower. The pupil is around 1.5-8 millimetres, which ensures that there is hardly any margin for error when measuring the eye. To measure the eyes requires glasses that can accurately measure the direction of the gaze [Aggarwal et al., 2007]. While the error margin could be much larger with full-body tracking since the surface is much larger to track. The articles showed that accuracy was influenced by several aspects or had controversial findings. These aspects or findings influenced the video recording or the body tracking.

There are multiple aspects that influence the video recording and could affect the accuracy.

Firstly, the accuracy of the 3D image used for body tracking. Both 2D and 3D images were considered high enough for measuring the workflow [Belagiannis et al., 2016]. The accuracy of the 3D image for body tracking is slightly higher [Belagiannis et al., 2016]. Since the mapping of the operating room in 3D results in the most information. The 2D imaging should not be completely excluded as it has viable accuracy and can possibly support the 3D image. The camera systems construct differently the 3D images. In addition to the fact that this affects the accuracy, it also affects the amount of calibration, computational capacity, and requirement of space [Kadkhodamhammadi et al., 2017]. Since the system with multiple cameras needs multiple devices to construct a 3D image. The time to compute the 3D image is higher in comparison with the InfraRed camera. The multiple devices also take up several places in the operating room. Because the cameras need a clear view of the operating table, which is not always possible as it can be busy and chaotic during surgery. When there is only one camera, for example, a camera with multiple lenses or an InfraRed camera, it is easier to take a place in the operating room with a clear view of the operating table. Furthermore, the position of the multiple cameras needs to be calibrated with each other to correctly calculate the 3D image. When the cameras are slightly moved, they need to be recalibrated and the measurement can be invalid. Since the infrared camera and camera with a lens are one device, they are less affected by it.

Secondly, the type of camera that was used for the body tracking. The reviewed articles could be categorized into three different camera categories: multiple cameras, infrared cameras, and cameras with multiple lenses. These categories have all demonstrated promising results, but they differ in terms of accuracy. Infrared cameras are influenced by factors such as occlusion [Hansen et al., 2019] and lighting [Strickland et al., 2013] in the operating room. Cameras with multiple lenses are also affected by occlusions [Rodrigues et al., 2022]. Multiple cameras used for tracking medical staff are less affected by occlusion or lighting [Belagiannis et al., 2016]. However, this camera system does not necessarily have the highest accuracy [Azevedo-Coste et al., 2019]. This is because the 3D image is constructed from multiple 2D images captured by each camera. Each camera has a certain deviation in accuracy when creating a 2D image and when multiple cameras are used to create a 3D image, this deviation may increase, leading to a relatively lower accuracy. However, the best result emerges from combining the colour and InfraRed camera [Beerends et al., 2022], using the combination of the 3D and 2D images.

Thirdly, the use of trackers in addition to video recording. There are multiple trackers that can be used as an addition to body tracking. However, only two were used in the included articles, namely, IMU [Azevedo-Coste et al., 2019; Birgand et al., 2019] and electromagnetic trackers [Berkfellner et al., 1998]. Besides, there are also markers used on the body of the medical staff to facilitate the tracking of the body for the video recorder [Stenmark et al., 2021].

The additional use of trackers would possibly resolve the problem that occurs with occlusion during video tracking [Berkfellner et al., 1998]. However, the trackers still have some downsides. The trackers need to be worn by the surgeon, for example on the hand, and this leads to discomfort for the surgeon during surgery [Kranzfelder et al., 2012]. In addition, in the usage of IMUs drift occurs during these measurements, which results in an increasingly large deviation [Ong et al., 2018]. The markers do not help prevent the occlusion and the wearing still leads to discomfort for the surgeon. The usage of markers and IMUs as trackers is excluded for additional help for body tracking with video recording. Because they have specific downsides that are not situation-appropriate for the tracking of surgeon

motion. However, if there is a possibility to reduce the discomfort of the surgeon during movement, for example by wearing it on the shoulders or head. Then wearing electromagnetic trackers can contribute to the reduction of occlusion during the tracking of the body.

Concluding, the three different cameras have their strength and their flaws. Combining the methods of 2D and 3D might contribute to additional accuracy and reduce the effect of certain factors that reduce the accuracy. Combining colour and a depth camera showed the best results. This combination of camera types is also used in 3D cameras, an example is the Azure Kinect DK. In addition, electromagnetic trackers might reduce the amount of occlusion that can occur, if the trackers can be worn without leading to limitation of the movement of the surgeon.

There are also multiple aspects that influence body tracking and therefore accuracy.

Firstly, tracking different body parts results in a difference in accuracy. There is a difference in accuracy when detecting the upper and lower extremities [Beerends et al., 2022]. An explanation is that the vision of the video camera on the lower extremities can be blocked by the operation table since the surgeon stands behind it. There is also a difference in the accuracy of the upper extremities. The head and shoulders have a lower detection error in comparison with the other extremities of the upper body such as the wrists and hands [Belagiannis et al., 2016; Kadkhodamhammadi et al., 2017; Hansen et al., 2019]. However, not measuring these body parts is not possible as tracking these body parts gives information on the specific movement of the surgeon during surgery. Which in turn can be used for phase detection, surgical education and identifying errors during surgery [Prigoff et al., 2016; Quach et al., 2023]. The hands are difficult to track with video recording because they are relatively smaller and move quickly. Besides, they are also more difficult to recognize due to occlusion or because the hand changes shape when holding medical equipment. Using markers on the medical equipment might result in a solution to this problem and will not limit the movement of the surgeon. Since markers on the medical instruments increase the accuracy of tracking these body parts [Stenmark et al., 2021]. However, this does not provide a solution for the occlusion of the hands or lower extremities. Tracking the exact location of the lower extremities is not important since it stand stationary and provides barely any information for the purposes of body tracking. To possibly reduce the occlusion in tracking the hands of the surgeon, the markers on the medical instruments can be exchanged for electromagnetic trackers. In addition, this will also influence the other difficulties of tracking the hand.

Secondly, the accuracy can be influenced by adding constraints such as using independent phase and ReID modelling in the body tracking software. The difference in accuracy is shown in the difference in purposes of the body tracking. Namely, analyzing the workflow has a lower accuracy compared to specific body tracking. On the contrary, in the article of Mateus et al. (2009), where the workflow was measured, the accuracy of body tracking was about the same as the accuracy of body tracking for analyzing the movement of the surgeon [Birkfellner et al., 1998; Kadkhodamhammadi et al., 2017]. Because there was a usage of constraints that influenced the accuracy of the body tracking [Mateus et al., 2009; Hu et al., 2022]. Independent phase modelling and ReID results in a possibility to facilitate the tracking and increase the accuracy. In tracking rapid movement, the images of the cameras can be blurred. With consecutive images, this can lead to errors in motion tracking. The margin of error can be reduced by analyzing each frame separately. The tracking is then less likely to assume based on the previous frames if there is a blurred image. This does result in a much higher computational capacity for calculating the motion tracking. Lastly, a larger data set results in higher accuracy or lower error percentage. Since a higher amount

of data increases the accuracy of the body tracking [Beerends et al., 2022]. With a larger data set, it is possible to have a better estimation of inaccurate movements in blurry or occluded images for example. These estimations can be made through anticipation or interpolation of the data. Both anticipation and interpolation of the missing data result in a need for higher computational capability, which can result in a longer computational time. In addition, interpolation requires the complete data set to fill in the missing data, resulting in it not being able to function as an immediate feedback system.

In conclusion, there are multiple aspects that affect the accuracy of body tracking. The accuracy can still be increased through adjustments, but this is a trade-off with the computational capacity. By adding constraints and additional data the number of errors can be reduced in body tracking but the computational capacity increases. In addition, the accuracy for tracking different body parts differs. This is task-dependent because body tracking is used for various purposes. In some cases, certain body parts can be ignored, while in others, additional trackers might offer a solution to the inaccuracies.

Limiting Factors

Using video-recorder for tracking the bodies of the medical staff is a state-of-the-art subject. Although it is widely discussed in the literature, it is only applied in a few studies. As a result, the included literature is somewhat different from each other. For example, body tracking was used for different purposes. Some studies aimed to investigate the accuracy of the hardware and software for body tracking [Heilbrun et al., 2000; Hu et al., 2022], while others utilized body tracking for different applications. For instance, tracking the eyes [Stenmark et al., 2021] requires high accuracy, while assessing infection risk through motion tracking [Azevedo-Coste et al., 2019] may require a lower level of accuracy. These varying applications may have influenced the author's opinion on the feasibility of using body tracking in the operating room. However, this gives an example of the wide usability of body-tracking with video recordings.

Additionally, the studies differed in measuring points and how many measurements were made. For example, the number of measuring points used to track the body differed per study. If the number of measuring points is higher, the results will be more robust compared with fewer measuring points.

Conclusion

According to the authors included in this review, the accuracy of body tracking with video recording was very promising. Although there are still errors made during the tracking. Since body tracking is used for multiple applications in the surgery room the required accuracy differs. For very specific applications such as eye tracking and incision tracking the error margin is too high to call the measurement accurate or robust. However, the accuracy of body tracking is accurate and robust enough for other applications in the surgery room that do not require the same level of precision. Examples include position detection, workflow monitoring or phase recognition.

The errors that occur with video recording can be reduced, by adjusting various aspects of body tracking or video recording. Taking into consideration that there is a trade-off between the accuracy and the computational capacity. The accuracy can be increased by using constraints or interpolation resulting in an increased computational capacity as well. In addition, the accuracy of the tracking varies per body part, and for some tasks, it is possible to exclude the tracking of specific body parts to increase accuracy. Thereafter, the use of trackers could be a solution for lower accuracy in the outer limbs and occlusion. Finally, combining 2D images of the Colour camera and 3D images of the InfraRed camera results in

the best accuracy and applicability in body tracking. Which makes it the most suitable choice for applications in the operating room.

However, body tracking is a state-of-the-art subject which results in limited research where body tracking with a video camera is used as an additional application in the operating room. In the future, research needs to be conducted to assess the applicability of body tracking in the operating room for assisting the medical staff. By, for example enhancing workflow planning or detecting radiation exposure in medical staff. This can contribute to the optimization of the technology in healthcare.

References:

Aggarwal, R., Grantcharov, T., Moorthy, K., Milland, T., Papasavas, P., Dosis, A., Bello, F., & Darzi, A. (2007). An evaluation of the feasibility, validity, and reliability of laparoscopic skills assessment in the operating room. *Annals of Surgery*, *245*(6), 992–999. https://doi.org/10.1097/01.sla.0000262780.17950.e5

Amin, M. S., Rizvi, S. T. H., & Hossain, M. M. (2022). A comparative review on applications of different sensors for sign language recognition. *Journal of Imaging*, *8*(4), 98. https://doi.org/10.3390/jimaging8040098

Azevedo-Coste, C., Pissard-Gibollet, R., Toupet, G., Fleury, E., Lucet, J., & Birgand, G. (2019). Tracking clinical staff behaviors in an operating room. *Sensors*, *19*(10), 2287. https://doi.org/10.3390/s19102287

Baashar, Y., Alkawsi, G., Ahmad, W. N. W., Alomari, M. A., Alhussian, H., & Tiong, S. K. (2023). Towards Wearable Augmented Reality in Healthcare: A Comparative survey and analysis of Head-Mounted Displays. *International Journal of Environmental Research and Public Health*, *20*(5), 3940. https://doi.org/10.3390/ijerph20053940

Belagiannis, V., Wang, X., Shitrit, H. B., Hashimoto, K., Stauder, R., Aoki, Y., Kranzfelder, M., Schneider, A., Fua, P., Ilic, S., Feussner, H., & Navab, N. (2016). Parsing human skeletons in an operating room. *Journal of Machine Vision and Applications*, *27*(7), 1035–1046. https://doi.org/10.1007/s00138-016-0792-4

Birgand, G., Azevedo, C., Rukly, S., Pissard-Gibollet, R., Toupet, G., Timsit, J., & Lucet, J. (2019). Motion-capture system to assess intraoperative staff movements and door

openings: Impact on surrogates of the infectious risk in surgery. *Infection Control and Hospital Epidemiology*, *40*(05), 566–573. https://doi.org/10.1017/ice.2019.35

Birkfellner, W., Watzinger, F., Wanschitz, F., Ewers, R., & Bergmann, H. (1998). Calibration of tracking systems in a surgical environment. *IEEE Transactions on Medical Imaging*, *17*(5), 737–742. https://doi.org/10.1109/42.736028

Beerend, G. A. (2022). 3D human pose estimation in multi-view operating room videos using differentiable camera projections. *Computer Methods in Biomechanics and Biomedical Engineering: Imaging & Visualization*, *11*(4), 1197–1205. https://doi.org/10.1080/21681163.2022.2155580

Datta, V., Mackay, S., Mandalia, M., & Darzi, A. (2001). The use of electromagnetic motion tracking analysis to objectively measure open surgical skill in the Laboratory-Based model. *Journal of The American College of Surgeons*, *193*(5), 479–485. https://doi.org/10.1016/s1072-7515(01)01041-9

Ganni, S., Botden, S. M. B. I., Chmarra, M. K., Li, M., Goossens, R., & Jakimowicz, J. J. (2020). Validation of motion tracking software for evaluation of surgical performance in laparoscopic cholecystectomy. *Journal of Medical Systems*, *44*(3). https://doi.org/10.1007/s10916-020-1525-9

Gordon, L., Reed, C., Sørensen, J. L., Schulthess, P., Strandbygaard, J., Mcloone, M., Grantcharov, T. P., & Shore, E. M. (2021). Perceptions of safety culture and recording in the operating room: Understanding barriers to video data capture. *Surgical Endoscopy and Other Interventional Techniques*. https://doi.org/10.1007/s00464-021-08695-5

Hansen, L., Siebert, M., Diesel, J., & Heinrich, M. P. (2019). Fusing information from multiple 2D depth cameras for 3D human pose estimation in the operating room. *International Journal of Computer Assisted Radiology and Surgery*, *14*(11), 1871–1879. https://doi.org/10.1007/s11548-019-02044-7

Heilbrun, M. P., McDonald, P., Wiker, J. C., Koehler, S., & Peters, W. (2012). Apparatus and method for photogrammetric surgical localization. *United States Patent*.

Hu, H., Hachiuma, R., Saito, H., Takatsume, Y., & Kajita, H. (2022). Multi-Camera Multi-Person tracking and Re-Identification in an operating room. *Journal of Imaging*, *8*(8), 219. https://doi.org/10.3390/jimaging8080219

Jebeli, M., Bilesan, A., & Arshi, A. R. (2017). A study on validating KinectV2 in comparison of Vicon System as a motion capture system for using in health engineering in industry. *Nonlinear Engineering*, *6*(2). https://doi.org/10.1515/nleng-2016-0017

Kadkhodamohammadi, A., Gangi, A., De Mathelin, M., & Padoy, N. (2017). Articulated clinician detection using 3D pictorial structures on RGB-D data. *Medical Image Analysis*, *35*, 215–224. https://doi.org/10.1016/j.media.2016.07.001

Klöpfer-Krämer, I., Brand, A., Wackerle, H., Müßig, J. A., Kröger, I., & Augat, P. (2020). GAIT Analysis – Available platforms for outcome assessment. *Injury-international Journal of The Care of The Injured*, *51*, S90–S96. https://doi.org/10.1016/j.injury.2019.11.011

Kranzfelder, M., Zywitza, D., Jell, T., Schneider, A., Gillen, S., Friess, H., & Feussner, H. (2012). Real-Time monitoring for detection of retained surgical sponges and team motion in the surgical operation room using Radio-Frequency-Identification (RFID) technology: a preclinical evaluation. *Journal of Surgical Research*, *175*(2), 191–198. https://doi.org/10.1016/j.jss.2011.03.029

Levin, M., McKechnie, T., Kruse, C., Aldrich, K. M., Grantcharov, T. P., & Langerman, A. (2021). Surgical Data Recording in the Operating Room: A Systematic Review of Modalities and Metrics. *British Journal of Surgery*, *108*(6), 613–621. https://doi.org/10.1093/bjs/znab016

Mackenzie, C. F., Yang, S., Garofalo, E., Hu, P., Watts, D., Patel, R., Puché, A. C., Hagegeorge, G., Shalin, V. L., Pugh, K., Granite, G., Stansbury, L. G., Shackelford, S., & Tisherman, S. A. (2021). Enhanced training Benefits of video recording surgery with automated hand motion analysis. *World Journal of Surgery*, *45*(4), 981–987. https://doi.org/10.1007/s00268-020-05916-1

Mao, W., Wang, M., Sun, W., Qiu, L., Pradhan, S., & Chen, Y. (2019). RNN-Based Room Scale Hand Motion Tracking. *Association for Computing Machinery*. https://doi.org/10.1145/3300061.3345439

Niehorster, D. C., Li, L., & Lappe, M. (2017). The accuracy and precision of position and orientation tracking in the HTC Vive virtual reality system for scientific research. *I-perception*, *8*(3), 204166951770820. https://doi.org/10.1177/2041669517708205

Ong, Z. C., Seet, Y., Khoo, S. Y., & Noroozi, S. (2018). Development of an economic wireless human motion analysis device for quantitative assessment of human body joint. *Measurement*, *115*, 306–315. https://doi.org/10.1016/j.measurement.2017.10.056

Padoy, N., Mateus, D., Weinland, D., Berger, M., & Navab, N. (2009). Workflow monitoring based on 3D motion features. *IEEE 12th International Conference on Computer Vision Workshops, ICCV Workshops*. https://doi.org/10.1109/iccvw.2009.5457648

Prigoff, J. G., Sherwin, M., & Divino, C. M. (2016). Ethical recommendations for video recording in the operating room. *Annals of Surgery*, *264*(1), 34–35. https://doi.org/10.1097/sla.0000000000001652

Quach, W. T., Vittetoe, K. L., & Langerman, A. (2023). Ethical and Legal Considerations for Recording in the Operating Room: A Systematic Review. *JSR Journal of surgical research*, *288*, 118–133. https://doi.org/10.1016/j.jss.2023.02.017

Reiley, C. E., Lin, H., Yuh, D. D., & Hager, G. D. (2010). Review of methods for objective surgical skill evaluation. *Surgical Endoscopy and Other Interventional Techniques*, *25*(2), 356–366. https://doi.org/10.1007/s00464-010-1190-z

Rodrigues, V. F., Antunes, R. S., Seewald, L. A., Bazo, R., Reis, E. S. D., Santos, U. J. D., Da Rosa Righi, R., Da S, L. G., Da Costa, C. A., Bertollo, F. L., Maier, A., Eskofier, B. M., Horz, T., Pfister, M., & Fahrig, R. (2022). A multi-sensor architecture combining human pose estimation and real-time location systems for workflow monitoring on hybrid operating suites. *Future Generation Computer Systems*, *135*, 283–298. https://doi.org/10.1016/j.future.2022.05.006

Smith, R., Schwab, K., Day, A., Rockall, T., Ballard, K., Bailey, M., & Jourdan, I. (2014). Effect of passive polarizing three-dimensional displays on surgical performance for experienced laparoscopic surgeons. *British Journal of Surgery*, *101*(11), 1453–1459. https://doi.org/10.1002/bjs.9601

Stenmark, M., Omerbašić, E., Magnusson, M., Andersson, V., Abrahamsson, M., & Tran, P. (2022). Vision-Based tracking of surgical motion during live Open-Heart surgery. *Journal of Surgical Research*, *271*, 106–116. https://doi.org/10.1016/j.jss.2021.10.025

Strickland, M., Tremaine, J., Brigley, G., & Law, C. (2013). Using a depth-sensing infrared camera system to access and manipulate medical imaging from within the sterile operating field. *Canadian Journal of Surgery*, *56*(3), E1–E6. https://doi.org/10.1503/cjs.035311

Tadano, S., Takeda, R., & Miyagawa, H. (2013). Three dimensional GAIT analysis using wearable acceleration and gyro sensors based on quaternion calculations. *Sensors*, *13*(7), 9321–9343. https://doi.org/10.3390/s130709321

Uslu, T., Gezgin, E., Özbek, S., Güzin, D., Can, F. C., & Çetin, L. (2021). Utilization of low cost motion capture cameras for virtual navigation procedures: Performance evaluation for surgical navigation. *Measurement*, *181*, 109624. https://doi.org/10.1016/j.measurement.2021.109624

Vörös, V., Page, A., Deprest, J., Kimpe, T., & Poorten, E. V. (2022). Motion and viewing analysis during minimally invasive surgery for autostereoscopic visualization. *International Journal of Computer Assisted Radiology and Surgery volume*, *18*, 527–535.

Weiss, K. E., Kolbe, M., Lohmeyer, Q., & Meboldt, M. (2023). Measuring teamwork for training in healthcare using eye tracking and pose estimation. *Frontiers in Psychology*, *14*. https://doi.org/10.3389/fpsyg.2023.1169940

Yan, X., Li, H., Wang, C., Seo, J., Zhang, H., & Wang, H. (2017). Development of ergonomic posture recognition technique based on 2D ordinary camera for construction hazard

prevention through view-invariant features in 2D skeleton motion. *Advanced Engineering Informatics*, *34*, 152–163. https://doi.org/10.1016/j.aei.2017.11.001

Appendix A: Search terms

Scholar searching terms.

("Body tracking" OR "Pose estimation" OR "Kinematics" OR "Motion tracking" NOT "Augmented Reality" NOT "Extended reality" NOT "Computer vision" NOT AI NOT robot)**)** AND ("Surgeons" OR "Medical staff") AND ("operation room" OR "surgery" OR "cath lab") AND ("Recording" OR "visual-audio media" OR "Visual information") AND language: English.

Espacenet searching terms.

((ta all "Body tracking" OR ta all "Pose estimation" OR ta all "Kinematics" OR ta all "Motion tracking") NOT ta any "Robot system") AND (ctxt any "Surgeons" OR ctxt any "Medical staff" OR ctxt any "Medical personnel" OR ctxt any "Doctors") AND (ctxt any "operation room" OR ctxt any "surgery" OR ctxt any "Medical procedure" OR ctxt any "cath lab") AND (ctxt any "Filming" OR ctxt any "Recording" OR nftxt any "video-audio media" OR ctxt any "Visual information")

Scopus searching terms.

("Body tracking" OR "Motion tracking") AND ("Surgeons" OR "Medical staff" OR "patients" OR "healthcare") AND ("healthcare" OR "surgery" OR "revalidation" OR "operation AND room" OR "clinical" OR "medical") AND ("video-recording" OR "filming")

PubMed searching terms.

("Body tracking" OR "Motion tracking" OR "position tracking" OR "kinematic analysis" NOT "Augmented Reality" NOT "Extended reality" NOT "Computer vision" NOT AI NOT robot) AND ("Surgeons" OR "Medical staff" OR "patients") AND ("Operation room" OR "healthcare" OR "surgery") AND ("video-recording" OR "filming" OR "Video-audio media" OR "visual information")

Appendix B: Selection of articles

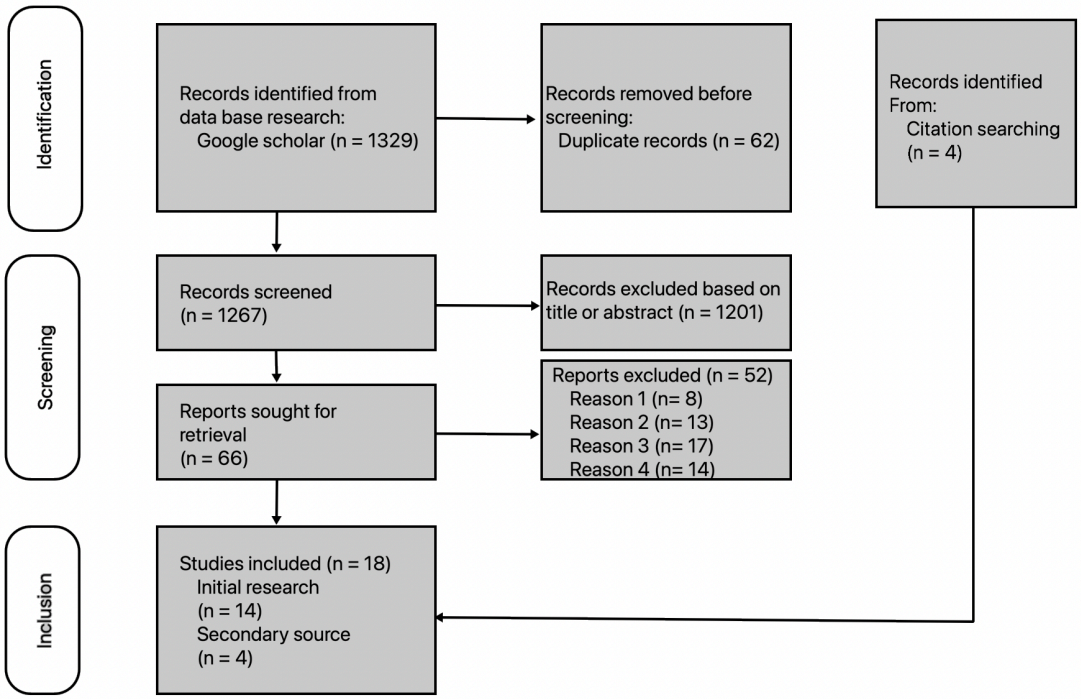

Figure 1: Databases search: Preferred reporting items for systematic reviews and meta-analyses (PRISMA)-diagram of the systematic search.

Appendix B: Measurement setup

Figure 22: Showing the setup in the Cath lab. A: The placement of the elevated Azure Kinect DK with the laptop that controls it. B: The surgeon's table where the phantom and the center are marked exactly in the middle. C: Shows how the orientation of the setup table for the Azure Kinect and the laptop is validated. D: Showing a line in the Cath lab as a reference position of the table for the Azure Kinect. E: The lines in the Cath lab are numbered for the positioning of the table for the Azure Kinect. Line 1 is positioned over line 2, so the lines are parallel. Line 4 is positioned parallel to line 3 at a certain distance. F: The bar handle is shown to adjust the orientation of the tabletop.

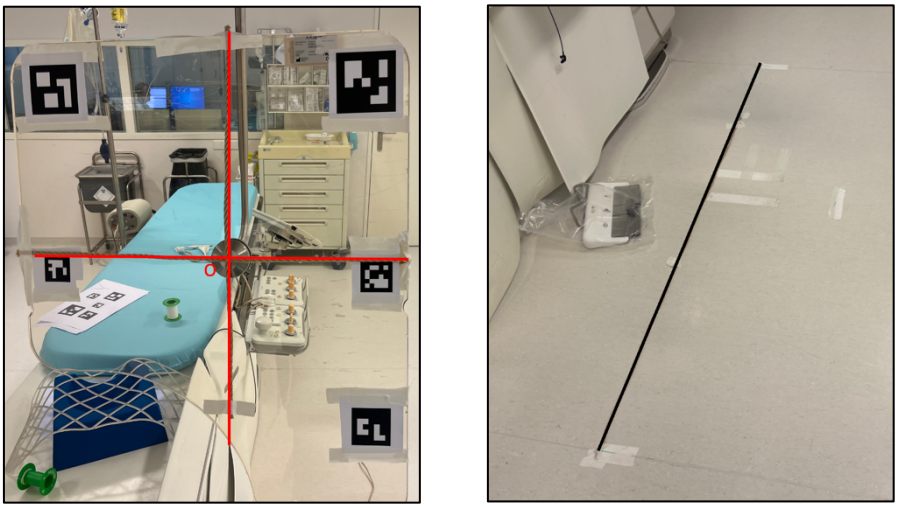

Figure 23: Shows some additional setup in the Cath lab. Left: Displays the 5 Aruco markers on the lead shield relative to the coordinate system of the center point of the lead shield. Right: This is a line parallel to the surgeon's table where the cardiologist stands.

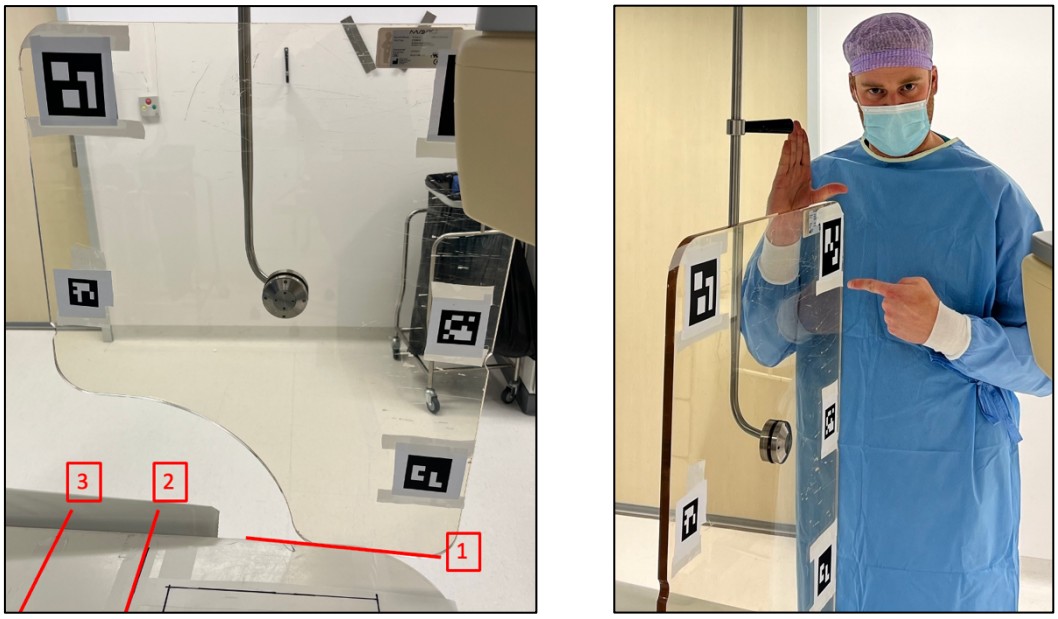

Figure 24: Displays the positioning of the lead shield in the dynamic measurement. Left: Shows the three different positions; position 1 is parallel to the table, position 2 is at 36,06 cm from the center of the phantom, position 3 is at a distance of 51,06 cm from the center of the phantom. Right: Displays the Cardiologist showing that position 2 and 3 of the lead shield are positioned perpendicular to the surgeon's table.

Reinier de Graaf

TU Delft
Delft University of Technology

Figure 25: Show the reference positions of the lead shield during the second part of the visualization measurements. Left: position 1 closes to the phantom. Middle: position 2 the middle position of the lead shield. Right: Position 3 the furthest away from the phantom.

Appendix C: Measurement Tables

Static Measurement: Extreme Positioning						
No.	**Angle of Stands**	**Position lead shield**	**Distance nose**	**Distance Left wrist**	**Distance Right Wrist**	**Distance Lead shield**
1	0°	1	*2272*	*2388*	*2465*	*N/A*
2	45°	1	*2292*	*2244*	*2345*	*1407*
3	90°	1	*2282*	*2302*	*2410*	*1078*
4	0°	2	*2373*	*2224*	*2260*	*N/A*
5	45°	2	*Not detected*	*Not detected*	*Not detected*	*1188*
6	90°	2	*Not detected*	*Not detected*	*Not detected*	*1136*
7	0°	3	*2541*	*2350*	*2470*	*N/A*
8	45°	3	*Not detected*	*Not detected*	*Not detected*	*1414*
9	90°	3	*2450*	*2352*	*2610*	*1132*

Table 3: Displays the results of the first measurement, where the distances towards the cardiologist and the middle of the lead shield are in millimeters. The cardiologist is positioned in different angles towards the Azure Kinect; 0, 45, ang 90 degrees. The lead shield is also positioned in three different positions: next to the cardiologist, partly occluding the cardiologist, and completely occluding the cardiologist.

Dynamic Measurement: Posture 1 (Anatomical posture)	No.	1	2	3
	Positions	Lead shield	Close	Far
		Cardiologist	1	1	1
Right Wrist	Dosimetry	0,632553	0,049128	0,525400
	Coordinates	[-116, 57, 0]	[-110, 53, -2]	[-114, 51, -4]
Right Elbow	Dosimetry	0,632553	0,736728	0,693713
	Coordinates	[-119, 68, 28]	[-115, 70, 26]	[-116, 64, 25]
Right Shoulder	Dosimetry	1,145931	0,745631	0,248008
	Coordinates	[-115, 65, 63]	[114, 64, 63]	[-116, 64, 62]
Right Ear	Dosimetry	0,926793	0,373548	0,041926
	Coordinates	[-103, 64, 93]	[-103, 64, 92]	[-103, 64, 92]
Neck Pelvis	Dosimetry	0,475071	0,190384	0,145709
	Coordinates	[-94, 71, 5]	[-92, 67,0]	[-93, 67, 0]
Neck Spine	Dosimetry	1,458630	0,848737	0,379712
	Coordinates	[-94, 70, 27]	[-94, 69, 24]	[-94, 68, 24]
Nose	Dosimetry	1,157517	0,431999	0,041926
	Coordinates	[-87, 52, 84]	[-85, 52, 83]	[-85, 52, 83]
Left Ear	Dosimetry	0,789403	0,204519	0,027318
	Coordinates	[-84, 74, 91]	[-82, 75, 90]	[-81, 74, 90]
Left Shoulder	Dosimetry	1,196101	0,391608	0,402432
	Coordinates	[-74, 77, 65]	[-73, 78, 59]	[-73, 75, 60]
Left Elbow	Dosimetry	1,674022	0,659092	0,666880
	Coordinates	[-70, 80, 29]	[-66, 76, 23]	[-65, 75, 24]
Left Wrist	Dosimetry	0,528096	0,160359	0,153996
	Coordinates	[-67, 70, 2]	[-63, 72, -6]	[-62, 71, -6]

Table 4.1: Displays the values of the first three postures of the second measurement where the cardiologist has an anatomical posture, the coordinates are [x, y, z]-axis in centimeters and the dosimetry is displayed in mSv. The first three values are the cardiologist positioned 100 cm in the x-axis away from the phantom.

4	5	6	7	8	9
No Lead shield	Close	Far	No Lead shield	Close	Far
2	2	2	3	3	3
*0,858652**	*0,903341*	*0,887520*	*0,554379**	*0,579117**	*0,559402**
[-151, 47, 0]	*[-150, 45, -1]*	*[-148, 46, 2]*	*[-193, 36, 2]*	*[-192, 32, 0]*	*[-193, 36, 1]*
*0,845707**	*0,880554**	*0,722558**	*0,574296**	*0,566927**	*0,506354**
[-159, 55, 29]	*[-155, 52, 29]*	*[-156, 52, 30]*	*[-198, 40, 30]*	*[-197, 40, 28]*	*[-198, 40, 30]*
*0,770735**	*0,771290**	*0,427664**	*0,601963**	*0,539343**	*0,367599**
[-155, 53, 65]	*[-154, 49, 66]*	*[-153, 51, 66]*	*[-192, 43, 65]*	*[-190, 40, 63]*	*[-191, 39, 62]*
0,924126	*0,610624*	*0,198333*	*0,634517**	*0,459540**	*0,214308**
[-142, 52, 92]	*[-141, 49, 91]*	*[-141, 50, 92]*	*[-181, 43, 89]*	*[-181, 42, 89]*	*[-181, 40, 86]*
0,933884	*0,867094*	*0,237979*	*0,729217**	*0,725553**	*0,690801**
[-132, 58, 3]	*[-130, 57, 3]*	*[-133, 59, 6]*	*[-172, 48, 4]*	*[-173, 46, 4]*	*[-172, 44, 4]*
1,213049	*1,106070*	*0,828943*	*0,774042**	*0,753892**	*0,634651**
[-133, 59, 27]	*[-132, 58, 27]*	*[-133, 57, 29]*	*[-172, 48, 27]*	*[-171, 46, 26]*	*[-173, 48, 27]*
1,014755	*0,659799*	*0,198333*	*0,796062**	*0,606233**	*0,305534**
[-123, 43, 83]	*[-122, 44, 82]*	*[-122, 43, 82]*	*[-162, 33, 83]*	*[-164, 29, 85]*	*[-164, 28, 84]*
0,904726	*0,475689*	*0,104679*	*0,769747**	*0,543647**	*0,238599**
[-125, 64, 93]	*[-125, 63, 93]*	*[-125, 63, 92]*	*[-164, 54, 89]*	*[-162, 50, 89]*	*[-164, 52, 90]*
1,083459	*0,665393*	*0,671916*	*1,013041**	*0,786407**	*0,499459**
[-115, 69, 64]	*[-115, 69,64]*	*[-114, 68, 65]*	*[-152, 56, 62]*	*[-152, 56, 61]*	*[-152, 56, 62]*
1,234487	*0,972392*	*0,949137*	*1,040236*	*0,955044*	*0,866961*
[-109, 71, -24]	*[-107, 70,28]*	*[-109, 70, 31]*	*[-150, 55, 28]*	*[-147, 57, 27]*	*[-149, 57, 27]*
1,357115	*0,132739*	*0,516963*	*0,908837*	*0,911710*	*0,932469*
[-104, 60, 0]	*[-98, 70, -1]*	*[-105, 59, 3]*	*[-144, 49, 0]*	*[-146, 47, 0]*	*[-149, 45, 2]*

Table 4.2: Displays the values of the fourth till ninth postures of the second measurement where the cardiologist has an anatomical posture, the coordinates are [x, y, z]-axis in centimeters and the dosimetry is displayed in mSv. The fourth till sixth values is the cardiologist positioned 130 cm in the x-axis away from the phantom. The seventh till ninth is the cardiologist positioned 160 cm in the x-axis away from the phantom.

Dynamic Measurement: Posture 2 (Turned)	No.	1	2	3
	Position Lead shield	No Lead shield	Close	Far
Position Cardiologist		1	1	1
Right Wrist	Dosimetry	0,91019	1,077431	1,059575
	Coordinates	[-113, 91, -4]	[-93, 78, 10]	[-88, 49, 12]
Right Elbow	Dosimetry	0,919844	1,495392	0,478447
	Coordinates	[-105, 92, 32]	[-95,80, 30]	[-91, 60, 31]
Right Shoulder	Dosimetry	1,041810	0,498815	0,094175
	Coordinates	[-102, 79, 62]	[-105, 81, 62]	[-103, 81, 59]
Right Ear	Dosimetry	0,957174	0,363009	0,039426
	Coordinates	[-99, 73, 79]	[-102, 73, 85]	[-102. 75, 86
Neck Pelvis	Dosimetry	0,862636	0,460639	0,294048
	Coordinates	[-87, 68, 9]	[-94, 73, 7]	[-89, 65, 5]
Neck Spine	Dosimetry	1,552920	0,806340	0, 295787
	Coordinates	[-88, 71, 27]	[-93, 71, 28]	[-87, 67, 26]
Nose	Dosimetry	1,032026	0,506442	0,064267
	Coordinates	[-102, 55, 88]	[-105, 53, 86]	[-104, 54, 89]
Left Ear	Dosimetry	0,863981	0,315169	0,023196
	Coordinates	[-84, 68, 89]	[-87, 61, 89]	[-85, 65, 89]
Left Shoulder	Dosimetry	1,479434	0,740358	0,708293
	Coordinates	[-74, 57, 60]	[-80, 54, 59]	[-78, 54, 59]
Left Elbow	Dosimetry	2,530941	1,971588	1,566311
	Coordinates	[-71, 54, 29]	[-75, 50, 26]	[-73, 56, 25]
Left Wrist	Dosimetry	0,606767	0,176841	0,104119
	Coordinates	[-76, 47, 3]	[-81, 43, 0]	[-85, 48, 0]

Table 5.1: Displays the values of the first three postures of the second measurement where the cardiologist has an anatomical posture and an angle of 45 degrees, the coordinates are [x, y, z]-axis in centimeters and the dosimetry is displayed in mSv. The first three values are the cardiologist positioned 100 cm in the x-axis away from the phantom.

4	5	6	7	8	9
No Lead shield	Close	Far	No Lead shield	Close	Far
2	2	2	3	3	3
*0,742206**	*0,672114**	*0,983207*	*0,883708**	*0,501123**	*0,653550**
[-160, 51, 6]	*[-171, 67, 9]*	*[-148, 27, 9]*	*[-195, 70, 12]*	*[-194, 73, 16]*	*[-171, 55, 11]*
0,993968	*0,740536**	*0,599737**	*0,592732**	*0,531810**	*0,366927**
[-147, 65, 26]	*[-154, 78, 29]*	*[-153, 70, 26]*	*[-189, 70, 36]*	*[-183, 72, 37]*	*[-182, 72, 36]*
0,943394	*0,677251*	*0,365868*	*0,662629**	*0,541901**	*0,407401**
[-146, 74, 59]	*[-145, 77, 62]*	*[-147, 73, 59]*	*[-181, 58, 66]*	*[-177, 63, 63]*	*[-163, 60, 59]*
0,925515	*0,612445*	*0,252284*	*0,748175**	*0,511403**	*0,314880**
[-147, 58, 85]	*[-146, 65, 85]*	*[-149, 63, 83]*	*[-167, 57, 82]*	*[-174, 56, 79]*	*[-164, 53, 74]*
1,339008	*1,053249*	*1,152118*	*0,731917**	*0,852471**	*0,754224**
[-127, 48, 11]	*[-136, 52, 9]*	*[-128, 47, 11]*	*[-176, 51, 12]*	*[-171, 50, 14]*	*[-166, 46, 15]*
1,333961	*1,077678*	*0,878122*	*0,757666**	*0,699026**	*0,701502**
[-129, 52, 31]	*[-136, 55, 31]*	*[-131, 53, 32]*	*[-172, 49, 32]*	*[-172, 52, 33]*	*[-163, 45, 32]*
0,957782	*0,643618*	*0,216750*	*0,628970**	*0,694305**	*0,430382**
[-137, 42, 85]	*[-138, 45, 87]*	*[-132, 40, 86]*	*[-183, 44, 86]*	*[-183, 39, 81]*	*[-182, 44, 82]*
0,910350	*0,492164*	*0,132566*	*0,723201**	*0,476269**	*0,128388**
[-132, 61, 93]	*[-129, 62, 95]*	*[-135, 62, 95]*	*[-170, 38, 84]*	*[-165, 43, 85]*	*[-182, 72, 36]*
1,251498	*0,939984*	*0,904306*	*0,994930**	*0,777194**	*0,660706**
[-122, 44, 65]	*[-124, 44, 65]*	*[-121, 45, 67]*	*[-155, 35, 59]*	*[-161, 33, 59]*	*[-161, 29, 56]*
1,648361	*1,431054*	*1,456386*	*0,858963**	*0,874942**	*0,847903**
[-118, 42, 31]	*[-121, 40, 32]*	*[-119, 42, 33]*	*[-153, 34, 29]*	*[-158, 36, 30]*	*[-155, 35, 30]*
1,326565	*1,178509*	*1,290868*	*0,830011**	*0,812097**	*0,830011**
[-122, 40, 5]	*[-132, 33, 6]*	*[-127, 37, 7]*	*[-161, 24, 5]*	*[-165, 29, 9]*	*[-164, 35, 8]*

Table 5.2: Displays the values of the fourth till ninth postures of the second measurement where the cardiologist has an anatomical posture and an angle of 45 degrees, the coordinates are [x, y, z]-axis in centimeters and the dosimetry is displayed in mSv. The fourth till sixth values is the cardiologist positioned 130 cm in the x-axis away from the phantom. The seventh till ninth is the cardiologist positioned 160 cm in the x-axis away from the phantom.

Dynamic Measurement: Posture 3 (Arms raised)				
	No.	1	2	3
	Position Lead shield	No Lead shield	Close	Far
Position Cardiologist		1	1	1
Right Wrist	Dosimetry	*1,128492*	*0,197316*	*0,76311*
	Coordinates	*[-105, 16, 37]*	*[-93, 17, 40]*	*[-87, 17, 42]*
Right Elbow	Dosimetry	*1,418136*	*0,773619*	*0,757942*
	Coordinates	*[-115, 40, 46]*	*[-108, 43, 47]*	*[-104, 33, 48]*
Right Shoulder	Dosimetry	*1,101336*	*0,786533*	*0,184536*
	Coordinates	*[-113, 68, 65]*	*[-110, 62, 61]*	*[-109, 63, 65]*
Right Ear	Dosimetry	*0,907831*	*0,340729*	*0,037781*
	Coordinates	*[-105, 69, 88]*	*[-103, 72, 91]*	*[-103, 72, 91]*
Neck Pelvis	Dosimetry	*0,835029*	*0,421323*	*0,228308*
	Coordinates	No Lead shield	Close	Far
Neck Spine	Dosimetry	*1,494854*	*0,764212*	*0,279669*
	Coordinates	*[-94, 69, 30]*	*[-91, 71, 26]*	*[-91, 70, 27]*
Nose	Dosimetry	*1,039252*	*0,407158*	*0,034192*
	Coordinates	*[-87, 61, 84]*	*[-87, 59, 82]*	*[-87, 58, 82]*
Left Ear	Dosimetry	*0,780392*	*0,220699*	*0,049075*
	Coordinates	*[-87, 79, 90]*	*[-84, 78, 87]*	*[-83, 81, 88]*
Left Shoulder	Dosimetry	*1,197793*	*0,367067*	*0,321792*
	Coordinates	*[-75, 75, 66]*	*[-66, 67, 61]*	*[-76, 88, 62]*
Left Elbow	Dosimetry	*2,037333*	*0,382781*	*0,351604*
	Coordinates	*[-61, 59, 42]*	*[-52, 83, 37]*	*[-50, 79, 38]*
Left Wrist	Dosimetry	*2,700573*	*0,442317*	*0,326759*
	Coordinates	*[-65, 33, 38]*	*[-37, 72, -6]*	*[-62, 36, 28]*

Table 6.1: Displays the values of the first three postures of the second measurement where the cardiologist has an anatomical posture with their arms raised, the coordinates are [x, y, z]-axis in centimeters and the dosimetry is displayed in mSv. The first three values are the cardiologist positioned 100 cm in the x-axis away from the phantom. The fourth till sixth values is the cardiologist positioned 130 cm in the x-axis away from the phantom. The ninth first three values are the cardiologist positioned 100 cm in the x-axis away from the phantom.

4	5	6	7	8	9
No Lead shield	Close	Far	No Lead shield	Close	Far
2	2	2	3	3	3
0,950491	*1,208611*	*0,900571*	*0,743188**	*0,358927**	*0,640611**
[-141, 15, 26]	*[-121, 24, 30]*	*[-145, 16, 37]*	*[-165, -4, 36]*	*[-186, -4, 44]*	*[-178, 8, 35]*
*0,867391**	*0,932923**	*0,756361**	*0,556798**	*0,558799**	*0,666204**
[-157, 37, 35]	*[-151, 29, 33]*	*[-158, 36, 39]*	*[-195, 24, 37]*	*[-198, 24, 35]*	*[-182, 31, 27]*
*0,801459**	*0,888164*	*0,397114*	*0,599486*	*0,523247**	*0,362942**
[-152, 54, 62]	*[-146, 29, 63]*	*[-145, 60, 66]*	*[-193, 44, 62]*	*[-191, 46, 63]*	*[-190, 43, 61]*
0,924126	*0,616481*	*0,175427*	*0,613390**	*0,447138**	*0,179078**
[-141, 56, 90]	*[-145, 56, 89]*	*[-142, 57, 92]*	*[-184, 48, 89]*	*[-184, 50, 85]*	*[-183, 47, 89]*
0,922032	*0,831418*	*0,924974*	*0,773906**	*0,789583**	*0,729937**
[-131, 55, 6]	*[-133, 60, 4]*	*[-131, 53, 7]*	*[-169, 43, 6]*	*[-167, 41, 7]*	*[-170, 42, 8]*
1,294192	*1,120539*	*0,740014*	*0,783541**	*0,773258**	*0,675335**
[-130, 56, 28]	*[-133, 57, 24]*	*[-134, 62, 28]*	*[-171, 46, 27]*	*[-169, 45, 26]*	*[-170, 43, 29]*
0,997671	*0,645856*	*0,179848*	*0,786867**	*0,476960**	*0,275799**
[-124, 46, 84]	*[-126, 47, 83]*	*[-124, 47, 84]*	*[-163, 40, 85]*	*[-165, 41, 84]*	*[-164, 39, 85]*
0,909720	*0,498079*	*0,105728*	*0,748942**	*0,511653**	*0,235191**
[-122, 65, 89]	*[-129, 68, 89]*	*[-125, 68, 89]*	*[-166, 60, 88]*	*[-167, 61, 87]*	*[-167, 59, 87]*
1,159972	*0,738514*	*0,667142*	*0,994930**	*0,761521**	*0,475055**
[-112, 64, 66]	*[-116, 64, 64]*	*[-114, 69, 64]*	*[-153, 54, 67]*	*[-153, 57, 63]*	*[-153, 50, 65]*
1,948103	*1,585989*	*1,592178*	*1,035125*	*0,989323*	*0,976852*
[-97, 52, 35]	*[-104, 43, 37]*	*[-99, 45, 39]*	*[-140, 32, 44]*	*[-139, 30, 44]*	*[-139, 27, 45]*
1,875923	*1,193906*	*1,326965*	*0,912214*	*0,909697*	*0,908334*
[-99, 27, 24]	*[-108, 16, 29]*	*[-106, 21, 32]*	*[-142, 3, 41]*	*[-138, 4, 45]*	*[-142, 0, 41]*

Table 6.2: Displays the values of the fourth till ninth postures of the second measurement where the cardiologist has an anatomical posture with their arms raised, the coordinates are [x, y, z]-axis in centimeters and the dosimetry is displayed in mSv. The fourth till sixth values is the cardiologist positioned 130 cm in the x-axis away from the phantom. The seventh till ninth is the cardiologist positioned 160 cm in the x-axis away from the phantom.

Visualization Measurement 1: Adjusting the Distance of the Cardiologist part 1	Position Cardiologist	1	2	3	2	4
Right Wrist	Dosimetry	0,3708	1,1068	2,8377	1,0280	0,8032
	Coordinates	[-235, 0, 18]	[-132, 23, 26]	[-40, 56, -26]	[-143, 40, 5]	[-160, 79, 12]
Right Shoulder	Dosimetry	0,3672	0,9968	0,7667	1,0095	0,7522
	Coordinates	[-242, 26, 64]	[-148, 46, 66]	[-54, 79, 68]	[-145, 53, 67]	[-165, 98, 61]
Right Ear	Dosimetry	0,3767	0,9370	0,3731	0,9351	0,8864
	Coordinates	[-234, 27, 90]	[-137, 54, 87]	[-41, 75, 90]	[-134, 50, 90]	[-152, 93, 87]
Nose	Dosimetry	0,4518	1,0529	0,3766	1,0871	0,9093
	Coordinates	[-214, 22, 81]	[-119, 44, 82]	[-28, 68, 78]	[-116, 41, 81]	[-136, 85, 77]
Left Ear	Dosimetry	0,4204	0,9971	0,3660	0,9403	0,9093
	Coordinates	[-222, 38, 91]	[-118, 52, 86]	[-23, 84, 89]	[-115, 60, 90]	[-136, 105, 89]
Left Shoulder	Dosimetry	0,4891	1,1378	0,6301	1,0957	0,9023
	Coordinates	[-213, 45, 65]	[-109, 68, 63]	[-15, 93, 67]	[-107, 67, 63]	[-127, 110, 62]
Left Wrist	Dosimetry	0,5500	1,4205	0,7031	2,0136	0,8019
	Coordinates	[-199, 22, 21]	[-105, 30, 11]	[-16, 76, 45]	[-107, 40, 18]	[-126, 89, 115

Table 7: Displays the measurement 1 of the first part of the visualization measurement, with the dosimetry in mSv and the coordinates [x, y, z] in centimeters. This measurement shows the software is able to track difference in positions and the effect of exposure of radiation.

Visualization Measurement 1: Adjusting the Distance of the Cardiologist part 2						
Position Cardiologist		3	2	1	2	4
Right Wrist	Dosimetry	1,2815	0,9588	0,3711	1,0437	0,6611
	Coordinates	[-51, 79, 15]	[-149, 22, 6]	[-235, 18, 24]	[-144, 39, 7]	[-176, 94, 1]
Right Shoulder	Dosimetry	0,6983	1,0008	0,3745	0,9818	0,9102
	Coordinates	[-52, 85, 67]	[-146, 50, 66]	[-240, 26, 62]	[-148, 57, 65]	[-143, 105, 67]
Right Ear	Dosimetry	0,3726	0,9287	0,3885	0,9295	0,8864
	Coordinates	[-41, 81, 90]	[-135, 52, 91]	[-230, 21, 90]	[-136, 53, 90]	[-152, 98, 93]
Nose	Dosimetry	0,3559	1,0568	0,4371	1,0821	1,0540
	Coordinates	[-27, 70, 79]	[-123, 40, 79]	[-217, 17, 82]	[-123, 40, 77]	[-124, 40, 78]
Left Ear	Dosimetry	0,3629	0,9670	0,4404	0,9142	0,9098
	Coordinates	[-23, 88, 90]	[-118, 55, 88]	[-217, 37, 90]	[-120, 64, 89]	[-135, 112, 93]
Left Shoulder	Dosimetry	0,6640	1,2448	0,5129	1,2462	0,9035
	Coordinates	[-12, 94, 68]	[-106, 63, 62]	[-208, 43, 65]	[-108, 62, 61]	[-125, 114, 62]
Left Wrist	Dosimetry	1,2563	1,6658	0,5133	1,3938	0,6118
	Coordinates	[-4, 85, 15]	[-104, 35, 10]	[-202, 14, 17]	[-110, 26, 9]	[-102, 109, 4]

Table 8: Displays measurement 2 of the first part of the visualization measurement, with the dosimetry in mSv and the coordinates [x, y, z] in centimeters. This measurement shows the software is able to track difference in positions and the effect of exposure of radiation.

Table 9: Displays measurement 1 of the second part of the visualization measurement, with the dosimetry in mSv and the coordinates [x, y, z] in centimeters. This measurement shows the software is able to track difference in positions of the lead shield and the effect of exposure of radiation.

Visualization Measurement 2: Adjusting the Distance of the Lead Shield part 1				
Position Lead Shield		1	2	3
Coordinates Aruco Marker Lead shield	**87**	*[-5, 28, 21]*	*[-154, 220, 54]*	*[-147, 59, 34]*
	70	*[-42, 14, 47]*	*[-147, 60, 71]*	*[-394, 145, 123]*
	66	*[-41, 13, 76]*	*[-254, 167, 183]*	*[-329, 92, 180]*
	42	*[-13, 25, 45]*	*[-37, 14, 45]*	*[-145, 60, 69]*
	24	*[4, 27, 76*	*[-40, 13, 76]*	*No depth Value*
Right Ear	**Dosimetry**	*0,5249*	*0,0409*	*0,0409**
	Coordinates	*[-103, 64, 93]*	*[-103, 64, 93]*	*[-103, 64, 93]*
Right Shoulder	**Dosimetry**	*0,8735*	*0,2247*	*0,2247**
	Coordinates	*[-115, 65, 63]*	*[-115, 65, 63]*	*[-115, 65, 63]*
Nose	**Dosimetry**	*0,6285*	*0,0364*	*0,0364**
	Coordinates	*[-87, 52, 84]*	*[-87, 52, 84]*	*[-87, 52, 84]*
Left Shoulder	**Dosimetry**	*0,5632*	*0,1239*	*0,1239**
	Coordinates	*[-74, 77, 65]*	*[-74, 77, 65]*	*[-74, 77, 65]*
Left Wrist	**Dosimetry**	*0,4324*	*0,2358*	*0,2358**
	Coordinates	*[-67, 70, 2]*	*[-67, 70, 2]*	*[-67, 70, 2]*

Visualization Measurement 2: Adjusting the Distance of the Lead Shield part 1					
Position Lead Shield		**3**	**2**	**1**
Coordinates Aruco Marker Lead shield	**87**	*[-146, 68, 34]*	*[-151, 221, 53]*	*[-56, 250, 51]*
	70	*No depth Value*	*[-152, 61, 88]*	*[-154, 219, 140]*
	66	*[-332, 81, 191]*	*[-211, 116, 186]*	*[-114, 145, 183]*
	42	*[-143, 62, 68]*	*[-37, 14, 44]*	*[-53, 249, 107]*
	24	*[-259, 167, 183]*	*[-40, 13, 75]*	*[-2, 27, 75]*
Right Ear	**Dosimetry**	*0,5249*	*0,0409*	*0,0409**
	Coordinates	*[-103, 64, 93]*	*[-103, 64, 93]*	*[-103, 64, 93]*
Right Shoulder	**Dosimetry**	*0,8735*	*0,2247*	*0,2247**
	Coordinates	*[-115, 65, 63]*	*[-115, 65, 63]*	*[-115, 65, 63]*
Nose	**Dosimetry**	*0,6285*	*0,0364*	*0,0364**
	Coordinates	*[-87, 52, 84]*	*[-87, 52, 84]*	*[-87, 52, 84]*
Left Shoulder	**Dosimetry**	*0,5632*	*0,1239*	*0,1239**
	Coordinates	*[-74, 77, 65]*	*[-74, 77, 65]*	*[-74, 77, 65]*
Left Wrist	**Dosimetry**	*0,4324*	*0,2358*	*0,2358**
	Coordinates	*[-67, 70, 2]*	*[-67, 70, 2]*	*[-67, 70, 2]*

Table 10: Displays measurement 2 of the second part of the visualization measurement, with the dosimetry in mSv and the coordinates [x, y, z] in centimeters. This measurement shows the software is able to track difference in positions of the lead shield and the effect of exposure of radiation.

Appendix D: Visualization of the Coordinates Acquisition

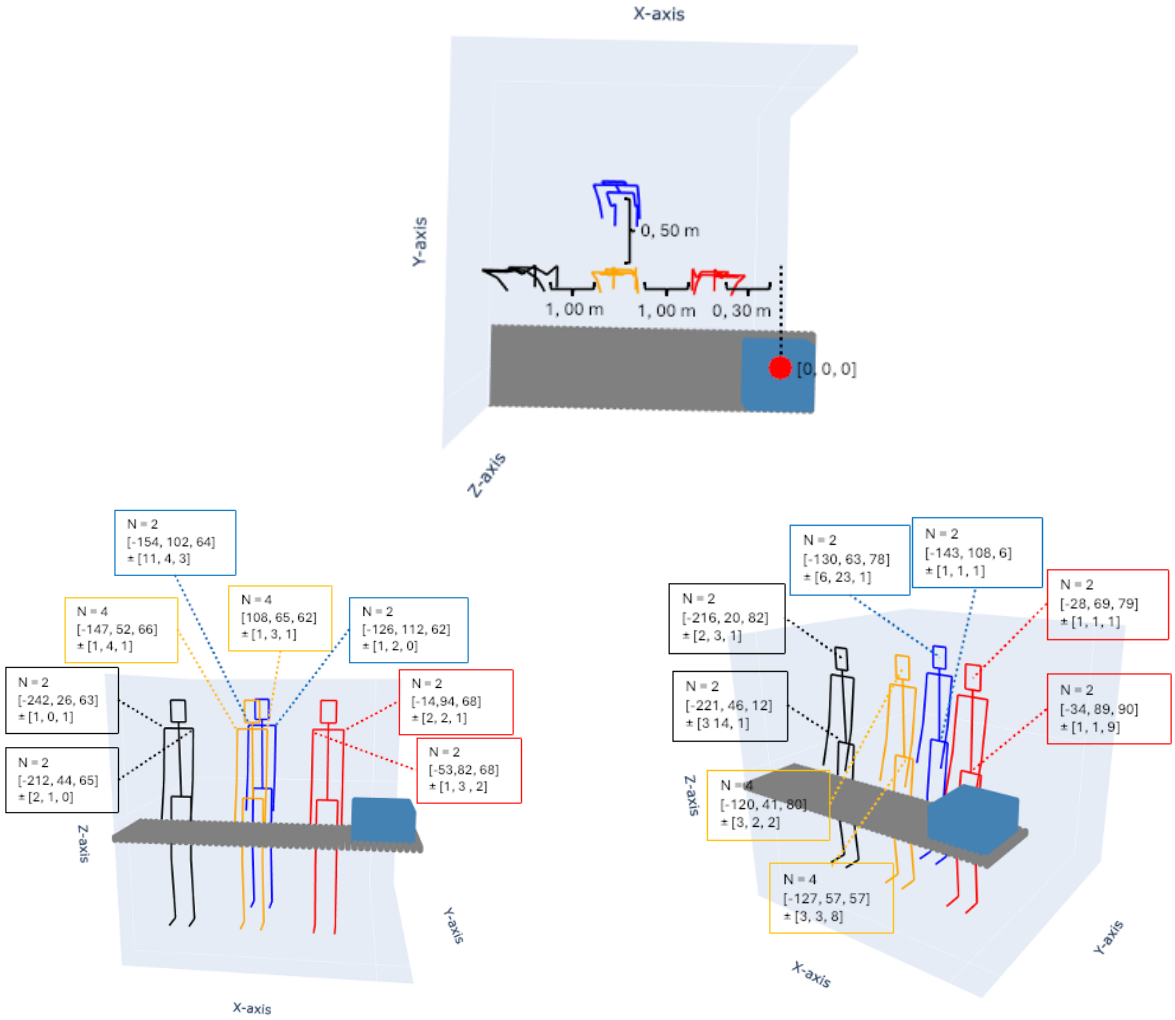

Figure 26: Displays the coordinates of part 1 of measurement three. The mean of the coordinates and the variation are shown for axes [x, y, z] in centimeters. A: Shows the positioning of the cardiologist in relation to the phantom. B: Shows the coordinates of the left and right shoulder of the four cardiologists. C: Shows the coordinates of the nose and the middle of the pelvis for the four positions.

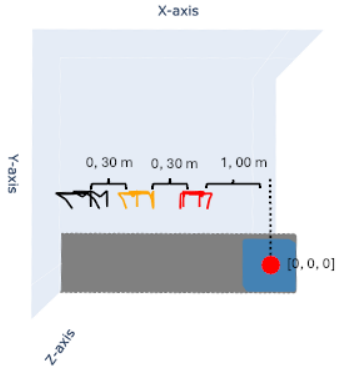

Figure 27: Displays the positioning of the positions of the cardiologist for the second measurement relative to the phantom

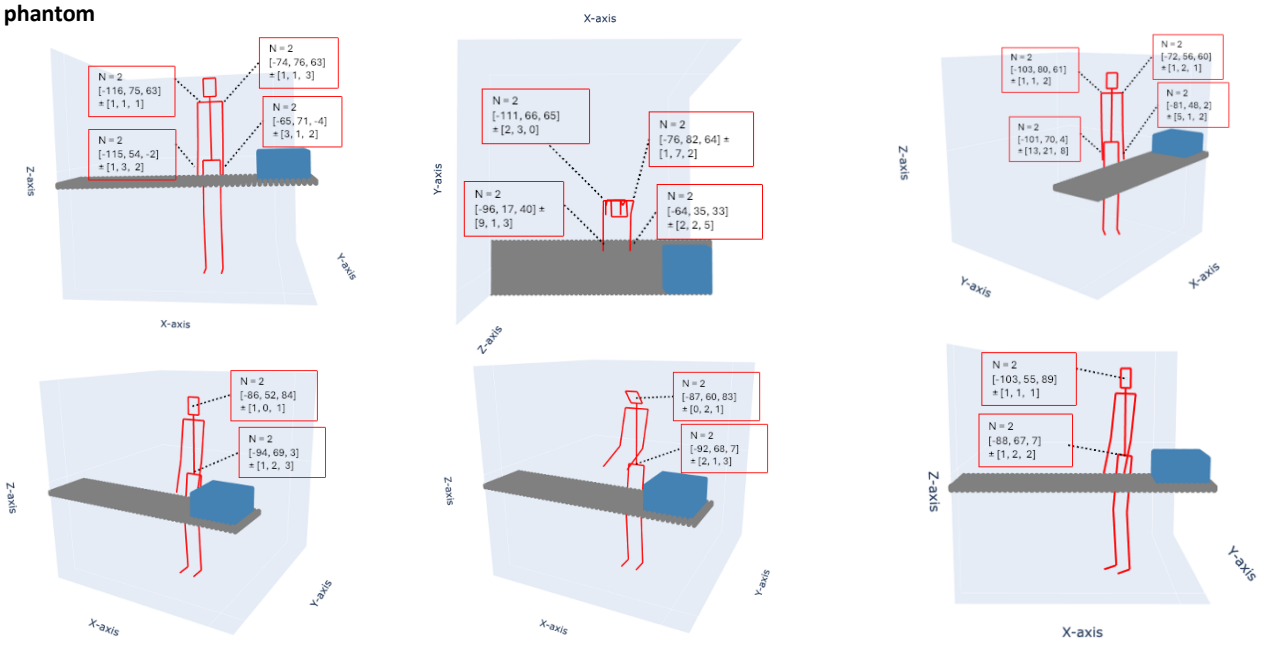

Figure 28: Displays six different angles of the three different postures of the cardiologist for position closest to the phantom for measurement 2. A: The cardiologist is in the anatomic posture positioned and the coordinates of left/right wrist and left/right shoulder are shown. B: The cardiologist is in the anatomic posture with the hands out with the coordinates of the same body parts. C: The cardiologist is turned 45 degrees and in the anatomic posture with coordinates of the same body parts. D: The cardiologist is in the anatomic posture positioned and the coordinates of the nose and middle of the pelvis are shown. E: The cardiologist is in the anatomic posture with the hands out with the coordinates of the same body parts. F: The cardiologist is turned 45 degrees and in the anatomic posture with coordinates of the same

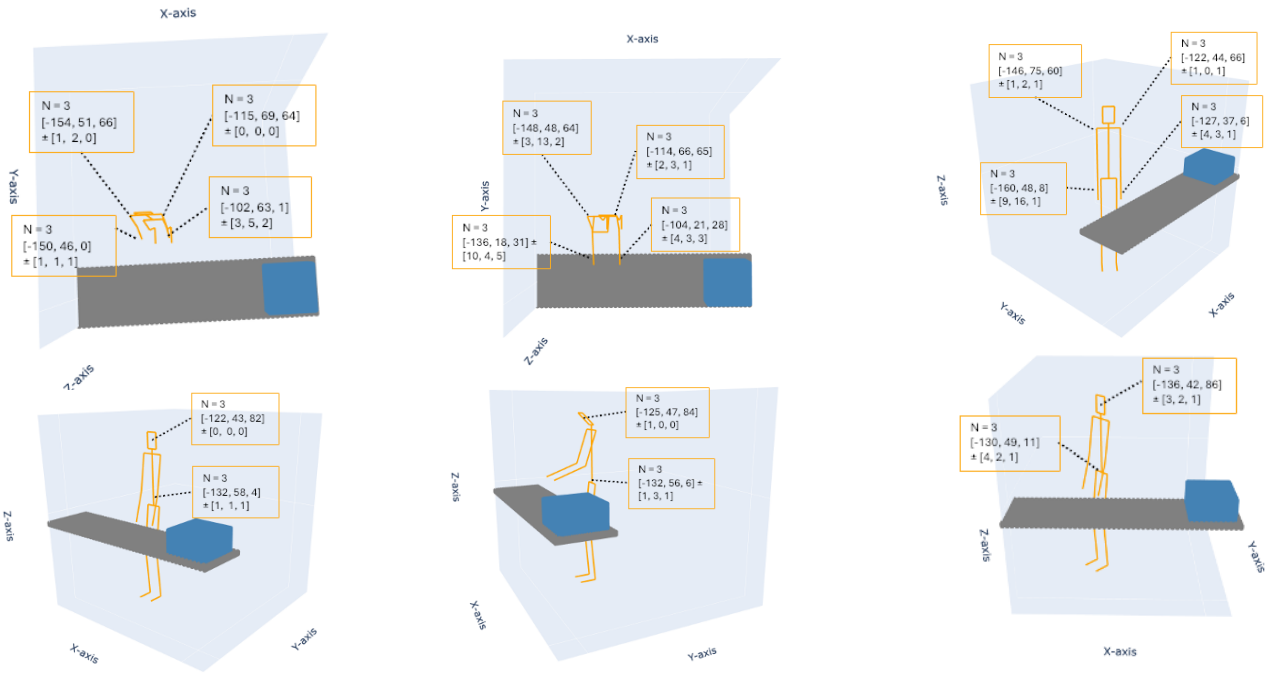

Figure 29: Displays six different angles of the three different postures of the cardiologist for position second closest to the phantom for measurement 2. A: The cardiologist is in the anatomic posture positioned and the coordinates of left/right wrist and left/right shoulder are shown. B: The cardiologist is in the anatomic posture with the hands out with the coordinates of the same body parts. C: The cardiologist is turned 45 degrees and in the anatomic posture with coordinates of the same body parts. D: The cardiologist is in the anatomic posture positioned and the coordinates of the nose and middle of the pelvis are shown. E: The cardiologist is in the anatomic posture with the hands out with the coordinates of the same body parts. F: The cardiologist is turned 45 degrees and in the anatomic posture with coordinates

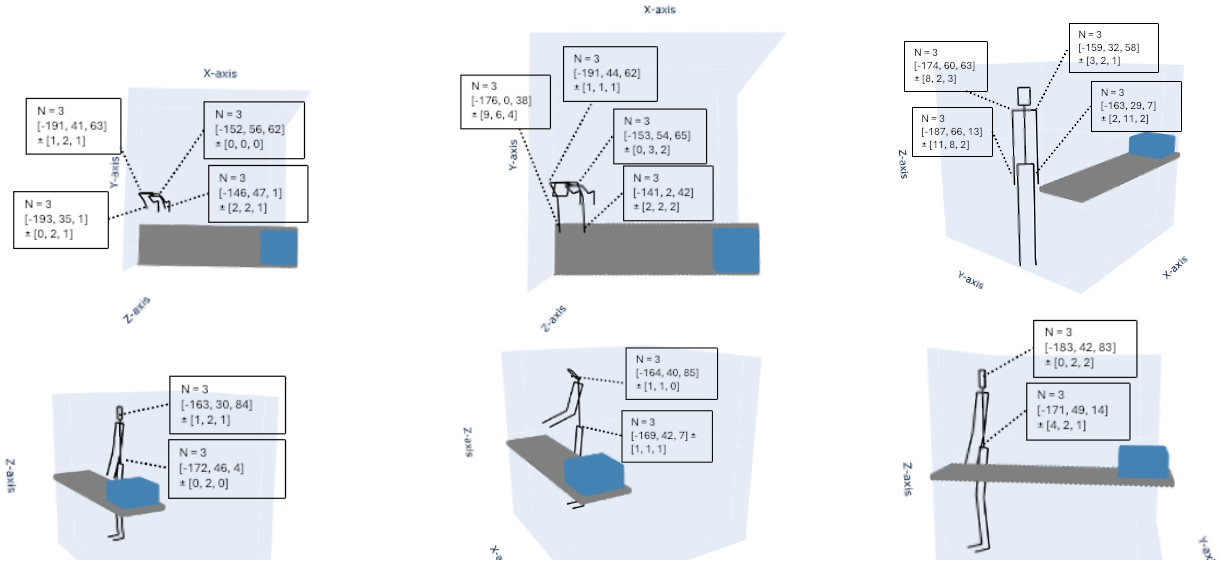

Figure 30: Displays six different angles of the three different postures of the cardiologist for position furthest away of the phantom for measurement 2. A: The cardiologist is in the anatomic posture positioned and the coordinates of left/right wrist and left/right shoulder are shown. B: The cardiologist is in the anatomic posture with the hands out with the coordinates of the same body parts. C: The cardiologist is turned 45 degrees and in the anatomic posture with coordinates of the same body parts. D: The cardiologist is in the anatomic posture positioned and the coordinates of the nose and middle of the pelvis are shown. E: The cardiologist is in the anatomic posture with the hands out with the coordinates of the same body parts. F: The cardiologist is turned 45 degrees and in the anatomic posture with coordinates

Appendix E: Visualization of Static Measurement

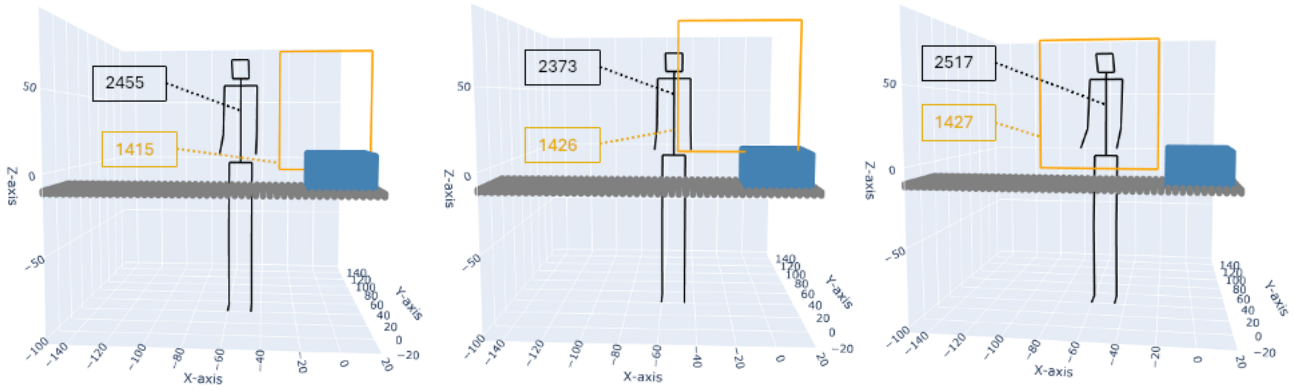

Figure 31: Displays the three different positions of the lead shield of measurement 1 and the distances towards the middle of the lead shield and the cardiologist in millimeters. A: Lead shield positioned next to the cardiologist. B: Lead shield partially covering the cardiologist. C: The lead shield completely covering the cardiologist.

Appendix F: Visualization of the Static Measurement

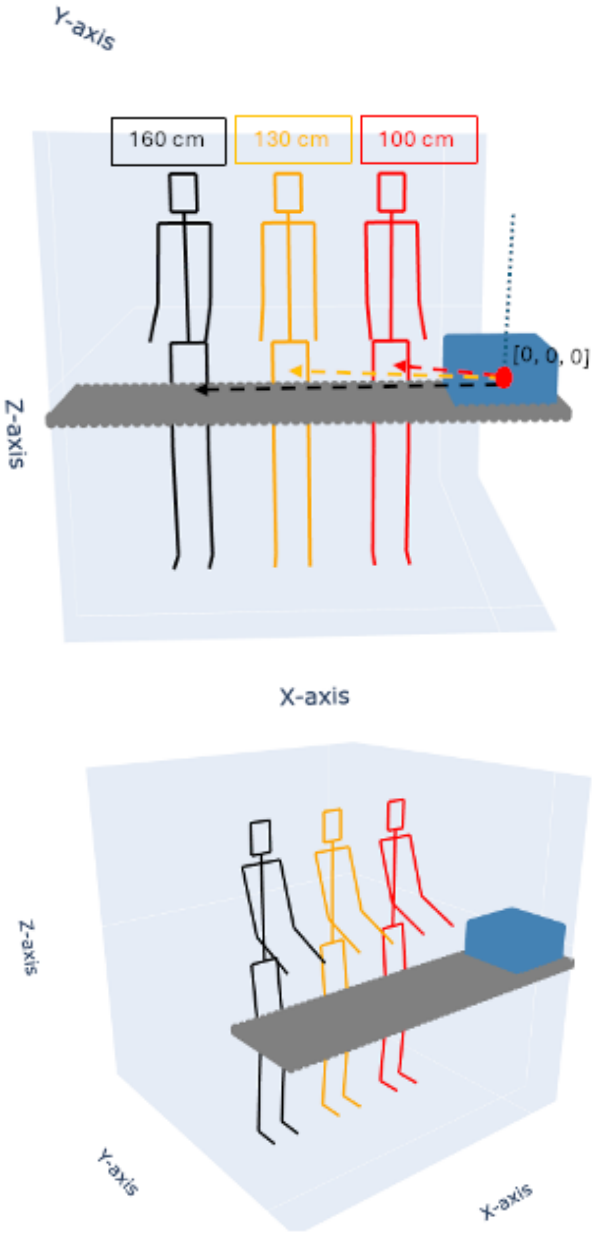

Body Parts	Different Position's Cardiologist:		
	100 cm	130 cm	160 cm
L Wrist	2,7006	1,8759	0,9122
L Elbow	2,0373	1,9481	1,0351
L Shoulder	1,1978	1,1600	0,9949
Nose	1,0393	0,9977	0,7879
Pelvis	0,8350	0,9250	0,7739
R Shoulder	1,1013	0,8015	0,5995
R Elbow	1,4181	0,8674	0,5568
R Wrist	1,1285	0,9505	0,7432

Figure 32: Displays the three different positions of the cardiologist when there is no lead shield used with the anatomical posture with the hands raised. A: Shows the relation of the positions towards the phantom. B: Shows a different angle of the three different postures of the cardiologist. TABLE: Shows the amount of radiation exposure in mSv for certain body parts for the different positions of the cardiologist.

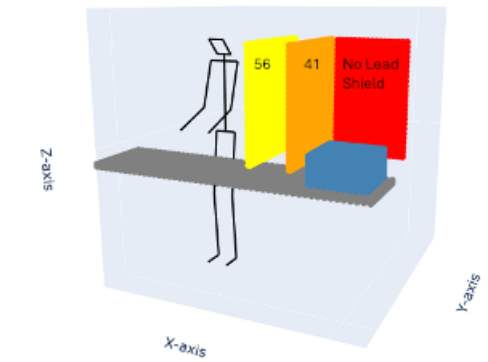

Body Parts	Different position's Lead Shield:		
	-	36 cm	51 cm
L Wrist	1,3571	0,1327	0,5170
L Elbow	1,2345	0,9724	0,6719
L Shoulder	1,0835	0,6654	0,6719
Nose	1,0148	0,6598	0,1983
Pelvis	0,9338	0,8671	0,2360
R Shoulder	0,7707	0,7713	0,4277
R Elbow	0,8457	0,8806	0,7726
R Wrist	0,8587	0,9033	0,8875

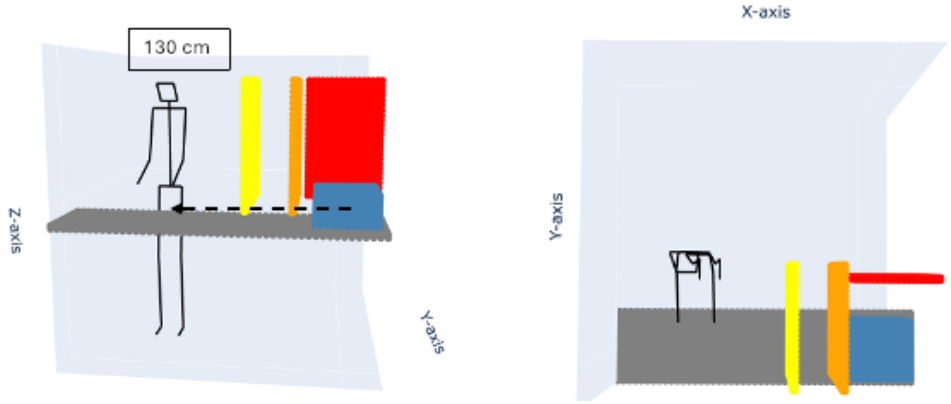

Figure 32: Displays the three different positions of the lead shield when the cardiologist is positioned at 130 cm in the x-axis from the phantom. A: Shows the relation of the positions of the lead shield towards the phantom. B: Shows the relation of the position of the cardiologist towards the phantom. C: Shows the view of above. TABLE: Shows the amount of radiation exposure in mSv for certain body parts for the different positions of the lead shield.

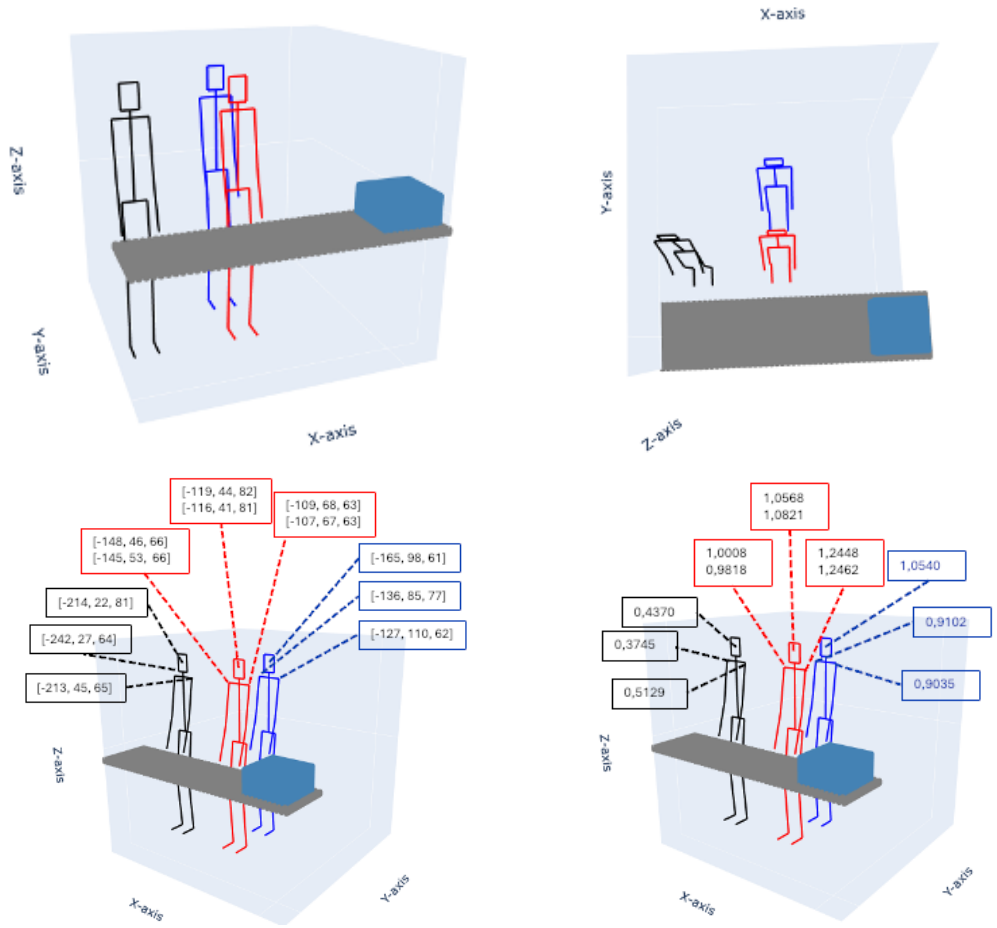

Figure 33: Shows the first measurement of part 1 of the visualization measurement. A & B: Show two different angles of the positions of the cardiologist, position 3 is removed due remarkable radiation exposure. C: Shows the coordinates of the cardiologists for the nose and the left/right shoulder in [x, y, z] axis in centimeters. D: Shows for the same body parts the amount of radiation exposure in mSv.

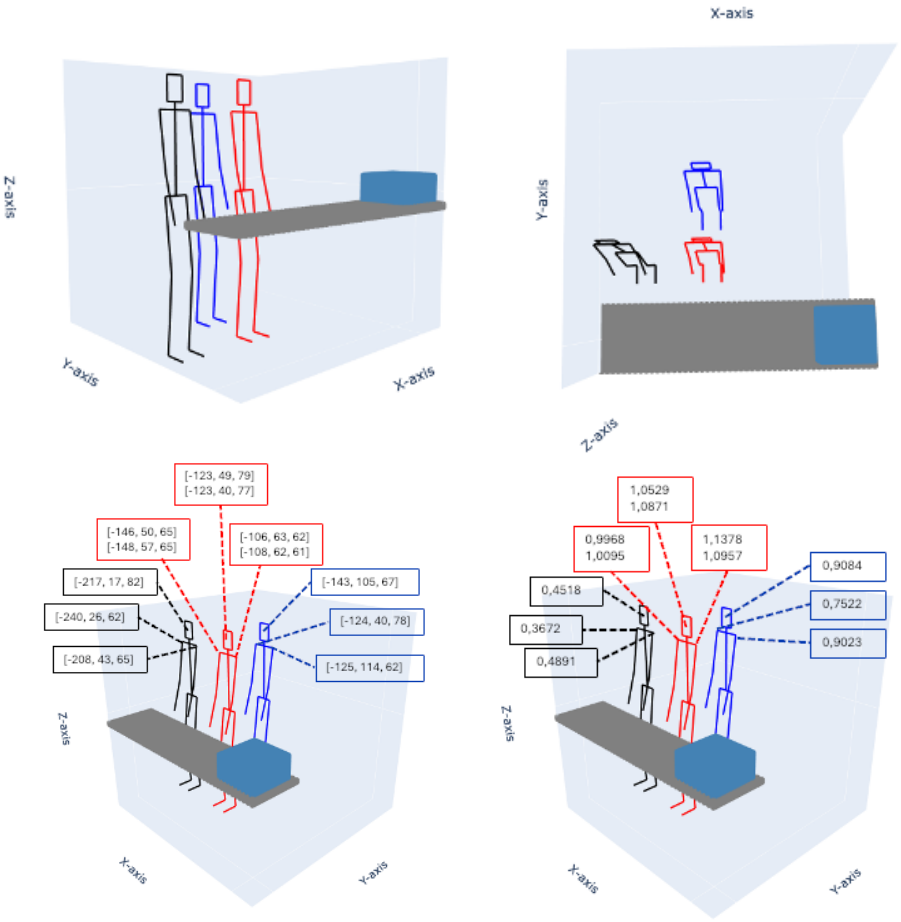

Figure 33: Shows the second measurement of part 1 of the visualization measurement. A & B: Show two different angles of the positions of the cardiologist, position 3 is removed due remarkable radiation exposure. C: Shows the coordinates of the cardiologists for the nose and the left/right shoulder in [x, y, z] axis in centimeters. D: Shows for the same body parts the amount of radiation exposure in mSv.

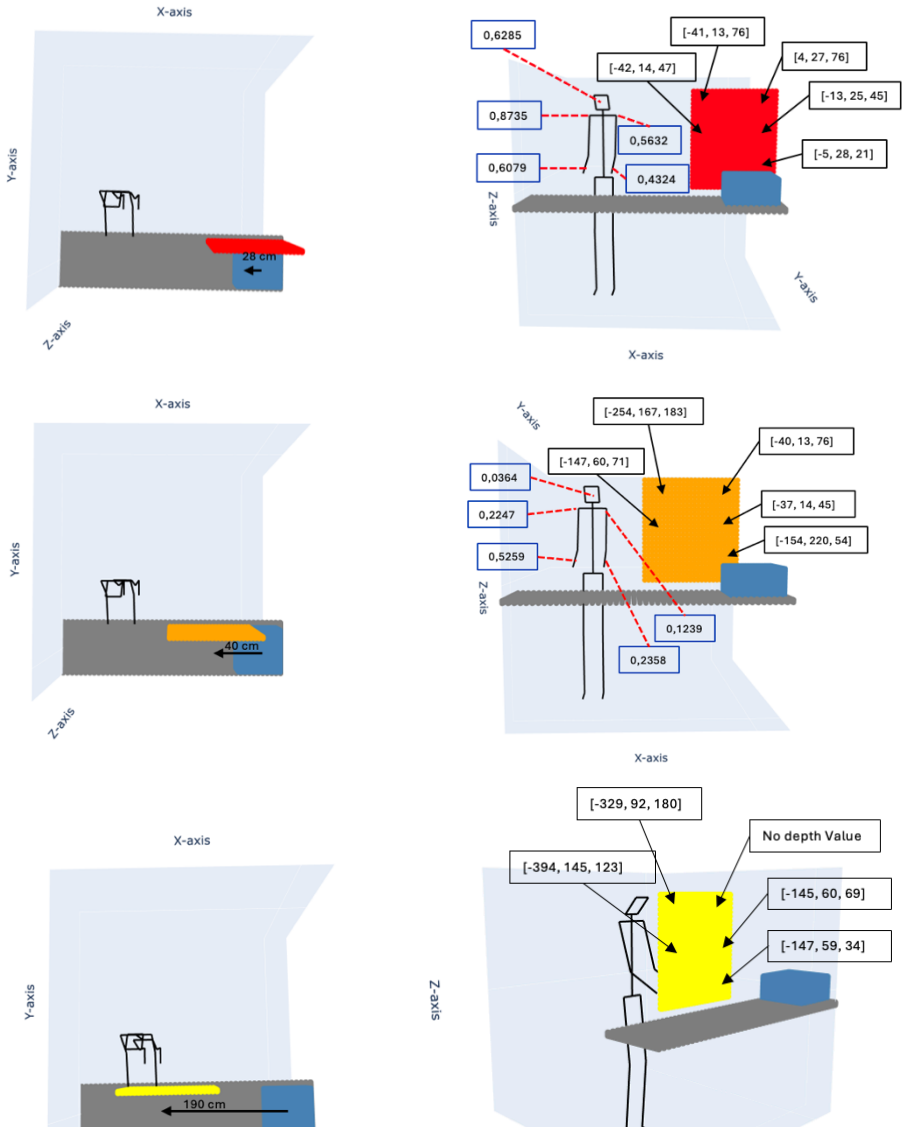

Figure 34: Shows the first measurement of part 2 of the visualization measurement. A & B: Show the first position of the lead shield. With A showing the distance of the center of the phantom towards the middle of the lead shield in the X-axis. B: Shows the coordinates of the left upper corner of the Aruco marker for [x, y, z] axis in centimeters and the amount of radiation exposure for the cardiologist in mSv. C & D: Show the second position of the lead shield. E & F: Show the third position of the lead shield.

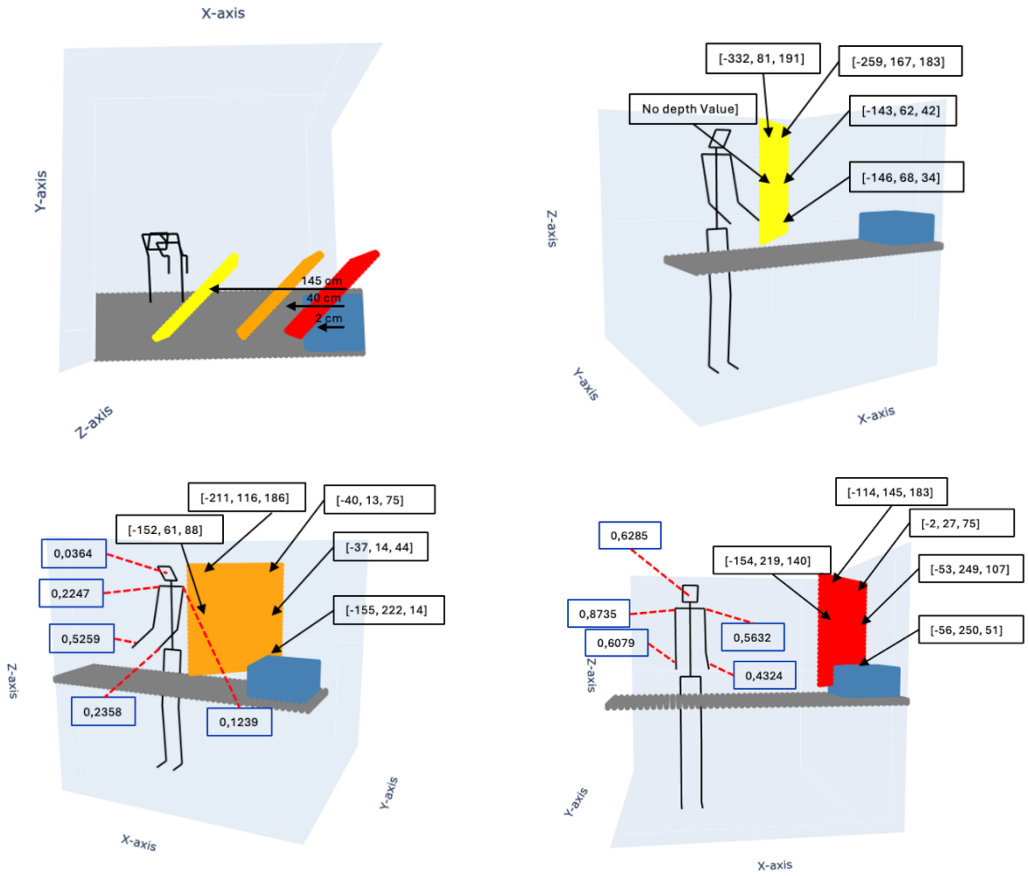

Figure 35: Shows the second measurement of part 2 of the visualization measurement. A: Shows the distances of the phantom towards the center of the lead shield in centimeters. B: Shows the first measurement with the lead shield positions farthest away, and the coordinates of the left upper corner of the Aruco marker are shown in centimeters for the [x, y, z] axes. C: Shows the second measurement. D: Shows the third measurement